UNIVERSITY OF CAPE TOWN

FACULTY OF ENGINEERING AND BUILT ENVIRONMENT

Department of Civil Engineering

Comparative Assessment of Single & Double Interface Shear Strength Properties: A Case Study of a Landfill Project in the Western Cape Province, South Africa

Author : Victor Sylivery

Supervisor : Prof. Denis Kalumba
Co-Supervisor : Byron Mawer (Pr. Eng)

A thesis submitted in partial fulfilment of the requirement for the award of the degree of Master of Science in Civil Engineering Specialising in Geotechnical Engineering at the University of Cape Town

February 2022

Plagiarism declaration

1. Plagiarism is to use another's work and pretend that it is one's own. I know that plagiarism is wrong.
2. I have used the UCT-Harvard convention for citation and referencing. Each significant contribution to and quotation in this report from the work or works of other people has been attributed and has been cited and referenced.
3. This thesis/dissertation is my work.
4. I have not allowed and will not allow anyone to copy my work to pass it off as their work.
5. This thesis/dissertation has been submitted to the Turnitin module (or equivalent similarity and originality checking software). I confirm that my supervisor has seen my report, and any concerns revealed by such have been resolved with my supervisor.

Signature: Signed by candidate …… Date: 01 February 2022

Student Name: Victor Kajungu Sylivery …….

Dedication

To

My Father, **Dennis Gabone Mwebuga**, whose love, care and support have geared me with the best education on a journey to becoming a responsible global citizen.

&

My Heavenly Father **God Almighty** and My Saviour Lord **Jesus Christ**, whose abundant love and grace is my everlasting hope.

Acknowledgements

This research was made possible by several amazing people whose vested interests and efforts in this work can never go unmentioned.

First and foremost, I would like to sincerely thank my supervisor, Prof. Denis Kalumba and co-supervisor, Mr Byron Mawer (Pr. Eng), for their guidance, knowledge, invaluable contributions, and constructive criticism towards achieving the objectives of this work. Additionally, I am grateful for their support in providing me with the necessary laboratory materials that enabled the undertaking of this study, ensuring its timely completion.

My sincere gratitude to the Executive Associate at JG Afrika (Pty) Ltd, Mr Richard Emery, for permitting me to utilise the site and project-specific geosynthetic and geomaterial samples in this study. Recognition to Mr Nkosinamandla Zwane (Engineer at JG Afrika), who delivered samples to the UCT Geotechnical Laboratory; thank you, Zwane.

I would also like to appreciate the general laboratory support received throughout this study from the following people within the UCT civil engineering laboratory: Mr Noor Hassen, Mr Elvino Witbooi and the late Mr Tahir Mukaddam. In addition, Mr Charles Nicholas and Mr Swayiza Masimthembe from the UCT civil engineering workshop were very helpful in assisting with geomembrane sample preparations.

UCT experience was phenomenal due to the presence of friends and colleagues, starting with Daniel Adeleke and Shade Muluti, who taught me how to use the Large Shear Apparatus and analysis of experimental data; Lebogang Sekhukhune, who proofread my dissertation during her precious time; and my fellow students, Rhonda Hyde, Gerald Otim, and Arthur Econi, who made this journey unforgettable. May you all please accept my deepest gratitude.

Lastly, my father Dennis Gabone, mother Evelyne Aliganyira, brother Francis Mutegeki, uncle Fabian Kalikawe and my amazing life partner Ms Dineo Kotu. I will forever be grateful for your kindness, patience, and encouragement in making me achieve this great milestone.

To those unmentioned, your invaluable support is equally recognised and appreciated. Many blessings to all of you, and I wish you well in all that you do.

With lots of love,

Victor Kajungu Sylivery.

Abstract

Geosynthetics are now stipulated inclusions in municipal solid waste (MSW) landfill's lining systems as they provide a competent hydraulic barrier, limiting environmental pollution and protecting public health. While these inclusions have considerable cost and technical benefits, they have presented several new potential interfaces for shear failure, particularly on side-slopes and basins of conventional hole-in-ground type MSW landfills. In the laboratory, interface shear strength properties of either soil-geosynthetic or geosynthetic-geosynthetic are determined through a single interface testing configuration as per standard testing practices like ASTM D5321 & D6243. However, there is little data on interface shear strength tests conducted through multiple-interface configurations. In addition, conducting single interface shear tests in the laboratory consumes time, effort, resources, and budget, especially when a multi-layered soil-geosynthetic lining system has been proposed. Therefore, this work aimed to ascertain the appropriateness of multiple-interface shear testing in the laboratory by comparing shear strengths mobilised at peak and at large displacements (LD) for single and double testing configurations. Moreover, the interface shear results obtained were applied on a typical side-slope and basal lining system design through the limit equilibrium method (LEM) to understand the implications on factors of safety (FS).

In this study, single interface testing configurations constituted only two lining components, either soil-geosynthetic or geosynthetic-geosynthetic. Multiple-interface testing configurations involved direct shearing of three lining components: geosynthetic-geosynthetic-geosynthetic, or soil-geosynthetic-geosynthetic, or soil-geosynthetic-soil, also referred to as double interfaces. The investigated MSW landfill components formed part of the proposed basal lining system for the MSW landfill cell in the Western Cape Province in South Africa. They included three nonwoven geotextiles, two smooth-sided geomembranes, a synthetic cuspate drain, sand, gravelly sand (GS), and leachate collection stone (LCS). All tests were conducted at applied normal pressures of 150, 300, & 450 kPa under saturated conditions with fresh tap water at a 1mm/min shearing rate as recommended by ASTM D5321.

The critical interface assessment revealed that failure within the lining components would likely occur at the same interface(s) regardless of the testing configuration. Specifically for this research, both testing configurations, i.e., single and double, involving smooth High-Density Polyethylene (HDPE) geomembrane with nonwoven geotextile combinations depicted the weakest shear resistances. Additionally, this work found that the peak strengths of the critical interface were highest for a double interface testing configuration. Conversely, the LD strengths obtained were either equal or less for a single interface testing configuration.

Ultimately, the assessment of both maximum and minimum FS using single and double interface shear results revealed that the former was conservative as it produced lower values of FS. As a result, interface direct shear testing through a double interface configuration enabled an understanding of the dynamics of shear strength transfer among the lining components proposed for the basal lining system of the landfill cell in the Western Cape Province in South Africa.

Contents

Figures

Tables

Abbreviations

AASHTO	-	American Association of State Highway and Transportation
ASTM	-	American Society of Testing and Materials
BES	-	Bentonite Enriched Soil
BS	-	British Standard
CBR	-	California Bearing Ratio
CCL	-	Compacted Clay Liner
CD	-	Cuspate Drain
CM	-	Crushed Material
CPE	-	Chlorinated Polyethylene
CSL	-	Compacted Soil Layer
CSL	-	Compacted Soil Layer
CSPE	-	Chlorosulfonated Polyethylene
DD	-	Dry Density
DEA	-	Department of Environmental Affairs
DSS	-	Direct Simple Shear
DWAF	-	Department of Water Affairs and Forestry
EIA	-	Environmental Impact Assessment
FoS	-	Factor of Safety
GCL	-	Geosynthetic Clay Liner
GCP	-	Geocomposite
GFM	-	Geofoam
GGR	-	Geogrid
GMB	-	Geomembrane
GNT	-	Geonet
GP	-	Poorly-graded Gravel
GPP	-	Geopipe
GS	-	Gravelly Sand
GTX	-	Geotextile
HDPE	-	High-Density Polyethylene
IRD	-	Initial Rate of Deposition
ISO	-	International Organization of Standardization
LCS	-	Leachate Collection Stone
LD	-	Large Displacement
LDPE	-	Low-Density Polyethylene
LEM	-	Limit Equilibrium Method
LLDPE	-	Linear Low-Density Polyethylene
LSA	-	Large Shear Apparatus
MD	-	Machine Direction
MDD	-	Maximum Dry Density
MDPE	-	Medium Density Polyethylene
MRD	-	Maximum Rate of Deposition

MSW	-	Municipal Solid Waste
NWMS	-	National Waste Management Strategy
OIT	-	Oxidative Induction Time
OMC	-	Optimum Moisture Content
PA	-	Polyamide
PET	-	Polyester
PP	-	Polypropylene
PS	-	Polystyrene
PVC	-	Polyvinyl Chloride
SANS	-	South African National Standards
SDR	-	Shear Displacement Rate
SP	-	Poorly-graded Sand
TD	-	Transverse Direction
UK	-	United Kingdom
USA	-	United States of America
USCS	-	Unified Soil Classification System
UV	-	Ultraviolet
VLDPE	-	Very Low-Density Polyethylene

Notations & Units

B	-	Width of the new waste mass at the level of the existing waste mass
B_{low}	-	The top width of waste mass with the lowest factor of safety
B_T	-	Width of the new waste mass at the top
C	-	Apparent cohesion between liner components for $C=C_A=C_P$
C'	-	Cohesion
C_A	-	Apparent cohesion between liner components beneath an active wedge, used at the back slope
C_c	-	Coefficient of Curvature
C_P	-	Apparent cohesion between liner components beneath passive wedge, used at the base
C_{SW}	-	Apparent cohesion of solid waste
C_u	-	Coefficient of Uniformity
E_A	-	Resultant/total force acting on the active wedge (E_{HA} & E_{VA})
E_{HA}	-	The horizontal component of E_A / normal force from passive wedge acting on active wedge
E_{HP}	-	The horizontal component of E_P / normal force from the active wedge acting on the passive wedge; $E_{HA}=E_{HP}$
E_P	-	Resultant/total force acting on a passive wedge (E_{HP} & E_{VP})
E_{VA}	-	The vertical component of E_A / frictional force acting on the side of the active wedge
E_{VP}	-	The vertical component of E_P / frictional force acting on the side of the passive wedge; $E_{VA}=E_{VP}$
F_A	-	Total shear strength along the back slope / frictional force acting on the bottom of the active wedge
F_P	-	Total shear strength along the base / frictional force acting on the bottom of the passive wedge
FS	-	Factor of safety for entire waste mass
$FS_{2.0}$	-	Factor of safety corresponding to $FS_V=2.0*FS$
FS_A	-	Factor of safety for active wedge
FS_{ave}	-	The average factor of safety
FS_{low}	-	The lowest factor of safety
FS_{max}	-	Maximum factor of safety, i.e., upper bound solution
FS_{min}	-	Minimum factor of safety, i.e., lower bound solution
FS_P	-	Factor of safety for passive wedge
FS_{true}	-	"True" factor of safety, i.e., exact solution
FS_V	-	Factor of safety at the interface between active and passive wedges

g/cm^3	-	grams per cubic centimetres
G_s	-	Specific Gravity
H	-	Depth of existing waste mass/height of side-slope
H_B	-	Depth of the existing waste mass when higher than proposed
H_T	-	Depth of new waste mass above the existing waste mass
l/hr	-	litres per hour
l/s/m/hr	-	litres per second per metre per hour
$l/s/m^2$	-	litres per second per square metres
kg/m^3	-	kilogram per cubic metres
kN	-	kilonewton
kN/m	-	kilonewton per meter
kPa	-	kilopascals
m	-	metres
m/s	-	metres per second
Mg/m^3	-	megagrams per cubic metres
mm	-	millimetres
mm/min	-	millimetres per minute
N	-	Newton
N/mm	-	Newtons per millimetre
N_A	-	Normal force acting on the base of an active wedge
N_P	-	Normal force acting on the base of a passive wedge
ϕ	-	The angle from horizontal to the slope of solid waste
ϕ'	-	The angle of internal friction
ϕ_{SW}	-	Internal friction angle of solid waste
R^2	-	Coefficient of Regression
W	-	Moisture Content
W_A	-	Weight of active wedge
W_P	-	Weight of passive wedge
W_T	-	Total weight of active and passive wedge; $W_T=W_A+W_P$
α	-	The angle of the front slope, measured from horizontal
β	-	The angle of the back slope, measured from horizontal
γ_{SW}	-	Unit weight of solid waste
δ	-	Interface friction angle between liner components for $\delta=\delta_A=\delta_P$
δ_A	-	Interface friction angle used at the back slope / Interface frictional angle of liner components beneath active wedge
δ_P	-	Interface friction angle used at the base / Interface friction angle of liner components beneath passive wedge
δ_P	-	Peak angle of interface friction
$\Delta_{s\text{-}LD}$	-	Large displacement horizontal displacement
$\Delta_{s\text{-}p}$	-	Peak horizontal displacement

θ	-	The angle of landfill cell subgrade, measured from horizontal
ξ	-	The back angle of the waste mass
σ_n	-	Applied normal pressure
τ_{LD}	-	Large displacement shear stress
τ_p	-	Peak shear stress
ω	-	The angle from horizontal to interactive wedge forces / Inclination angle of interwedge force (i.e., E_A or E_P), measured from horizontal

1 Introduction

1.1 Background

Municipal Solid Waste (MSW) landfills (commonly called *sanitary landfills*) are engineered containment facilities that undergo careful design and construction before operation. The primary function of MSW containment facilities is to provide a competent hydraulic barrier that prevents intermixing of the contained solid wastes and their associated leachate against groundwater and surface water resources hence, protecting the environment and public health at large (Feng & Lu, 2016).

Leachate is a liquid that is derived from the decomposition processes of solid wastes in a landfill (also known as *primary leachate*) and through water infiltration facilitated by rainfall percolation into the solid waste body (also known as *secondary leachate*) (Shukla, 2016). Leachate composition includes a high percentage of solvent and a relatively small percentage of dissolved solutes, which make up for a chemically harmful fluid. To avoid the possibility of having leachate leakage in MSW landfills, geosynthetics are usually incorporated into the landfill lining systems. Common geosynthetics in the lining systems include geotextiles, geomembranes, and geo-composites such as geosynthetic clay liners (GCLs). Geomaterials such as stone and compacted soil layers are also included as leak detection and leachate management measures.

Geosynthetics have been used extensively in different geotechnical projects fulfilling functions such as; fluid barrier, reinforcement, separation, filtration, drainage and protection (Shukla, 2016). For landfill design engineers, designing basal and cover lining systems is of great value as it ensures the integrity of the entire MSW landfill during its construction, service, and after-service (Feng & Lu, 2016; Punetha & Samanta, 2020). One of the main objectives of having an engineered MSW containment facility is to achieve a maximum disposal capacity by increasing the elevation, thereby creating steep slopes on the sides and bases of MSW landfills (Stark, Niazi & Keuscher, 2015). As several layers of geosynthetics and geomaterials are being introduced in MSW landfills, as seen in Figure 1-1, a situation of possible shear failure along geosynthetic-geosynthetic and geosynthetic-soil interfaces on landfill slopes arises (Lopes & Silvano, 2010; Zamara et al., 2012; Bacas, Cañizal & Konietzky, 2015; Feng & Lu, 2016; Cen, Wang & Sun, 2018). As a result, therefore, interface shear strength assessment becomes a point of focus when designing these sensitive geo-environmental structures.

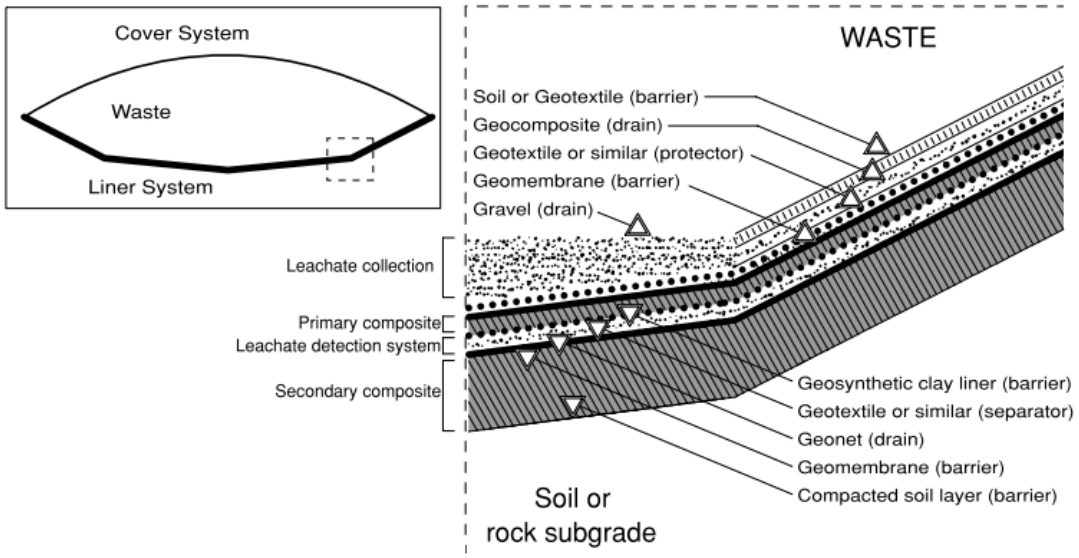

Figure 1-1: Lining system of an engineered MSW landfill (after De Brito Galvão et al., 2008)

1.2 Research Justification

Interface shear strength assessment of landfill lining components in the laboratory using 305mm×305mm direct shear apparatus typically involving either soil-geosynthetic or geosynthetic-geosynthetic interfaces has usually been done based on a single interface configuration (Sikwanda, Kalumba & Nolutshungu, 2019; Muluti, 2021). Single interface friction properties between two landfill lining components are typically evaluated following ASTM D5321 and ASTM D6243 standards. However, MSW landfill liners consist of multi-layered lining components comprised of compacted soils and geosynthetics, usually project and site-specific. The interface shear strength parameters of these lining components obtained in the laboratory rely on many factors, which include; testing conditions, the expertise of a test conductor, material types and their properties and most of all, the proposed liner arrangement in the field (Stark, Niazi & Keuscher, 2015; Muluti, 2021).

The arrangement of lining components in the field depends entirely on the functions intended and the designer's choice of materials to achieve the intended functions. The designing process involves using interface shear test results from the laboratory, usually obtained through a single interface configuration, to analyse the critical interface, which would then dictate the suitability of materials on side-slopes of MSW landfills (Stark & Newman, 2010). However, conducting single interface shear strength tests in the laboratory consumes time, effort, resources and budget, especially when multi-layered geosynthetic-soil materials have been proposed for the project (Eid, 2011). As a result, this could have implications in delaying the project execution.

As investigated by Stark, Niazi & Keuscher (2015), it was noted that overestimating shear strength parameters of liner interaction could result in substantial landfill failure, thereby endangering the environment and resulting in high remedial costs to the client and the public at large. Therefore, laboratory testing of interface shear strength properties is critical and needs to be done to a maximum attainable accuracy to avoid under or overdesigning of MSW landfill liners, especially on side-slopes.

This research investigated the comparability of interface shear results obtained from single and double interface testing configurations and their implications on a typical design application for the proposed landfill cell in the Western Cape Province in South Africa. This study was anticipated to benefit landfill designers and other stakeholders in understanding the implications of different testing configurations for interface shear strength assessment of landfill lining components. Most of all, the effort was vested in understanding the similarities and dissimilarities of a double interface to single interface shear testing of landfill lining components.

Double interface shear strength assessment involved testing a three-component sandwich of landfill liners with combinations such as geosynthetic-geosynthetic-geosynthetic or soil-geosynthetic-geosynthetic, or soil-geosynthetic-soil. In this test configuration, the middle geosynthetic layer was left loose/unclamped between the other two materials, either clamped for geosynthetics or compacted to the target densities for the case of geomaterials.

Tests in both configurations had to be conducted depending on the liner arrangement at the anticipated normal stresses under saturated conditions to compare single and double interface shear strength properties for the basal lining layer works. The evaluated landfill cell utilised several geosynthetics, including three nonwoven geotextiles, two smooth-sided geomembranes and a synthetic cuspate drain. It also incorporated compacted soil layers and granular materials in the leachate management systems.

1.3 Research Objectives

The main research objective of this study was to compare the shear strength parameters obtained through single and double interface testing configurations for the basal lining system of the proposed landfill cell in the Western Cape Province in South Africa.

There were two specific objectives in this research project which provided a pathway to ensuring that the main objective was achieved, and these included:

- To determine the shear strength parameters by developing strength envelopes using Mohr-Coulomb failure criterion at peak and LD for single and double interface testing configurations using a 305mm×305mm direct shear device at different applied normal pressures under saturated conditions.

- To examine the design implications through a detailed side-slope stability analysis using the limit equilibrium method (LEM) by determining factors of safety (FS) using interface shear results of a single interface and comparing them to those of a double interface for the landfill cell.

1.4 Scope and Limitations to the Study

This study mainly focused on evaluating two interface shear testing configurations, i.e., single interfaces and double interfaces, the comparability of results obtained therein and consequently, the design implications of using the results from both configurations on a practical landfill side-slope stability design. The study covered a basal lining system of the proposed landfill cell in the Western Cape Province, South Africa. The geomaterials and geosynthetics utilised in this study were obtained locally in South Africa and were specific to those used on the actual project. A 305mm×305mm *ShearTrac-III* Large Shear Apparatus (LSA) was used to evaluate these interface shear strength properties for both testing configurations at peak and at large displacements (LD) following standards such as ASTM D5321 for soil-geosynthetic & geosynthetic-geosynthetic interfaces. Additionally, the determined interface shear results were used to assess the side-slope and basal lining system stability conducted by evaluating maximum and minimum factors of safety (FS) using the limit equilibrium method (LEM).

Even though the research output from this study is locally based on the proposed landfill cell in the Western Cape Province, the methodological approach, analysis of results, and detailed side-slope stability analysis could be applied anywhere without the basis of the geographical location. Additionally, other important landfill considerations such as settlement analysis of the landfill specifically after closure, liner stability during leachate attack because of leakage and sustainability of geosynthetics in the long-term in MSW landfills were beyond the scope of this study.

1.5 Research Overview

This chapter introduces the topic with background knowledge and significance for undertaking the study. It also outlines the scope of the research and the limitations thereof. An extensive literature review about landfills, geosynthetics and their functions, shear strength studies on landfill liners, and ultimately, previous and recent research developments are presented in Chapter 2.

In Chapter 3, a detailed methodological approach undertaken in this study with equipment and material descriptions is presented. An overview of how quality control was attained, the testing program and the repeatability of results were ensured are also included in the same chapter.

Chapter 4 presents a detailed analysis of results with an extensive discussion outlining the similarities and dissimilarities of the two testing configurations. In contrast, Chapter 5 illustrates a detailed practical case study of the side-slope stability of the MSW landfill cell. The analysis utilises results obtained under single and double interface testing configurations; the same chapter also carefully assesses the design implications. General conclusions resulting from this study with recommendations for more related studies on different lining materials and testing configurations to create an extensive database are provided in Chapter 6.

2 Literature Review

2.1 Introduction

This chapter reviews the literature on the background of landfills, incorporation of geosynthetics into landfill's lining systems, their functions and failure mechanisms in engineered landfills. Interface shear testing studies on landfill lining components for geosynthetics and soils on both single and multi-layered interface configurations are also evaluated, specifically on the influencing factors and interpretation of results. A summary of literature review findings concludes this chapter.

2.2 Overview on Landfills

2.2.1 Historical Background

Through its document for minimum waste disposal requirements, the Department of Water Affairs and Forestry (DWAF) in South Africa defined a landfill as the deposition of waste by land through filling into the excavations or landfilling on grades (DWAF, 1998). Waste disposal by landfills is relatively cheap and convenient (Nanda & Berruti, 2021). However, it poses many environmental and health risks compared to other methods such as incineration and composting. Some short-term ecological impacts of waste disposal by a landfill include air pollution, odour, vectors, littering and unattractiveness, while the long-term consequences include water regime pollution and the generation of landfill gas leading to air pollution (DWAF, 1998; DEA, 2013).

Landfills were first utilised in the Minoan civilisation between 3000 BC and 1000 BC, where wastes were sent to a particular disposal site (Tammemagi, 1999). When the disposal site was full, it was covered by soil and vegetation. This method of landfilling has remained popular even today in some parts of the world. Later, a slightly similar way of handling solid wastes was employed in other civilisations, such as the Greeks and Romans. The Greeks had a regulation whereby each household was responsible for dumping their wastes outside the city's gates, while the Romans had a collection system of transporting their wastes to the pits using horse-drawn carts (Tammemagi, 1999). The Roman's landfilling approach was prominent later in Europe before industrialisation.

Until the "age of sanitation", public health had been at high risk as the European continent was becoming more populous and urbanised whilst land and other natural resources were becoming scarce (Lancione & McFarlane, 2016). As a result, the issue of solid waste management became fundamental and highly significant. From the 1880s to the 1930s, landfilling was the most prevalent method of waste disposal (Bonaparte, Bachus & Gross, 2020). However, it had raised public health concerns over unmanaged and uncontrolled large dumpsites. Incineration was also becoming a waste disposal method together with dumping of wastes in water bodies such as

oceans and rivers. However, these practices created even more significant public health problems. In the 1890s, similar to Europe, the United States started responding to the problem of solid waste management, which was catalysed by the high industrialisation pace and the call for a clean environment (Chang, Mitchell & Seed, 1999; Hodson, Martin & Prinn, 2010).

In the early days of landfilling practice, landfills were shallow and underlying liners were seldom used (Rowe, 2011). This created leaching problems of harmful waste liquids into groundwater resources, generating toxic landfill associated gases and other related public health concerns (Bonaparte, Bachus & Gross, 2020). It was not until 1950s that a "sanitary landfill" was introduced (Allen, 2001). Figure 2-1 illustrates a modern engineered sanitary landfill. This type of landfill involved an engineered method of disposing of wastes in small volumes, compacting, and covering the wastes at the end of the working day. Another significant engineered advancement in landfilling technology was the collection of data on waste quantities and the generation rates used to properly handle waste disposal (Nanda & Berruti, 2021). The use of proper soil covers and clear waste transportation routes, among others, were also crucial.

Between 1970s and 1980s, the groundwater contamination problem by landfilling practices had become prominent, thereby needing quick remediation measures (Rowe & Shoaib, 2017). This problem was critical because it increasingly became a challenge to treat contaminated groundwater. During this period, bottom liners made of natural low absorbent materials such as clay and synthetic materials such as High-Density Polyethylene (HDPE) geomembranes were introduced to minimise and ultimately stop the leaching problem. Other systems included cover materials with similar properties as bottom liners to limit rainfall percolation. The use of gas collection systems and modified landfill operation routine of monitoring groundwater, surface water, and gas quality became prominent.

As though landfills have been known to offer a cheap solution for managing MSW, in sub-Saharan Africa, most of the MSW landfills are non-engineered (Idowu et al., 2019). These MSW landfill sites pose a serious environmental threat, including biological, chemical, or physiochemical. Additionally, the associated landfill gases generated from non-engineered landfill sites degrade air quality, leading to several forms of threats to public health at large. Economically, non-engineered landfill sites make it extremely difficult to harness waste resources into valuable products for commercialisation (Schenck et al., 2019; Wilson et al., 2022). It should be noted that waste generation in sub-Saharan Africa is estimated at 62 million tonnes per year, with urban populations producing between 0.3 to 1.4 kg per capita per day (Idowu et al., 2019). Due to these high waste generation rates, a call for proper waste management is of utmost importance and developing engineered MSW landfills should be one of the priorities in sub-Saharan African countries. However, in most of these countries, the substitution of an engineered landfill has been a compacted clay liner (CCL) of hydraulic conductivity less than 1×10^{-8}m/s (Park, Park & Lee, 2007; Dai et al., 2016). This criterion, however, is difficult to prove due to different clay types available and non-stringent waste management regulations by the responsible governments. It should be noted that some of the

major reasons hindering inadequate waste management in developing countries include the level of technical know-how, inadequate finances, limited government waste management policies and containment structures (Schenck et al., 2019).

Despite the hurdles of waste management in sub-Saharan Africa, engineered landfills are still a standard practice in most parts of the world, including South Africa, and they form part of an integrated environment (Nanda & Berruti, 2021). However, new challenges are rising due to the associated ground impediments with geosynthetics and waste composition variabilities. It has been noted that these engineered state-of-art landfills could eventually fail at some point, and this has triggered more research into the subject of landfill lining systems, especially on the stability and integrity of landfill structures in the long term (Allen, 2001).

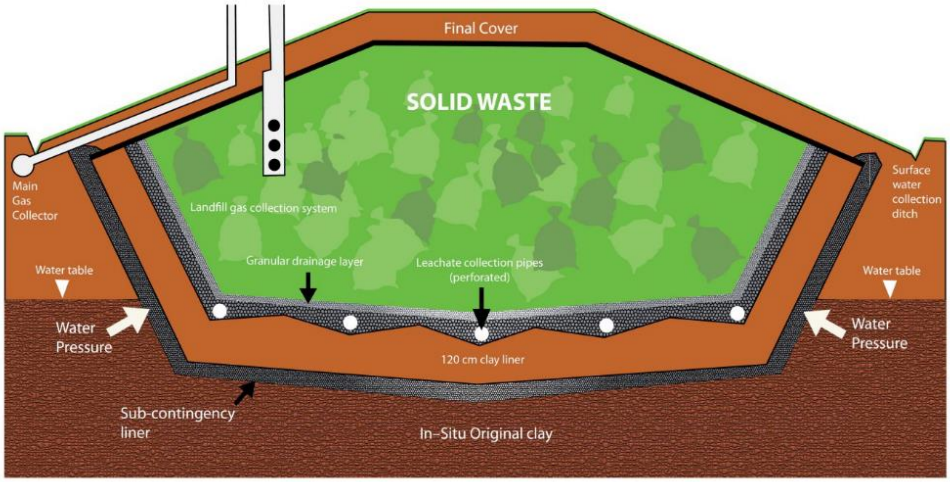

Figure 2-1: A typical engineered MSW landfill (after Koda et al., 2019)

2.2.2 Classes of Landfills

In South Africa, landfills are classified based on the nature of waste they are set to receive, the level of toxicity the waste stream is likely to produce, and the possibility of generating a significant amount of leachate (DWAF, 1998; DEA, 2013). The classification task on landfills is vital because it helps in the design process of lining systems. Landfills may generally be categorised into two main groups, predominantly determined by the nature of the waste stream as described in the sub-sections below:

2.2.2.1 General Waste Landfills

General waste landfills are landfills where wastes such as domestic, commercial, a portion of industrial and builder's rubble may be disposed of. However, the characteristics and composition of these wastes should not be harmful to pose a significant effect on the environment or public health, at least if adequately managed (DWAF, 1998). Additionally, general waste landfills

require careful operation detail and monitoring to ensure that harmful substances are not disposed of. These landfills normally constitute basal lining layers, as shown in Figure 2-2 (a).

2.2.2.2 Hazardous Waste Landfills

Hazardous waste landfills are landfills where the waste composition contains substances that, primarily due to their physical and chemical properties, can cause adverse impacts on the environment and public health (DWAF, 1998). Wastes generally found in these landfills are of toxic organic and inorganic nature, oily wastes, putrescible wastes, and many others that may be deemed hazardous by relevant authorities. The disposal of hazardous wastes also follows a hazard rating developed by the DWAF in their document for waste disposal by a landfill, also adopted by the DEA in the government gazette for waste management. Therefore, the operation and monitoring of hazardous wastes has always been critical due to their adverse impacts.

Hazardous waste landfills are further classified based on the hazard rating, which according to the DWAF (1998), starts from 1 to 4, with one being more hazardous and 4 being less hazardous. It also follows a further categorisation with H:H landfills accepting all forms of hazardous waste whilst H:h landfills only taking moderate and low hazard wastes. The lining system for his landfill type normally constitutes components, as shown in Figure 2-2 (b).

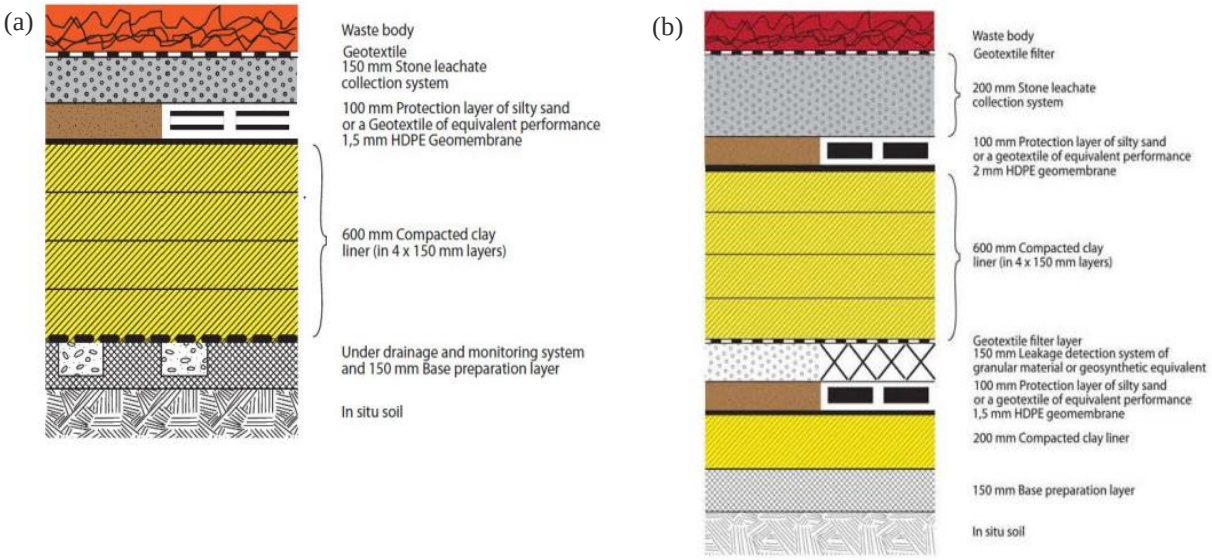

Figure 2-2: Basal liners for (a) General & (b) Hazardous Waste Landfills (DEA, 2013)

2.2.3 Typical MSW Landfill Components

MSW Landfills generally comprise different components, including the subgrade, basal lining system, solid waste, and cover lining system. These components perform different functions; for instance, the subgrade acts as a foundation to the entire landfill structure; the basal lining system provides a competent hydraulic barrier that prevents leachate from reaching groundwater resources; the cover lining system protects the landfill to ensure that the biodegradable processes

are not affected by external factors such as rainfall percolation which may lead to significant leachate generation, this layer also limits vectors and odours to the surrounding environment. The following sub-sections explain the possible failure mechanisms orchestrated by these typical MSW landfill components.

2.2.3.1 Subgrade

Several factors influence the subgrade where the MSW landfill lining system sits. These include possible basal heave, the possible presence of voids, the subgrade's compressibility level, and slope instabilities in the case of steep slopes (Fowmes, Dixon & Jones, 2007; Guarena, Dominijanni & Manassero, 2020). As a result, an adequate geotechnical site investigation is inevitable. These factors also depend on whether the new MSW landfill lining system will sit on the natural ground or an engineered subgrade or be overlain by the existing solid waste from the pre-existing landfill. For the latter condition, the type of solid waste disposed of before needs to be cautiously assessed to know the level of degradation when constructing a new lining system. This must be evaluated together with the placement and compaction efforts implemented. If these scenarios are well understood, the possibility of void formation and the extent of settlements will be avoided or at least well predicted.

Whether the subgrade is on a flat, gentle slope or steep slope terrain, it should be ensured that it is stable enough to allow for construction activities of the new lining system without immediate failure in deformation or void formation. For instance, when the subgrade is made up of fine-grained soils, more failure mechanisms related to time need to be assessed in both the short-term (without dissipation of excess pore pressures) and long-term (when excess pore pressures have been entirely dissipated) (Park & Lee, 2002). For other subgrades like rock or quarry, attention should be paid to common patterns with rock mass assessment to understand rock slopes.

2.2.3.2 Basal Lining System

Typically, a basal lining system is comprised of layers that function as barriers, offer protection, and allow drainage. The primary function of the MSW landfill's basal lining system is to provide a barrier function required to limit leachate leakage and associated landfill gases from the solid waste body into the surrounding environment (Rowe, 2011; Nanda & Berruti, 2021). Barrier layers currently in use include compacted clay liner (CCL), geosynthetic clay liner (GCL), bentonite-enriched soil (BES) and polymeric geomembranes among others. An example of a basal lining system is seen in Figure 2-3. These barrier layers are sometimes used in combination as composites depending on their availability, the toxicity of the retained solid waste mass and the geologic conditions of the site (Nanda & Berruti, 2021). To further lower the hydraulic conductivity of the harmful MSW landfill leachate, a common practice involves using geomaterials such as CCL with geosynthetic materials such as geomembranes. It is also common to protect the geomembrane against failures resulting from puncturing from the overlying granular material in the drainage layer, which controls the leachate hydraulic head using a thick geotextile (Rowe & Shoaib, 2017).

The basal lining system has two possible failure mechanisms: one is attributed to subgrade incompetency, and the other is within the lining elements attributed to overstressing. Overstressing is caused mainly in two ways: during the construction phase by construction machinery or during waste placement by compaction efforts leading to loss of function in the lining system (Fowmes, Dixon & Jones, 2007; Bonaparte, Bachus & Gross, 2020). The primary principle in designing the basal lining system is to ensure that its integrity with the subgrade and the retained solid waste allows for stability and continuous function over its design life.

Another failure mechanism in the basal lining system could be contributed by developing fluid pressures and heaving in the subgrade (Stark, Huvaj-Sarihan & Li, 2009). Fluid pressure development in the subgrade is usually contributed by the groundwater level fluctuations resulting in hydraulic gradients in the subgrade-basal lining interface. In the case of subgrade comprised of fine-grained soils such as clays, this action will lead to soil softening and, consequently, shear failure. The consideration of under-drainage needs to be carefully implemented to alleviate these scenarios, as such shortcomings in MSW landfills have been documented by Stark et al. (2012). Moreover, the MSW landfill design needs to account for fluid pressure development in the subgrade (commonly implemented during interface shear testing under submerged or saturated conditions). Additionally, it should be noted that in the short-term, i.e., undrained conditions, the geological barrier (in this case, fine-grained soil) exhibits a relatively high shear strength compared to the long-term, i.e., drained conditions (Touze-Foltz, Xie & Stoltz, 2021).

The following is worth understanding for the heaving of the subgrade layer leading to a potential failure in the basal lining system. When pore pressure develops in the subgrade at a reasonably greater depth than the stress generated from the overlying strata, basal heaving is likely to occur. This heaving action in the landfill base is further facilitated because the developed fluid pressure has no void to dissipate. Heaving is usually observed before waste placement when the basal lining system has not experienced any overlying stress or during waste placement, given that low unit weight is placed on the lining system.

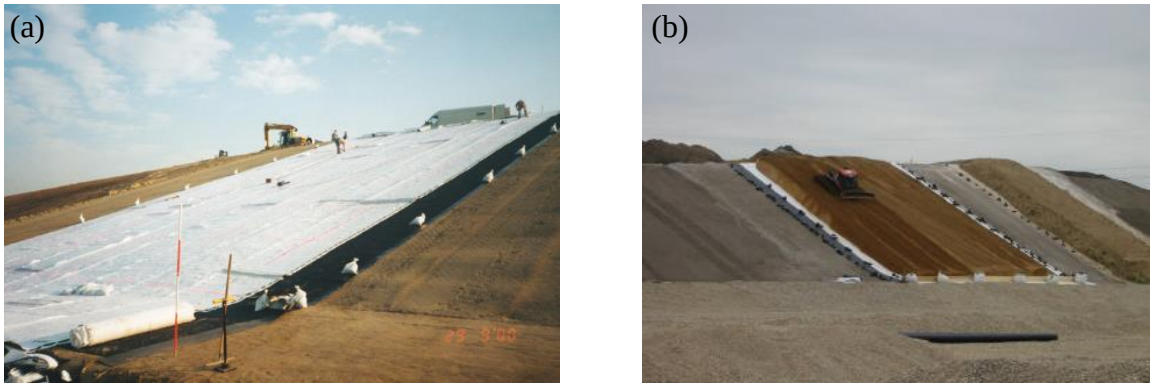

Figure 2-3: Typical basal & side-slope lining systems (after Müller & Saathoff, 2015)

2.2.3.3 Side-Slope Lining System

The side-slope lining system forms part of the basal lining system as the two are integrated and are ideally meant to work in the same manner, as seen in Figure 2-3. The stability of the subgrade and lining components before and after the solid waste placement is a significant focus in this category. As solid waste is placed in MSW landfills accompanied by the required compaction efforts, additional stresses are introduced coupled with time-dependent solid waste decomposition and creep effects after the operational period. Nevertheless, side-slopes on MSW landfills need to be designed for integrity and stability. In addition, leachate and landfill associated gases need to be contained.

Like most geomaterials, solid waste in MSW landfills also experiences settlement, resulting in induced strains on the lining elements within the lining system. Settlement of solid waste is evidenced via two forms: one is through the waste placement practice, which involves compaction of several solid waste layers, and the second form is through subsequent decomposition of the contained solid waste due to biological and chemical reactions resulting in creep (Park & Lee, 2002; Park, Park & Lee, 2007). As solid waste settles in the MSW landfill, drag forces are formed. To reduce or prevent overstressing and the loss of functionality in the lining system, the down drag forces generated from the solid waste settlement must be dissipated. Due to these issues in MSW landfills, designers usually implement two countermeasures: designing a robust lining system to undertake all the resulting extra stresses without losing functionality (El-Fadel et al., 1999). And another countermeasure is to provide a preferential slip surface through sacrificial geomaterials, which can undertake the extra stresses and, therefore, relieve the lining system (Nanda & Berruti, 2021; Touze-Foltz, Xie & Stoltz, 2021).

Another important consideration as far as the side-slope lining system is concerned is the anchorage of geosynthetic materials. In most cases, geosynthetic materials used on the side-slopes of MSW landfills are typically anchored (Hegde & Roy, 2018). The anchorage minimises uncontrolled deformations due to sliding effects and avoids toppling of the lining system. While anchorage gives confidence to designers that slippage movements are controlled, the resulting stresses get transferred to the lining system, thereby developing strains within the geosynthetic materials forming part of the lining system (Bonaparte, Bachus & Gross, 2020). A challenge still stands when several geosynthetics are used on the side-slopes as to which material must be anchored and which one should be loose. In some instances, the lower layer of geosynthetics is anchored as this cannot be let slip; other layers can then be anchored depending on their interface shear strength and pull out values (Fowmes, Dixon & Jones, 2007). The anchorage is usually avoided for geosynthetic components with high interface shear strength and those placed on relatively gentle slopes (Touze-Foltz, Xie & Stoltz, 2021).

2.2.3.4 Solid Waste

For most MSW landfills, the type of solid waste retained is highly heterogenic, which means that predicting its properties is complex (Sivakumar Babu & Lakshmikanthan, 2015). As a result,

conservative parameters of solid waste are normally used, even though these also depend on waste placement technologies, including compaction efforts and the waste stream. It is common for solid waste in landfills to fail significantly when the shear angles surpass shear strength values (Naveen, Sumalatha & Malik, 2018). In some scenarios, landfill's solid waste instabilities can be orchestrated by relic layers, such as leachate & landfill associated gas pressures, short-term soil covers and weak solid waste layers (Fowmes, Dixon & Jones, 2007), as illustrated in Figure 2-4. Translational solid waste failures are also common (Qian, Koerner & Gray, 2003).

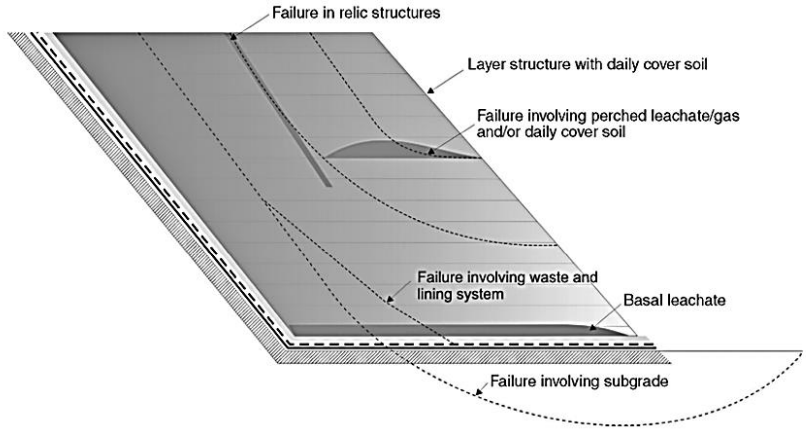

Figure 2-4: Waste slope failure mechanisms (after Fowmes, Dixon & Jones, 2007)

2.2.3.5 Cover Lining System

The cover lining system works contrary to the basal lining system as its purpose is to cover solid wastes. Several failure mechanisms can be experienced by the MSW landfill's cover lining systems, including differential settlements which result from the potential further decomposition of the retained solid waste. Other failure mechanisms are as seen in Figure 2-5. These would impact both the stability and integrity of the landfill's cover lining system. A landfill failure resulting from stability issues of the cover lining system has been reported by Stark & Newman (2010).

Nonetheless, MSW landfill lining systems work as a single integrated system at the stage of landfill closure when the landfill cover lining system has been placed. It is important to note that failure in the cover lining system could be attributed to other components such as subgrade, basal lining system, side-slope lining system and solid waste. In heavy rainfalls, even when the drainage layer is provided on the cover, the landfill cover system is susceptible to over-saturation, leading to instability issues (Zhang et al., 2013). Moreover, landfill associated gasses, if not well managed, could lead to a significant impact of degrading the landfill cover system, making it lose its intended function.

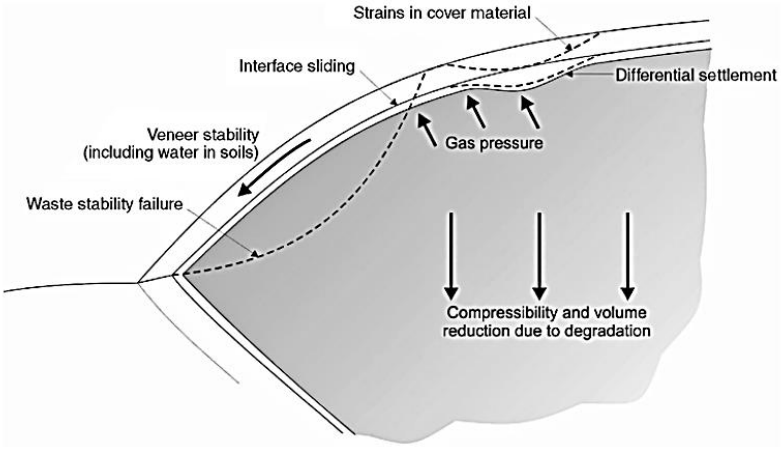

Figure 2-5: Failure mechanisms in the cover system (after Fowmes, Dixon & Jones, 2007)

2.2.4 Landfill Failure Mechanisms

MSW landfill stability relies on the integrity of materials incorporated in its construction, the competence of the contractor who ensures that quality control and assurance have been adhered to and most importantly, proper routine operations of the landfill, including monitoring of lining systems, among other things. Failure mechanisms of MSW landfills and other engineered landfills, in general, have been discussed by several authors, e.g., Chang, Mitchell & Seed (1999); Stark, Huvaj-Sarihan & Li (2009); Peng et al. (2016) and Bonaparte, Bachus & Gross (2020). In summary, though, these failures can be narrowed down to rotational and translational slope failures.

Qian, Koerner & Gray (2003) further categorised MSW landfill failure mechanisms tracing back to what could have been the cause. This categorisation listed the following: sliding failure orchestrated within the leachate collection system, rotational failure directed along with the side-slope & basal lining or through the waste mass, lining system & subgrade, and lastly, translational failure initiated by the movement along with the lining system as seen on Figure 2-6. As Buthelezi, Kalumba & James (2016) & Buthelezi (2017) discussed, the translational failure mechanism within the lining system is highly likely to occur in engineered landfills that have been inadequately designed and constructed without ensuring proper quality control. Along with the landfill's geometry, other considerations such as loading levels, moisture contents within the waste mass and adjacent lining systems contribute to stabilising or destabilising an engineered landfill.

To properly simulate the translational failure of MSW landfills, Qian, Koerner & Gray (2003) and Qian (2006) proposed numerical, analytical approaches that account for many parameters contributing to this failure pattern. In these numerical approaches, the conventional limit equilibrium method (LEM) is applied to a two-part wedge system to assess the potential of landfill failure. Ultimately, the method provides a representative factor of safety (FS), aiming to show that the shear strength within the landfill isn't exceeded anywhere on the waste mass.

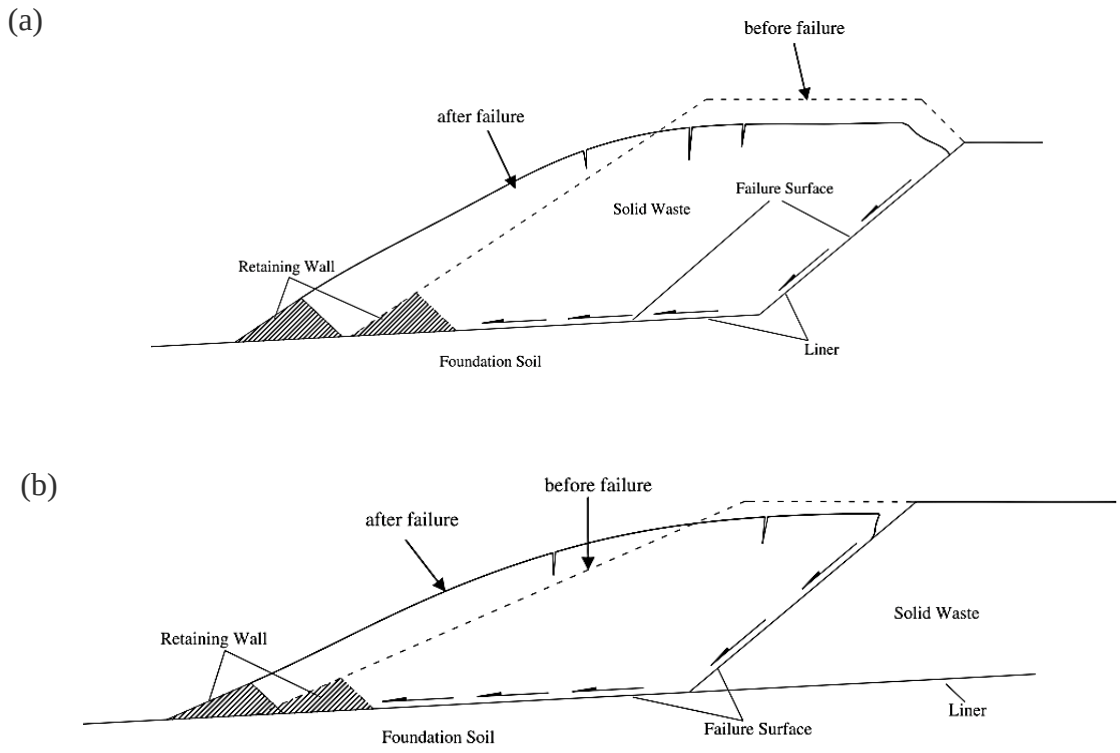

Figure 2-6: Translational failure of MSW landfill (a) Total sliding & (b) Partial sliding (after Feng et al., 2010)

2.2.5 Design & Construction Practices of Landfills

MSW landfill design and construction practices require careful attention among design engineers and contractors because a failure of these sensitive geo-environmental structures is progressive and usually initiated by inadequate site investigations, inadequate design practices and little understanding of groundwater fluctuations (Chang, Mitchell & Seed, 1999). Most failures resulting from landfill constructions can quickly be remediated once failure signs are displayed during the construction phase. However, these failures can substantially damage the environment, leading to significant cost implications when left without being attended to. For example, in 2003, the UK report on landfills indicated that 85 landfills experienced minor and significant failures, and most were remediated at extremely high costs (Fowmes, Dixon & Jones, 2007). Another example is the progressive landfill failure in the US, which was remediated at an extra charge of $1.4 million on top of the $2 million initial overall project cost (Stark & Newman, 2010).

Landfill design requires an in-depth understanding of both in-situ subgrade, groundwater properties, engineered materials such as geosynthetics which are incorporated into the design and sometimes mechanical properties of the solid waste itself (Ghazizadeh & Bareither, 2021; Nanda & Berruti, 2021; Touze-Foltz, Xie & Stoltz, 2021). Depending on the product's polymer properties, density, thickness, and predicted design life for geosynthetics, allowable strains in the

barrier layers should also be considered. For example, the design life of a polymeric geomembrane will depend on factors such as polymer type, additive pigment on the polymer, the temperature at which the geomembrane is exposed to in the landfill and the chemistry of leachate (Rowe, 2012; Naveen, Sumalatha & Malik, 2018). It can be noted that, however, the design life of geosynthetics can be predicted since these products are bound to degrade in the long term. Therefore, this loss of functionality needs to be accounted for in designs. For geomaterials such as fine-grained soils, the allowable strains will depend on plasticity, with high plasticity soil experiencing substantial deformations compared to low plasticity soil (Burland, 1990).

Another vital consideration in MSW landfill designs is the interface shear strength considerations (Palmeira, 2009; Rowe, 2011; Adeleke et al., 2021). The utilisation of planar surfaces originating from geosynthetics creates planes of weakness where slippage may occur. As with any other engineering design, the interfaces resulting from geosynthetics present a high variability due to material differences from one manufacturer to another and the testing laboratory expertise (Müller et al., 2008; Shi et al., 2020). Therefore, site and project-specific testing is usually recommended to restrain the uncertainty in testing and increase confidence in the obtained shear strength parameters (Müller & Saathoff, 2015). It is also advised that literature data on interface shear testing for real-life projects be avoided, especially at the detailed design stage (McCartney, Zornberg & Swan, 2009). However, it may prove useful as a preliminary reference for initial decision making.

In some cases where a GCL is used, an internal shear strength assessment is customarily conducted. In cases of composite interaction, failure is likely to occur at any path, whether internally or at the interface (Rowe, 2020). Additionally, leachate and landfill gas pressures could be present at the interface in some instances, and due to their chemical properties, possible influence on the interface shear strength parameters could be considered. It is worth noting that the choice of shear strength parameters could have significant impacts, especially on the factor of safety calculated in the limit equilibrium analyses (Belczyk & Smith, 2012; Adeleke et al., 2021). Ultimately, the fundamentals for a safe MSW landfill design lie in correctly predicting potential slip failures in the lining systems to account for the MSW landfill's stability and integrity.

In summary, it is essential for design engineers to consider almost all failure mechanisms that could lead to MSW landfill failures and make sure that the design addresses them accordingly. It should also be noted that a good plan is worthless if quality control and quality assurance have not been adhered to during construction (Allen, 2001). Monitoring schemes are also essential to ensure the integrity and stability of MSW landfills, most especially on leakage and groundwater level fluctuations, as these could orchestrate landfill failures (Pandey & Shukla, 2020).

Landfill design is derived from a proper site investigation, including geotechnical and suitability, coupled with a thorough Environmental Impact Assessment (EIA) (DWAF, 1998). This ensures that both short and long-term adverse environmental impacts are avoided. Still, more proactively,

the interaction of harmful leachate with both surface and groundwater resources is minimised and eventually prevented.

The design of an engineered landfill begins with the determination of the Maximum Rate of Deposition (MRD), which according to DWAF (1998), is defined as the projected maximum average annual rate of waste deposition during the expected service life of a landfill. MRD is responsible for determining the landfill class, and its calculation is dependent on the Initial Rate of Deposition (IRD).

IRD is determined from the multiplication of the population serviced by the landfill with the waste generation per capita. Once IRD has been chosen depending on the local authority guidelines, MRD is then determined through Equation 2-1;

$$\mathrm{MRD} = (\mathrm{IRD})(1 + \mathrm{d})^{\mathrm{t}} \qquad \textbf{Equation 2-1}$$

Where:

MRD = the maximum rate of deposition in tonnes/day during the final year of the landfill's operation

IRD = the initial rate of deposit of refuse on site in tonnes/day

D = the expected annual development rate, based on the expected population growth rate in the area served by the landfill

t = the period planned life of the site expressed in years

According to DWAF (1998), the size of the waste stream of the landfill will then be assigned according to MRD, as summarised in Table 2-1.

Table 2-1: Description of landfill class sizes (adapted from DWAF, 1998)

Landfill Class Size	Symbol	MRD [Tonnes/day]
Communal	C	MRD < 25
Small	S	25 < MRD < 150
Medium	M	150 < MRD < 500
Large	L	MRD > 500

After carefully determining the landfill class size, the estimation of leachate generation and leachate management then follows. A concept of climatic water balance is adopted to determine whether a landfill will generate a significant leachate quantity. According to DWAF (1998), the climatic water balance (B) is the difference between rainfall and evaporation. It indicates whether the climate in which a proposed landfill is located will influence the generation of significant leachate, hence requiring leachate management measures. Climatic Water Balance (B) may be determined using Equation 2-2.

$$B = R - E \qquad \textbf{Equation 2-2}$$

Where:

B = is the climatic water balance in mm of water

R = is the rainfall in mm

E = is the evaporation from a soil surface, taken as:

0.70×A – pan evaporation in mm or

0.88×S – pan evaporation in mm

The site water balance concept is also adopted in optimising landfills to ensure that leachate is contained correctly. Some critical site water balance components include the moisture content of the landfilled solid waste, surface or groundwater ingress into the waste body, poor drainage design, and poor landfill siting (DWAF, 1998; DEA, 2013). Together with the climatic water balance, leachate generation is well managed. A summary of landfill classification is seen in Table 2-2.

Table 2-2: Landfill classification system (after DWAF, 1998)

Waste Class	**G General Waste**								**H Hazardous Waste**	
Size of Landfill Operation	C Communal Landfill		S Small Landfill		M Medium Landfill		L Large Landfill		H:h Hazard Rating 3&4	H:H Hazard Rating 1-4
Site Water Balance	B^-	B^+	B^-	B^+	B^-	B^+	B^-	B^+		
Minimum Requirements										
Notes: B^- = No significant leachate will be generated in the Site Water Balance (Climatic Water Balance + Site-Specific Factors), so a leachate management system is not required. B^+ = Significant leachate will be generated in the Site Water Balance (Climatic Water Balance + Site-Specific Factors), so a leachate management system is required. h = A containment landfill that accepts Hazardous waste with Hazard Ratings 3 and 4 H = A containment landfill that accepts all Hazardous waste, i.e., with Hazard Rating 1,2, 3 and 4										

2.2.6 South African Regulatory Frameworks on Waste Management

In South Africa, waste management is being overseen by the Department of Environmental Affairs (DEA), which sets out guidelines on good practices and proper ways to control and manage waste as an integrated approach to preserving the natural resources in the environment. According to the DEA (2011) & (2013), the National Waste Management Strategy (NWMS) is implemented as a legislative requirement of the National Environmental Management: Waste

Act, 2008 (Act No. 59 of 2008), notably known as the "Waste Act". The purpose of the NWMS revolves around eight specific objects, including:

- Promoting waste minimisation, re-use, recycling, and recovery of waste,
- Ensuring the effective and efficient delivery of waste services,
- Acceleration of the contribution of the waste sector to the green economy
- Ensuring that people are aware of the impacts of waste on their health, well-being, and the environment at large,
- Achieving integrated waste management frameworks,
- Ensuring proper budgeting and financial management for waste services,
- Providing measures to remediate contaminated land, and
- Establishing effective compliance with and enforcement of the Waste Act.

Additionally, a summary of waste management systems in South Africa is provided in Figure 2-7.

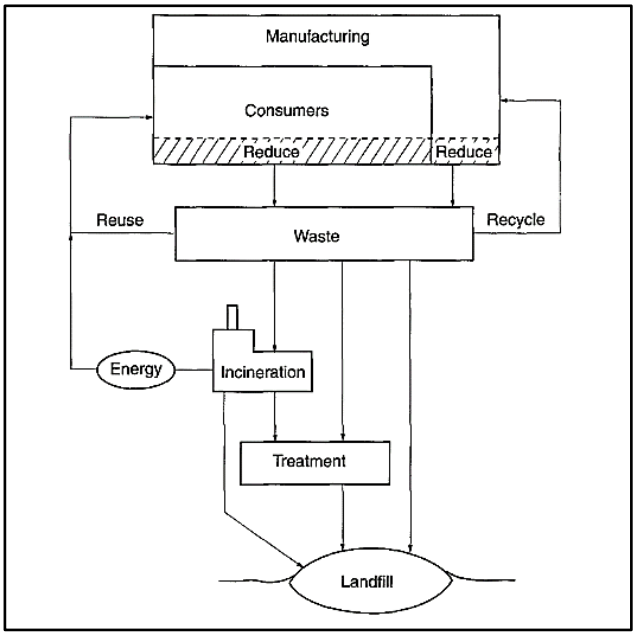

Figure 2-7: Waste Management Systems in South Africa (after DWAF, 1998)

2.3 Geosynthetics

2.3.1 Overview

Geosynthetics are manufactured planar products from polymers whose main application involves contact with soil or rock, thereby forming part of a civil engineering structure or system (Shukla,

2002; Shukla & Yin, 2006). The polymers used in manufacturing geosynthetic products are primarily synthetics originating from crude petroleum oils and other materials such as rubber and fibreglass (Koerner, 2005). Geosynthetics have been used in civil engineering projects since 1970s and have become popular because they are environmentally friendly, offer a cost-effective alternative solution to other conventional materials, provide technical efficiency, and are energy resilient and aesthetically pleasing (Müller & Saathoff, 2015).

Generally, geosynthetics offer sustainable solutions to the civil engineering industry and, most significantly, the geotechnical engineering sub-discipline with other sectors such as agricultural and mining benefitting from them (Shukla, 2016). They can wholly or partly replace conventional building materials such as clay and sand. Geosynthetic products include geotextiles, geomembranes, geogrids, and geocomposites such as geosynthetic clay liners (GCLs).

2.3.2 Functions of Geosynthetics

Geosynthetics perform six main functions in civil engineering, mining, and agriculture. These functions are reinforcement, separation, filtration, drainage, fluid barrier, and protection. One geosynthetic type can perform one or more functions, and these functions will generally be classified as primary and secondary functions, as seen in Table 2-3.

Table 2-3: Geosynthetics and their Functions (adapted from Shukla, 2016)

Function	Category	Typical geosynthetics used
Separation	Primary	GTX, GCP & GFM
	Secondary	GTX, GGR, GNT, GMB, GCR & GFM
Reinforcement	Primary	GTX, GGR & GCP
	Secondary	GTX & GCP
Filtration & Protection	Primary	GTX & GCP
	Secondary	GTX & GCP
Drainage	Primary	GTX, GNT, GCP & GPP
	Secondary	GTX, GCP & GFM
Fluid Barrier	Primary	GMB & GCP
	Secondary	GCP
Notes: GTX = Geotextile, GGR = Geogrid, GNT = Geonet, GMB = Geomembrane, GFM = Geofoam, GPP = Geopipe & GCP = Geocomposite		

2.3.2.1 Reinforcement

When soil material's mechanical properties are insufficient to resist the applied loads or provide the required settlement criteria, geosynthetic inclusion may improve the properties by forming a reinforced soil material (Mawer & Kalumba, 2014; Kiptoo et al., 2017). The composite material usually possesses high compressive and tensile strengths, thereby acting as a tensioned member to the ground through shear strength properties and interlocking with confinement which

ultimately creates the intended stability of the structure (Koerner, 2005). The reinforcement mechanisms of geosynthetics with soils are further elaborated in Figure 2-8.

Shukla (2016) classified a tensile member from a tensioned member in that a tensile member supports planar loads while a tensioned member supports both planar and normal loads. When the geosynthetic works as a tensile member, two crucial mechanisms come into play, i.e., shear and anchorage. In summary, therefore, geosynthetics incorporated as reinforcing members can resist the following:

- Shear failure (also known as *shear stress reduction effect*) by supporting planar loads because of sliding effects of the soil,
- Anchorage failure by supporting planar loads originating from the pull-out effects from the soil material, and
- Membrane failure (also known as *membrane effect*) by supporting both planar & normal loads originating from the deformable soil material.

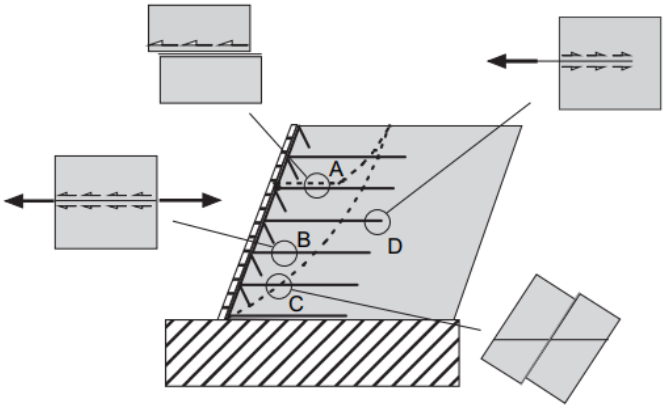

Figure 2-8: Reinforcement Mechanism of Geosynthetics in Soils (after Palmeira, 2009)

2.3.2.2 Separation

A geosynthetic product is said to perform a separation function when used to separate two different geomaterials to facilitate construction activities or perform throughout the project's design life. This function is more relevant to pavement designs in roads and railway projects, shallow foundations, and embankments where layers of fine/soft soil materials are separated from granular layers. Geosynthetic products such as geotextiles or geocomposites such as geogrids combined with geotextiles are used to ensure the separation of adjacent dissimilar materials while ensuring the structural integrity and intended performance of the whole system (Biswas et al., 2015; Wang et al., 2018; Biswas, 2019). In such scenarios, geosynthetics perform double functions, thus, separation and reinforcement. The separation mechanism is illustrated in Figure 2-9.

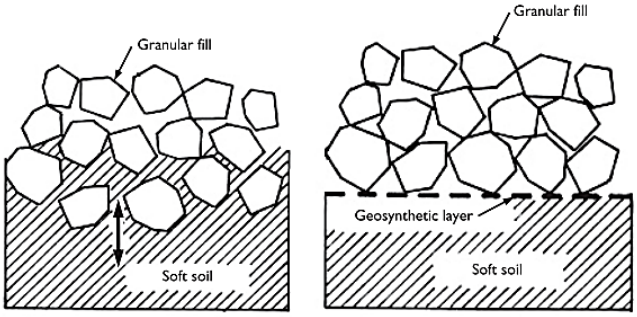

Figure 2-9: Separation mechanism of geosynthetics (after Shukla, 2016)

2.3.2.3 Filtration

When fluid flow is required through adjacent soil materials with different grain sizes, a geosynthetic product may be used to facilitate the filtration of such a fluid while limiting the migration of soil particles across the plane. However, the effects of seepage flow may be experienced, especially when a condition of equilibrium is not well established at the soil-geosynthetic interface leading to continuous piping action (Koerner, 2005). The situation worsens when the soil particles near the geosynthetic filter have smaller diameters than the filter opening sizes. This function also provides a secondary separation and sometimes reinforcement process, therefore giving double benefits to the geosynthetic application in the field. The filtration mechanism is illustrated in Figure 2-10.

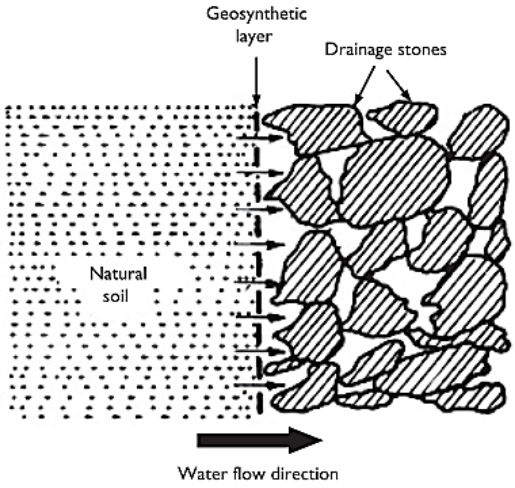

Figure 2-10: Filtration mechanism of geosynthetics (after Shukla, 2016)

2.3.2.4 Drainage

This function is closely related to the separation function. When a geosynthetic product permits adequate fluid flow while limiting soil particles migration in its plane, it is said to perform a fluid transmission function or drainage function (Özer & Akay, 2021). A retaining wall application exhibits a typical drainage function among geosynthetic products since the geosynthetic layer collects water behind the wall and redirects it to the weep hole, as seen in Figure 2-11. While

performing the drainage function, the geosynthetic automatically performs a filtration function to some extent, allowing for the dissipation of excess pore water pressures by facilitating fluid flow in and across the plane.

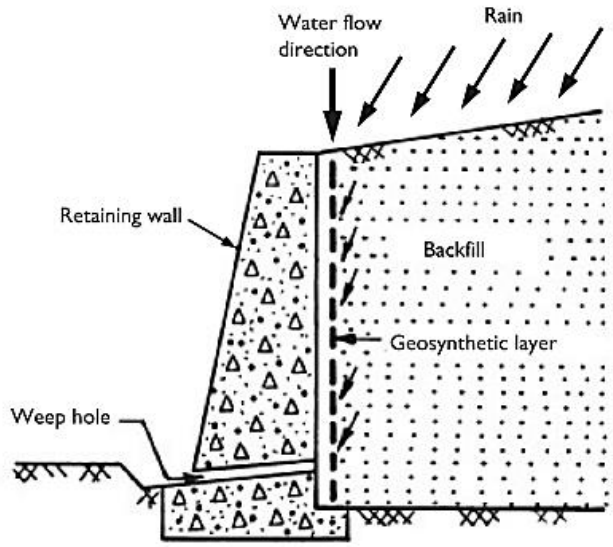

Figure 2-11: Drainage mechanism of geosynthetics (after Shukla, 2016)

2.3.2.5 Fluid Barrier

When a fluid migration needs to be strictly prevented during or after the service of geo-environmental structures like landfills, a geosynthetic product with impermeable characteristics such as a geomembrane can perform a fluid barrier function (Jingjing, 2014; Gapak et al., 2017). Figure 2-12 shows a typical geosynthetic membrane liner performing a fluid barrier function.

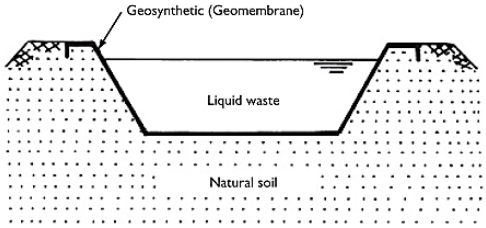

Figure 2-12: Fluid barrier mechanism of geosynthetics (after Shukla, 2016)

2.3.2.6 Protection

A geosynthetic product performs a protection function when placed between two materials that are likely to influence each other's functional abilities due to the resulting stresses and strains (Adeleke, Kalumba & Hardie, 2019). In this scenario, a geosynthetic product distributes such stresses and strains and protects materials. A good example is granular soils placed directly over the geomembrane; in this case, a thick geotextile would be used to cushion the geomembrane, protecting it against puncturing effects from the granular soil layer. Figure 2-13 further illustrates a protection function by geosynthetics.

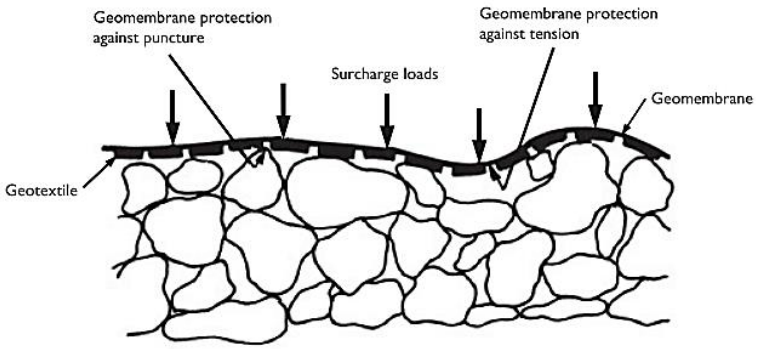

Figure 2-13: Protection mechanism by geosynthetics (after Shukla, 2016)

2.3.3 Classification of Geosynthetics

Factors such as durability, availability, cost, constructability, and specifications influence the selection of geosynthetics for a particular function. The durability of geosynthetics is derived from the type of polymers used to manufacture them. These polymeric pigments also determine the cost of the entire geosynthetic product. To specify geosynthetics for a particular application, basic knowledge of how they are manufactured, polymers used and how these affect the properties in the short and long term is imperative (Palmeira, 2009). Table 2-4 shows polymers commonly used to manufacture geosynthetic products, and this is the basis of the geosynthetic classification.

Geosynthetics are viscoelastic polymeric products; under applied stresses in the field, their performance is influenced by conditions such as temperatures, duration of the applied pressures and the applied rate (Rowe, 2011; Nanda & Berruti, 2021; Touze-Foltz, Xie & Stoltz, 2021). A microscopic view of geosynthetic properties needs to be understood during the design stages to ensure their stability and serviceability under the action. The properties of geosynthetic products are mainly divided into:

- Physical properties such as specific gravity, unit mass, thickness & stiffness,
- Mechanical properties like compressibility, tensile, survivability and soil-geosynthetic & geosynthetic-geosynthetic interface properties,
- Hydraulic properties like geosynthetic pore characteristics, percentage opening area and permeability, and
- Endurance and degradation properties including creep, abrasion, long-term flow characteristics and durability.

Table 2-4: Polymers used in Geosynthetics (adapted from Shukla, 2016)

Types of polymers		Abbreviations
Polypropylene		PP
Polyester (polyethylene terephthalate)		PET
Polyethylene	Low-density polyethylene	LDPE
	Very low-density polyethylene	VLDPE
	Linear low-density polyethylene	LLDPE
	Medium low-density polyethylene	MDPE
	High-density polyethylene	HDPE
	Chlorinated polyethylene	CPE
	Chlorosulfonated polyethylene	CSPE
Polyvinyl chloride		PVC
Polyamide		PA
Polystyrene		PS

2.3.4 Geosynthetics Application in MSW Landfills

In MSW landfills, different types of geosynthetics are used to perform several functions. The main ones are to prevent leachate from infiltrating the soil and drain leachate off the landfill, i.e., fluid barrier and drainage functions (Rowe, 2012; Jingjing, 2014). The design of soil-geosynthetic structures revolves around understanding the failure modes as discussed in Section 2.2.4. These will then dictate the relevant laboratory tests that can accurately simulate the field conditions to ensure geosynthetics' stability, strength, and overall serviceability over the entire design life.

As presented by Shukla (2002) & (2016) and Koerner (2005), there are several design approaches for soil-geosynthetic structures, including:

- Design by experience,
- Design by cost and availability,
- Design by specification, and
- Design by function.

The last approach is the most adopted among civil/geotechnical engineers (Koerner, 2005). Some of the geosynthetics used in MSW landfills to achieve the functions discussed in Section 2.3.2 are described below:

2.3.4.1 Geotextiles

Geotextiles are mostly porous to water flow across and within their manufactured planes. The degree of porosity among geotextiles varies widely because of pores in their structure. Depending on the thickness of the geotextile fluid, transmission ranges from moderate to a high degree. Geotextiles are manufactured from different polymers, fibres, and fabric styles, influencing the

geotextile performance in the field and making it a flexible sheet (Kalumba, 1998; Adeleke, Kalumba & Oriokot, 2019). The manufacturing process of geotextiles involves a two-step process where linear elements, i.e., yarns or fibres from polymer pellets, are made. They are then combined under heat and pressure to make a fabric structure (Shukla, 2002). Fibres are flexible, refined and have a high ratio of length to thickness, making them efficient load-carrying elements coupled with adequate tensile strengths (Koerner, 2005).

Geotextiles are divided into four main groups, i.e., woven, nonwoven, knitted and stitch-bonded geotextiles, as seen in Figure 2-14. Furthermore, nonwoven geotextiles are divided into three main groups differing in bonding, i.e., mechanical, thermal, or chemical. This creates variation in orientation, size, density, and curvature of the filaments used in geotextiles (Kim & Frost, 2011).

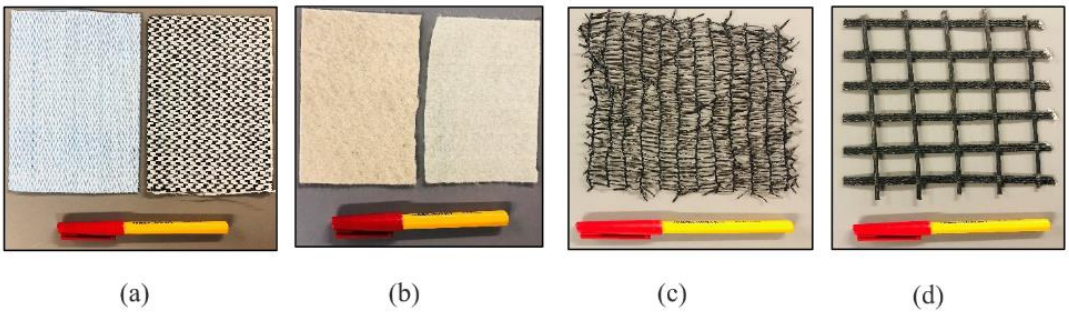

Figure 2-14: Types of Geotextiles: (a) woven,; (b) nonwoven; (c) knitted & (d) stitched (after Muluti, 2021)

2.3.4.2 Geomembranes

Geomembranes are planar, impermeable geosynthetic products with permeability coefficients ranging from 5×10^{-13} m/s to 5×10^{-16} m/s (Rowe & Shoaib, 2017). These coefficients of permeability values are lower than those of CCLs, making geomembranes be used extensively as fluid barriers in landfills. In addition, geomembranes offer excellent durability and are resistant to the effects of chemicals and UV light (Jafari & Stark, 2017; Adeleke, 2020). Moreover, geomembranes offer superior weldability and flexibility, allowing easy installation without compromising their integrity (AKS Lining Systems (Pty) Ltd, 2015). The minimum thickness for most geomembranes is 0.75mm, while 1.5mm is usually the required minimum thickness (Koerner, 2005).

HDPE geomembranes are the most used type of geomembranes for the case of landfills since they offer excellent performance to chemical attacks (Rowe, 2012). However, if greater flexibility is required, LLDPE geomembranes are typically used because they possess low molecular weight resin that can conform to non-uniform surfaces, thereby offering greater flexibility during construction and operations (Jingjing, 2014).

Geomembranes are manufactured through three methods, i.e., spread coating, calendering, and extrusion (Adeleke, 2020). Calendering is the most used manufacturing method for most geomembranes (AKS Lining Systems (Pty) Ltd, 2015). This process involves heating a polymeric compound by passing it through a series of heated rollers of the calender while rotating under hydraulic pressure or by mechanical means, as illustrated in Figure 2-15.

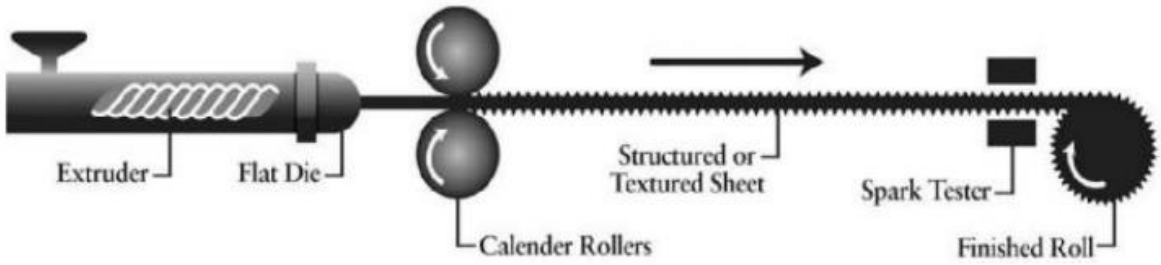

Figure 2-15: Calendering process (after Adeleke, 2020)

Textured geomembranes can be made with projections or indentations on either one or both sides, a process made possible through blown film coextrusion or impingement of hot PE particles (AKS Lining Systems (Pty) Ltd, 2015). The purpose of a textured geomembrane is to enhance friction properties between the geomembrane and soils or with other geosynthetics such as geotextiles (Adeleke, 2020; Adeleke et al., 2021). Figure 2-16 shows types of geomembranes.

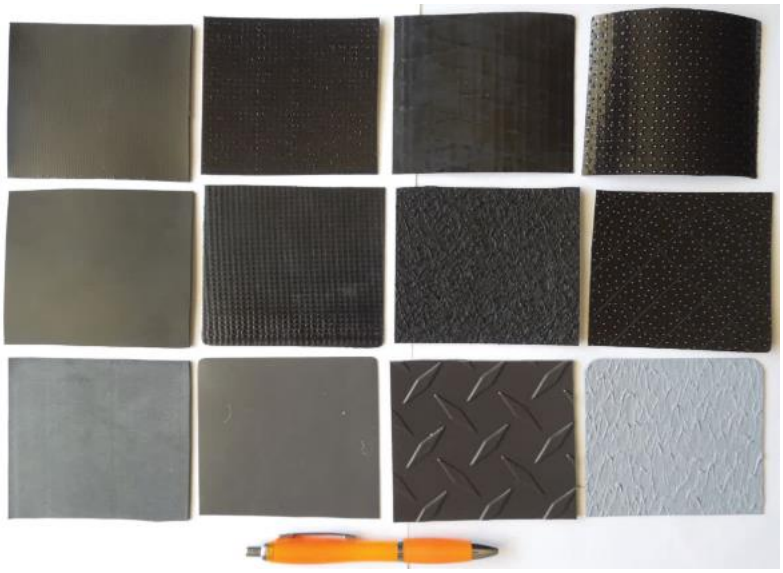

Figure 2-16: Typical geomembranes faces (after Shukla, 2016)

2.3.4.3 Geocomposites

Geocomposites are manufactured from either exclusively polymeric materials or combinations with other materials such as fibreglass or steel, sand, dried clay, or bitumen to perform functions such as tensile reinforcements or allowance for swelling in landfills' liner or waterproofing (Shukla, 2016). Geocomposites are commonly desired when a geosynthetic product cannot fulfil

all the intended functions and requirements (Chinkulkijniwat et al., 2017). An excellent example in landfill application is the geomembrane-geonet-geomembrane geocomposite used as a leak detection system. Another example is geosynthetic clay liner, a geotextile-clay-geotextile or geotextile-clay-geomembrane geocomposite, used as an impermeable liner to prevent leachate transport to the groundwater resources. The latter combination of the GCL offers greater flexibility since the clay layer minimises the leakage rate from any holes from the geomembrane. In contrast, the geomembrane prevents cracks in the clay originating from wet and dry cycles.

Geosynthetic Clay Liners (GCLs) are geosynthetic products whose primary purpose is to perform a hydraulic barrier function. These are manufactured using geotextiles or geomembranes, which sandwich a thin layer of clay mineral, usually sodium or calcium bentonite and held together by mechanical means such as needle-punches or stitch-bonds as illustrated in Figure 2-17, or through the use of chemical adhesives (Koerner, 2005; Shukla, 2016). GCLs have a hydraulic conductivity (also known as *permeability*) that is between 20 to 100 times lower than that of a typical Compacted Clay Liner (CCL) (Kloprogge, Komarneni & Amonette, 1999; Rowe & Orsini, 2003; Dananaj, Frankovská & Janotka, 2005; Wang et al., 2014). Therefore, they are highly preferred in applications such as landfill lining and cover systems. When hydrated, the sandwiched bentonite creates an impermeable sheet typically 4 to 6 mm thick with mass per unit area between 3.2 to 6 kg/m^2. GCLs also have a typical width of 4 to 5.2 m and a length of 30 to 60 m. Figure 2-18 shows a standard GCL product manufactured by a process, as seen in Figure 2-17.

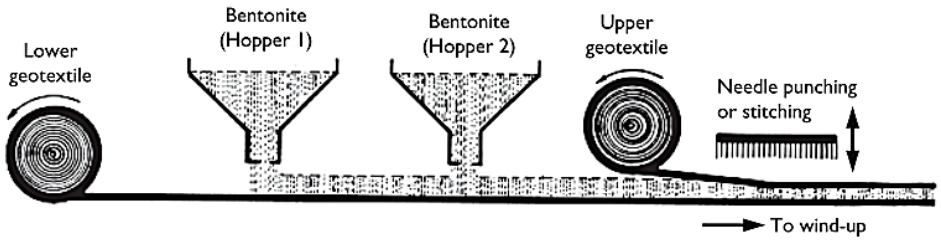

Figure 2-17: Manufacturing process of GCLs (after Shukla, 2016)

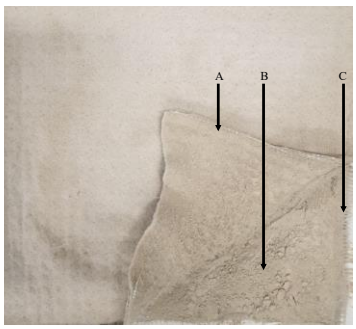

Figure 2-18: Geosynthetic Clay Liner (a) Nonwoven geotextile; (b) Sodium bentonite & (c) Woven geotextile

2.4 Shear Strength Properties of Geosynthetics in Landfills

There are two main scenarios in which the interaction between geosynthetics and other geomaterials, such as soil in MSW landfills, becomes critical. These include sliding soil over geosynthetics and pulling out of geosynthetics from the soil when the tensile load has been mobilised (Kalumba, 1998; Kalumba & Scheele, 1999). The soil-geosynthetic interaction's performance is equally vital in other geotechnical structures such as retaining walls, embankments, slopes, and foundations reinforced with geosynthetics. Interface interaction is purposefully significant in transferring stresses from the soil to geosynthetics, an action that ensures that the intended geosynthetic function is performed.

The objective of engineered MSW landfills, as discussed in Section 2.3.4, is to ensure complete waste disposal in the available space by creating steep slopes while warranting that leachate and landfill associated gases are well managed for stability and integrity of the landfill (Rouncivell, 2007; Rowe, 2011; Sikwanda, 2018; Muluti, 2021; Nanda & Berruti, 2021). However, the resulting steep side-slope geometry of the MSW landfill has been shown to contribute immensely to landfill failures, leading to catastrophic environmental consequences (Qian, Koerner & Gray, 2003).

Most MSW landfill failure cases originate from the shear failure, whether involving the lining system or the solid waste stream, as reported by Chang, Mitchell & Seed (1999); Fowmes, Dixon & Jones (2007); Belczyk & Smith (2012) and Bonaparte, Bachus & Gross (2020). Shear failure in landfills mainly occurs when the shear forces have transcended the shear strength of the lining system subjected (Fowmes, 2007; Sikwanda, 2018). Additionally, on a steep slope, the length of a slope is increased and its angle, thereby orchestrating shear forces through gravity, which could lead to a slipping plane, mainly if induced beyond what the lining component can resist. In other words, landfill lining stability is controlled by the interface properties between the lining components of soil-geosynthetic or geosynthetic-geosynthetic.

Currently, there are four laboratory tests employed to assess soil-geosynthetic and geosynthetic-geosynthetic interface interaction (Muluti, 2021; Touze-Foltz, Xie & Stoltz, 2021). These include a direct shear test, pull-out or anchorage test, an inclined plane test, and a torsional ring shear test. For purposes of this study, a focus was concentrated on the interface shear strength assessment by direct shear using the 305mm×305mm *ShearTrac-III* Large Shear Apparatus (LSA) seen in Figure 2-19. It should also be noted that using a direct shear box with relevant standards like ASTM D5321 and ASTM D6243 has proven reliable results, especially at higher normal stresses exceeding 25kPa (Lopes & Silvano, 2010; Stark & Newman, 2010; Bacas, Cañizal & Konietzky, 2015).

Figure 2-19: *ShearTrac-III* Large Shear Apparatus (after Geocomp, 2018)

2.4.1 Direct Shear Test

A modified conventional direct shear device is normally used to measure peak and ultimate (or LD) interface shear strength parameters, i.e., angle of interface friction and an apparent adhesion between soil-geosynthetic and geosynthetic-geosynthetic interfaces (Kalumba, 1998; Buthelezi, 2017; Sikwanda, 2018; Muluti, 2021). In this test, interface shear resistance properties are determined by placing and clamping the geosynthetic material on the bottom half shear box and soil material on the top half shear box (usually compacted to the required density). The representative constant normal force (N) is then applied to the top shear box on a constant area (A) to give a normal applied pressure ($\sigma = N/A$). Shear force (F) is then steadily applied to the bottom box at a constant shear rate usually dictated by the relevant standard (e.g., 0.1mm/min for tests involving fine-grained soils & 1.0mm/min for tests involving coarse-grained soils) (ASTM, 2020a,b). During the shearing stage, the bottom box where shear force is applied moves horizontally relative to the top box to a particular horizontal displacement value (e.g., 75mm). At the end of the test, the shear stress is reported against the horizontal displacement for the three representative normal stresses as a minimum threshold.

For most interfaces tested by this method, peak strength that defines the maximum shear strength is typically observed after a relatively small displacement, as shown in Figure 2-20. After attaining the peak strength, the interface undergoes the strain-softening phase, a behaviour also known as plastic deformation, until the residual shear strength value is reached. However, the residual state is never reached for some interfaces for various reasons, such as the amount of horizontal displacement that the LSA can achieve; thus, large displacements (LD) shear strength values are typically reported (Sikwanda, Kalumba & Nolutshungu, 2019; Muluti, 2021). After the test, specimens are further inspected visually or by sophisticated means such as microscopic examination, allowing for easy pinpointing where the failure might have occurred during the test (Adeleke, 2020).

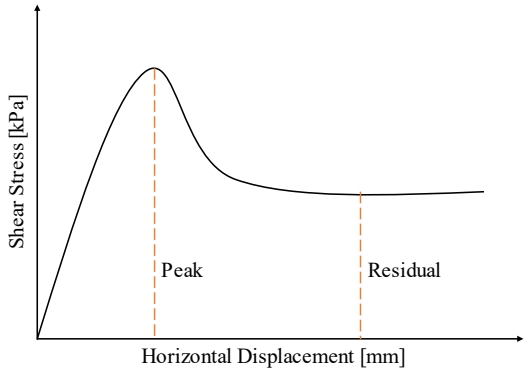

Figure 2-20: Shear stress-displacement relationship

Peak and residual (or LD) shear stresses are usually plotted against the corresponding values of normal stresses. A line of best-fit is traced to determine the shear strength parameters. The slope of the best-fit line gives the value of the interface friction angle between the soil-geosynthetic or geosynthetic-geosynthetic. In contrast, the vertical axis' intercept gives the value of an apparent adhesion between the two materials (ASTM, 2020a,b).

Despite the advantages offered by the direct shear test, this test is not ideal for stress-strain relationships of test specimens because of the non-uniformity in the shear force and recorded displacements (Lopes & Silvano, 2010). The resistance observed could result from the sliding nature of geosynthetic surfaces, strain effects of the geosynthetic specimens, soil particles interlocking with the sample, or rolling effects on the surfaces (Kalumba, 1998; Vangla & Latha, 2015; Yamsani, Sreedeep & Rakesh, 2016; Sikwanda, Kalumba & Nolutshungu, 2018; Adeleke, Kalumba & Oriokot, 2019).

2.4.2 Analysis of Data from LSA

At the beginning of the 20th century, Mohr pioneered a theory that the failure of materials is influenced by the combination of normal and shear stresses (Sikwanda, 2018; Adeleke, 2020; Muluti, 2021). The analysis of data obtained from LSA relies on the Mohr-Coulomb failure criterion to get shear strength parameters used in the design of lining systems of MSW landfills.

The Mohr-Coulomb failure criterion stipulates a linear relationship between applied normal and shear stresses at peak and residual (or LD) states. The Mohr-Coulomb failure criterion is presented in Equation 2-3 and a schematic presentation in Figure 2-21.

$$\tau = \alpha + \sigma_n \tan\delta \qquad \textbf{Equation 2-3}$$

Where:

τ = Shear stress
α = Apparent adhesion
σ_n = Applied normal stress

δ = Interface or internal friction angle

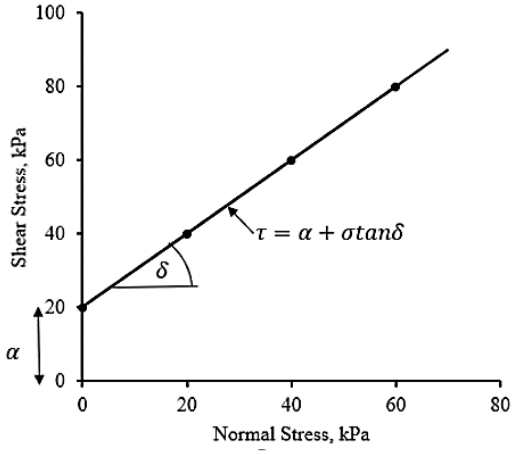

Figure 2-21: Mohr-Coulomb failure criterion (after Sikwanda, 2018)

According to Adeleke (2020), if the plotted shear stress curve against applied normal pressure, as seen in Figure 2-21, doesn't represent the anticipated field conditions, the values used to plot the graph are then incorrect. Consequently, the determined shear strength parameters are wrong.

Mohr-Coulomb failure criterion is widely used in understanding the mechanics of different materials whose compressive strengths exceed their tensile strengths. This understanding is fundamental in several geotechnical conventional and computer-aided analyses to define strength parameters. However, for some geotechnical applications, such as in geosynthetics, the Mohr-Coulomb failure criterion might not accurately predict the correct strength parameters, especially when the geosynthetics are loaded at very high normal stresses (Kalumba, 1998). Scholars such as Sharma, Fleming & Jogi (2007) and Muluti (2021) discussed the importance of interpreting the LSA data using the non-linearity approach on plots of shear, especially when the geosynthetic materials are tested on a wide range of normal stresses. To further illustrate the implications of the non-linearity approach in understanding the Mohr-Coulomb failure criterion of geosynthetics' interface shear testing, Figure 2-22 is presented.

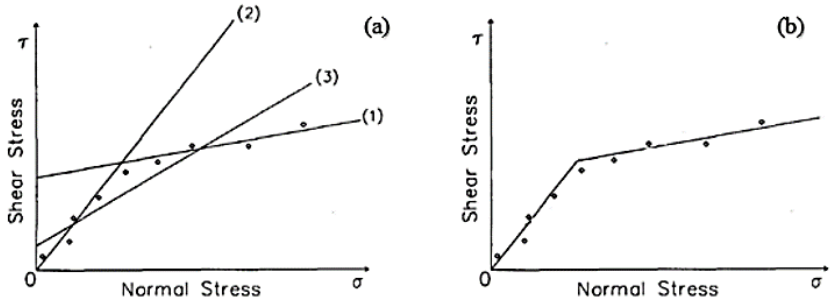

Figure 2-22: Mohr-Coulomb Failure Criterion for Geosynthetics (after Muluti, 2021)

For the same materials tested on a wide range of applied normal stresses, straight line 1 in Figure 2-22 (a) provides a reasonably fair estimate of shear strength parameters at high applied normal stresses. In reverse, straight line 2 on the exact Figure 2-22 (a) presents a reasonable estimation of shear strength parameters at a low applied normal stress range. However, straight line 3 in Figure 2-22 (a) is recognised as the best-fit line that would give reasonably shear strength parameters for both low and high applied stress ranges (ASTM 2020a,b). Bonaparte, Bachus & Gross (2020) and Muluti (2021) discussed that selecting a straight line 3 could incorrectly estimate shear strength parameters. Therefore, a bilinear envelope resulting from the combination of straight-line 1 & 2, as seen in Figure 2-22 (b)**,** would best define the shear strength parameters of these materials.

2.4.3 Factors Influencing Interface Shear Properties

2.4.3.1 Applied Normal Stress

The use of LSA in determining shear strength properties of soil-geosynthetic and geosynthetic-geosynthetic interfaces requires the application of normal stress. According to ASTM (2020a,b), a minimum of three applied normal stresses are necessary to correctly estimate the shear strength parameters using the Mohr-Coulomb failure criterion. Many scholars, for instance, McCartney, Zornberg & Swan (2009); Eid (2011) and Bacas, Cañizal & Konietzky (2015), pointed out that the applied normal stress range affects the shear strength parameters in a way that shear stresses increase with increasing applied normal stresses. Additionally, researchers such as Sikwanda (2018); Adeleke (2020) and Muluti (2021), who have conducted interface shear tests on a wide range of normal applied stresses, concluded that Mohr-Coulomb failure criteria could be bilinear or curvilinear due to the effects associated with normal pressure ranges tested.

This shows that the choice of normal stresses for interface shear testing must always reflect the anticipated field conditions to establish shear behaviour correctly. For instance, the range of normal pressures applied to the basal lining system cannot be the same as those applied to the cover lining system in the case of MSW landfills. For the suitable approximation of shear strength parameters, the choice of normal stresses should reflect all loading conditions, i.e., low, intermediate, and high. In cases where one stress value is the only known value, then the increment should at least be either 100% or 150% (ASTM, 2020a,b; Muluti, 2021).

Failure mechanisms on interface shear strength testing have been shown to depend on values of applied normal stresses. For example, a geomembrane-geotextile interaction will have a different interface shear failure mechanism, one of which involves the interlocking together with the frictional mechanism at low normal stresses of <50kPa, while a matrix level mechanism is observed at high normal applied pressure, thus >50kPa (Adeleke, Kalumba & Oriokot, 2019). On another interface, such as the soil-geotextile interface, the friction mechanism appears at low normal applied stresses of approximately <100kPa, while at high normal applied stresses of >100kPa, internal friction of soil seems to be the mechanism (Bacas, Cañizal & Konietzky, 2015).

2.4.3.2 Shear Displacement Rate

During a shearing stage, the shear force is progressively applied to the interface tested by the LSA, and at this stage, the shear displacement rate (SDR) becomes of great concern. In simple terms, SDR may be defined as the speed at which the bottom shear box with one of the specimens travels laterally relative to the top shear box (Geocomp, 2018). The choice of SDR during interface shear testing is essential as it simulates the progressive failure of the tested materials in the field (Stark & Choi, 2004; Eid, 2011; Bacas, Cañizal & Konietzky, 2015; Stark, Niazi & Keuscher, 2015; Sikwanda, 2018; Muluti, 2021). SDR is also emphasised in the ASTM standards for evaluating shear strength by a direct shear method whereby, for all materials involving coarse-grained soils and geosynthetics apart from GCLs, SDR of 1mm/min is normally preferred. While for all tests involving fine-grained soils and GCLs, SDR of 0.1mm/min is usually sufficient to avoid any positive or negative pore pressure build-up during the test (ASTM, 2020a,b).

Sikwanda (2018) stated that if a faster SDR is applied during interface shear testing in the laboratory, the quality of the results obtained, and consequently the shear strength parameters may be subjected to effects of tension/slippage and may not adequately simulate field conditions. Conversely, some researchers such as Stark, Williamson & Eid (1996) stated that SDR choice has a negligible impact on geosynthetics' measured shear strength parameters such as geotextile and geomembranes. However, since SDR reflects the strain rate action on the tested materials, its choice should be to give results for the long-term shear characteristics of the landfill lining components (Muluti, 2021).

2.4.3.3 Hydration

Normally, if hydrated conditions are expected in the field where the landfill lining components will be utilised, then the interface shear tests in the laboratory are run under hydrated conditions. ASTM standards for the interface and internal shear strength assessment by direct shear method require that the type of hydration liquid be specified, especially when the interface tests involve geosynthetics, particularly geomembranes and GCLs (ASTM, 2020a,b). Therefore, this means that the hydration conditions affect the shear strength parameters of geosynthetics. The standards further require that the method to which the materials have been hydrated be stated in the final report, i.e., whether the materials were spray-wetted or were fully submerged prior to shearing and for how long. Hydration conditioning has also been proven to give minor favourable shear strength parameters compared to interface shear tests run under dry conditions (Fox & Stark, 2015).

A particular geosynthetic material that requires proper hydration conditioning is the GCL. The sodium bentonite layer within a GCL component is chemically active, and depending on how the hydration conditioning has been implemented, this layer could swell to a maximum. Studies conducted by Chiu & Fox (2004) and McCartney, Zornberg & Swan (2009) revealed that complete hydration of GCLs will result in critical state failure; however, under ideal field working conditions of the GCL, this is unlikely to be the case. Moreover, studies conducted by

Zanzinger (2016) revealed that to achieve a complete hydration conditioning of the GCL, it needs to be saturated for longer than 24hrs under a small seating load (usually 17kPa) to allow for a complete swelling before the shearing stage. This is because sodium bentonite in the GCL affects the shear strength parameters during the shearing stage.

It is worth noting that the above conditioning can only be achieved in laboratory conditions if several direct shear machines are available to avoid the strains on resources such as time and cost. Standards such as ASTM (2020a) clearly state that for proper GCL hydration conditioning, the material needs to be hydrated within the direct shear machine to avoid complications resulting from transfer issues to the LSA. The applied normal stress expected during the shearing step should also be applied during hydration conditioning. For other types of geosynthetics other than GCLs, a hydration time of 1hr or less is generally preferred and acceptable by ASTM standards. This time allows for proper geosynthetic engagement before shearing (Stark, Niazi & Keuscher, 2015; ASTM, 2020b).

2.4.3.4 Consolidation

Consolidation may be defined as the vertical compression of geomaterials such as soil or geosynthetics such as GCL over a specified amount of time resulting from the expulsion of excess pore water pressures. In interface shear strength testing by the direct shear method, consolidation occurs concurrently with the hydration step. Usually, 1hr for specimens not involving clay and 24hr for specimens involving clay, assuming that 90% of consolidation has occurred. This is because tests are run under consolidated drained (CD) conditions (ASTM, 2020a,b).

If the consolidation period is insufficient, interface shear results will likely be affected due to the effects associated with pore water pressure build-up, which are not given sufficient time to be expelled (Fox & Stark, 2015). However, it is worth noting that for some geosynthetics such as GCLs, consolidation periods are difficult to ascertain purely because of the high variability of the sodium bentonite component from different manufacturers. Some researchers, including Zaini, Kasa & Nayan (2012); Lin et al. (2014) and Lin, Zhang & Xiong (2018), conducted shear tests of GCLs and expressed that the material under different consolidation periods, different shear strength parameters were obtained.

2.4.3.5 Specimen Gripping Systems & Fixation

Direct shear testing of landfill lining components uses LSA, which has two large shear boxes, i.e., top and bottom. To run an interface test, say for the soil-geosynthetic or geosynthetic-geosynthetic interface, geosynthetic specimens are usually clamped on top of a gripping surface for the case of the bottom box or vice versa for the case of the top box. Gripping surfaces allow geosynthetics to not slide against the shearing blocks. This action allows the shearing to occur at the intended interface (Sikwanda, 2018; Sikwanda, Kalumba & Nolutshungu, 2018). The gripping surfaces used in the interface shear testing should also allow field conditions to be replicated (Kalumba, 1998).

Clamping devices play an essential role, especially when the gripping surfaces cannot fully mobilise adequate resistance and facilitate shear measurements, these act like anchors in the field (Chiu & Fox, 2004). Clamping devices assist in holding the specimens in their position during shear testing, thereby allowing the failure to occur at the intended interface (Sikwanda, Buthelezi & Kalumba, 2018).

Without an excellent gripping surface and a clamping mechanism, a geosynthetic material will slide on the shearing block, thereby developing unintended tensile forces and producing inaccurate results. At the same time, it also results in a progressive failure since the portion of the applied normal pressure is lost, eventually generating reduced shear strength parameters both at peak and residual (or LD) (Sikwanda, 2018). ASTM standards relevant for interface shear strength measurement of soil-geosynthetic and geosynthetic-geosynthetic interfaces, unfortunately, do not explicitly specify a type of gripping surface. However, they state that the surface has to be textured enough to allow sufficient shear resistance mobilisation, of course, with the help of a suitable clamping system that will hold the geosynthetic specimen in place (ASTM, 2020a,b).

Different gripping surfaces have been employed in running shear interface testing using the LSA, such as textured steel, adhesive bonding, nail plates Figure 2-23 (a) and sandpaper Figure 2-23 (b). The effects of gripping surfaces are noticeable in shear strength tests of landfill lining components. For instance, using nail plates as gripping surfaces, peak stress is achieved at lower shear displacement due to early engagement and intimate contact of specimens with the gripping surfaces (Sikwanda, 2018). This is the opposite for sandpaper gripping surfaces, as seen in Figure 2-24. This phenomenon is noticed at high normal stresses, e.g., at 200, 295 & 400 kPa, compared to lower pressures where the difference is almost negligible. Another mechanism called stick-slip, where the specimens slip against the gripping surfaces, is also noticed at high applied normal stresses. The tested specimens' repeated build-up best explains this phenomenon and subsequent collapse attributed to the increasing confining pressure (Sikwanda, 2018; Sikwanda, Kalumba & Nolutshungu, 2018). Another important observation is that regardless of the gripping system used, the change in critical interface is noticed, as seen in Figure 2-25.

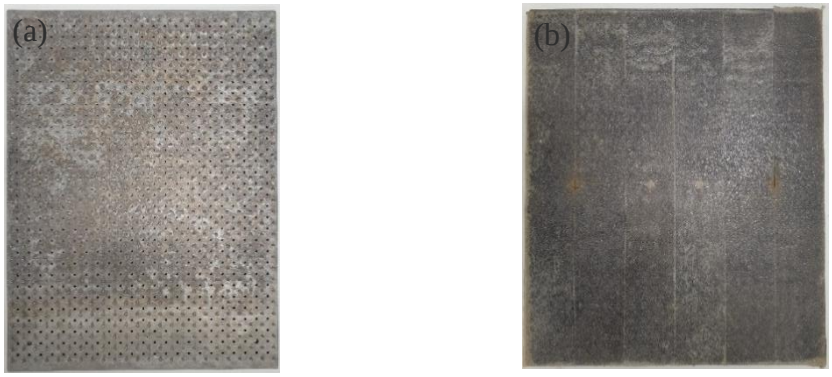

Figure 2-23: Gripping surfaces (a) Nail Plate & (b) Sandpaper

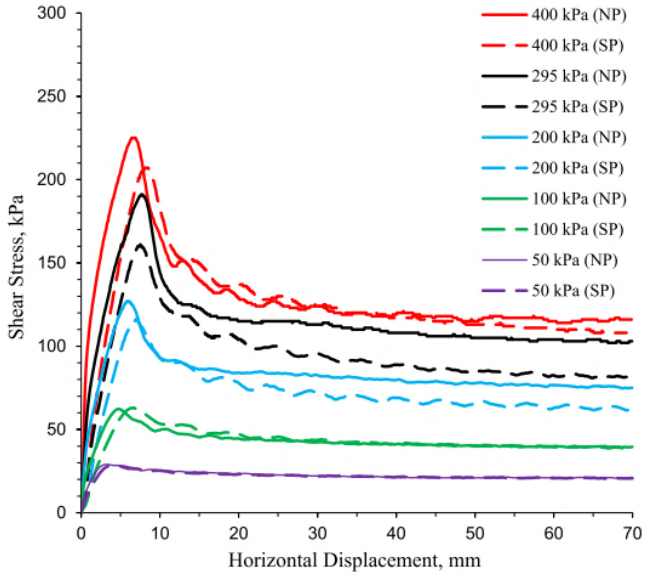

Figure 2-24: Shear stress – horizontal displacement relationship of an interface with different gripping systems (after Sikwanda, 2018)

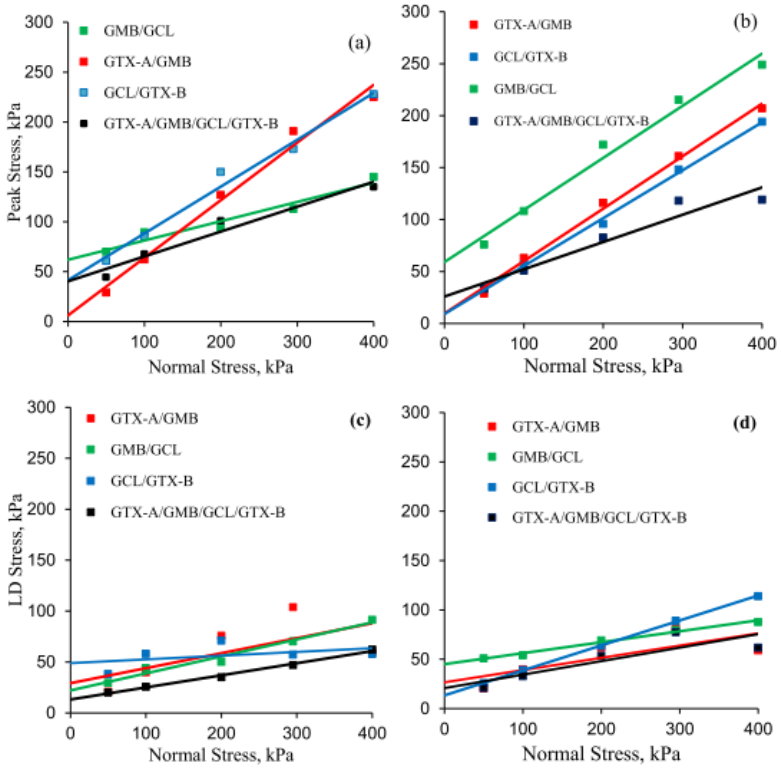

Figure 2-25: Mohr-Coulomb failure criteria for single- and multi-interfaces (after Sikwanda, 2018)

2.5 Review of Previous Research

Due to strict environmental regulations imposed by local government authorities and public concerns over solid waste management, the demand for engineered MSW landfills requiring extensive use of lining systems has evolved in most parts of the world, South Africa included (Nanda & Berruti, 2021). To assess the stability of the lining systems within an engineered landfill, single interface shear strength tests of either soil-geosynthetic or geosynthetic-geosynthetic are typically conducted. This approach is widely accepted for various reasons, such as confidence in the obtained results (Sikwanda, Kalumba & Nolutshungu, 2019). However, the single interface configuration poses disadvantages, such as overestimating shear strength parameters due to specimen confinement (Stark, Niazi & Keuscher, 2015), while in most cases, not simulating field characteristics of the liner arrangement, which is usually a composite of multi-layered lining system (Sikwanda, 2018; Muluti, 2021). Single interface shear assessment of landfill lining components has also been noted to consume time and money.

When geosynthetics are used with other geosynthetics or geomaterials, their interaction becomes pertinent as failure could be mobilised on their interfaces. Being one of the failure modes, direct sliding between a soil block and geosynthetic or between geosynthetic materials is critical at landfill slopes in engineered MSW landfills (Lopes & Silvano, 2010). A study by Kim & Frost

(2011) identified that shear failure of MSW landfill slopes is a progressive behaviour; therefore, the rigidity behaviour on sloped surfaces is less relevant since differential elongation of geosynthetics during such an advanced shear failure is usually observed.

Ideally, in the field, failure in the lining systems could occur at any weakest interface through different possible failure mechanisms, as discussed briefly in Section 2.2.4. It is worth noting that running single interface shear strength tests in the laboratory doesn't capture these complicated scenarios accurately. The limitations of single interface shear testing, however, can be controlled and well captured in the double or multi-interface shear testing, as discussed in detail in studies by Stark, Niazi & Keuscher (2015); Khilnani, Stark & Bahadori (2017) and Muluti (2021)

Consequently, double or multi-interface shear testing emanates with its challenges, including only critical shear strength parameters and not parameters of other interfaces that could also be of interest are determined (Muluti, 2021). However, it should be noted that, even when other interfaces would be relatively stable compared to the critical interface during the test, their behaviours during shearing are imperative. As mentioned earlier, shear failure of landfill lining components is a progressive process, and more than one interface could fail concurrently. Nonetheless, running a multi-interface shear strength test is related to the proposed landfill lining arrangement. Depending on the design, some landfill lining arrangements may not allow running interface shear tests of more than three landfill lining components at one go, i.e., multi-interface. A double interface shear strength test could be suitably employed in such cases.

The evolution of double interface shear tests is also motivated by the presence of double-lined landfill systems, which were legislated on the national specification and used in MSW landfills in the United States since 1986 with extended applications in dams and tunnels (Kim & Frost, 2011). Double interface shear strength testing involves testing only three landfill lining specimens adjacent to each other, thereby understanding the shear characteristics of only two interfaces. Specific benefits of running double interface shear tests over multi-interfaces are related to the easiness of understanding interface shear results similar to those of single interface, as double interface testing gives fewer complications than multi-interface testing.

However, due to the limitations associated with the LSA as far as setting a shear gap is concerned, challenges arise when running double interfaces and multi-interfaces of landfill lining components. As a result, therefore, it becomes necessary at least to run one interface shear test via a single interface approach to establish consistency in testing; the interface of choice is usually the critical interface as this can easily be compared with the results obtained via double and multi-interface approach (Stark, Niazi & Keuscher, 2015; Muluti, 2021).

In analysing soil-geosynthetic frictional properties, three interfaces are very important: geomembrane-clayey soil, geomembrane-geotextile, and GCL-clayey soil, as discussed by Chai & Saito (2016). When a geomembrane interacts with soil, two failure mechanisms exist, i.e., sliding and ploughing shear, which relies on the extent of confining stress and the stiffness of the

geomembrane. When the geomembrane is too soft and the confining pressure is relatively higher, the ploughing shear mechanism is likely to occur. In any case, the properties of the two materials contribute significantly to the shear behaviour with the adjacent topsoil. Additionally, for soil-geosynthetic interface shear strength tests, particularly for nonwoven geotextiles, higher interface angles of friction have been observed due to soil particles' ability and significantly smaller particle sizes penetrating the geotextile (Choudhary & Krishna, 2016).

The failure mechanism of the geotextile-geomembrane interface results from a combined action between the two materials facilitated by tension and surface contact deterioration (Kim & Frost, 2011; Adeleke et al., 2021). When utilized on slopes, the geomembrane-geotextile interface experiences tension forces developed from the construction machinery and the settlement originating from the overlying solid wastes, as discussed in Section 2.2.3. The interaction between a geomembrane and a geotextile is typical, as the geotextiles are used in conjunction with the geomembrane to provide a protective layer. Geotextiles dominate the stability criteria for this interface, while geomembranes are less subjected to shear failure. When there is lateral confinement, however, the increase in tensile strength becomes dependent on the rise in the geotextile stiffness.

Different liner systems were proposed by Stark, Niazi & Keuscher (2015), as seen in Figure 2-26 (a), and Khilnani, Stark & Bahadori (2017)**,** as seen in Figure 2-26 (b). The interface shear strength testing for these lining systems had the objective of developing strength envelopes at peak and residual (or LD) states for single and multi-interface testing arrangements.

From Figure 2-26 (a), a maximum shear displacement of 75mm was chosen, accompanying five applied normal stresses ranging from 70 to 2070 kPa. The proposed landfill was estimated to have a unit weight of 12.55kN/m^3 and a maximum vertical height of 165m. The deliberate choice of small normal stresses, i.e., 70 & 170 kPa, was considered a better definition of shear strength of a typical lining system as numerous MSW landfills are usually exposed at such low normal stress values.

Stark, Niazi & Keuscher (2015) observed that the measured shear strength parameters at peak and LD for single and multi-interface configurations involving HDPE GMB were reasonably comparable for low normal stresses applied, i.e., 170 & 690 kPa, as seen in Figure 2-27. However, this was not the case for the high applied normal pressures of 1380 & 2070 kPa, where multi-interface configurations yielded higher peak and LD shear strength parameters. Some interesting findings in Khilnani, Stark & Bahadori (2017) research was that the weakest or critical interface through single interface configuration on the side-slope lining system was determined to be GMB-GC for the entire range of normal stresses evaluated. This critical interface was also confirmed by the multi-interface shear testing configuration where shear displacement occurred at the GMB-GC interface. The peak strengths for both single and multi-interface test configurations proved to be similar.

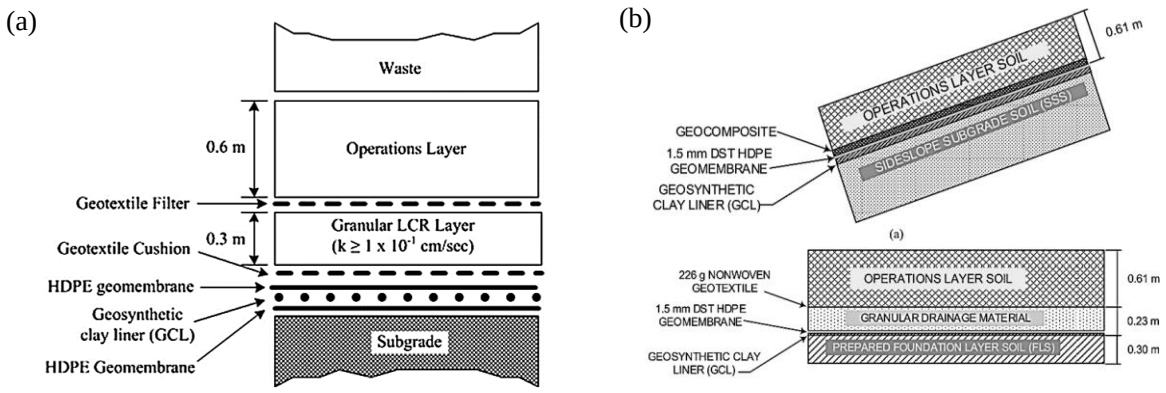

Figure 2-26: Basal and side-slope lining systems (after Stark, Niazi & Keuscher (2015) and Khilnani, Stark & Bahadori (2017))

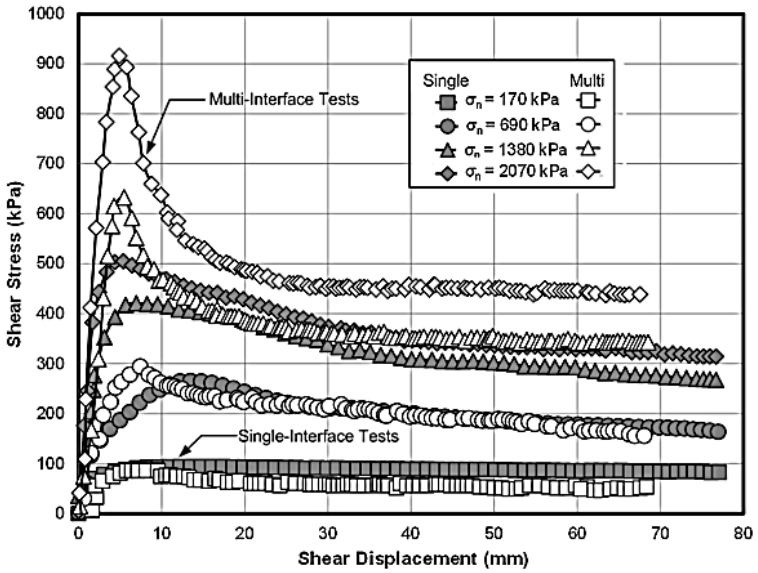

Figure 2-27: Shear stress – horizontal displacement relationship (after Stark, Niazi & Keuscher, 2015)

The philosophy behind single interface shear testing is to determine the critical interfaces within the landfill lining system over a range of required normal stresses. In interface shear testing, a critical interface may be defined as one whose shear strength values are the lowest of all the other interfaces (Buthelezi, Kalumba & James, 2016; Buthelezi, 2017). This depends on several factors discussed in Section 2.4.3, with the main one being the applied normal stress.

Direct shear testing of MSW landfill lining systems exhibits stress-dependent shear characteristics when subjected to a wide range of applied normal stresses. An excellent example of this is seen on the single interface shear testing by Stark, Niazi & Keuscher (2015), where at peak, the weakest interface at an applied normal stress of 870kPa altered from a GMB-GCL-GMB fully hydrated to GMB-CSL (compacted soil layer) exposed to pre-wetted conditioning as

seen in Figure 2-28 (a). However, this trend was not observed for LD strength assessment, where the lowest LD strengths still originated from the same lining components tested under full hydration, i.e., GMB-GCL-GMB, as seen in Figure 2-28 (b). Additionally, the GMB-CSL interface showed more overlapping at the LD state by crossing through the GMB-GCL-GMB exposed to un-hydrated conditioning at around 700kPa and through GMB-GTX exposed to pre-wetting conditioning at 1350kPa, as seen in Figure 2-28 (b).

Due to such variabilities in determining the weakest failure planes within landfill lining components, the construction of a failure envelope requires a combination of the lowest peak strength values from all the segments tested, especially if the failure criteria overlap (Sikwanda, 2018).

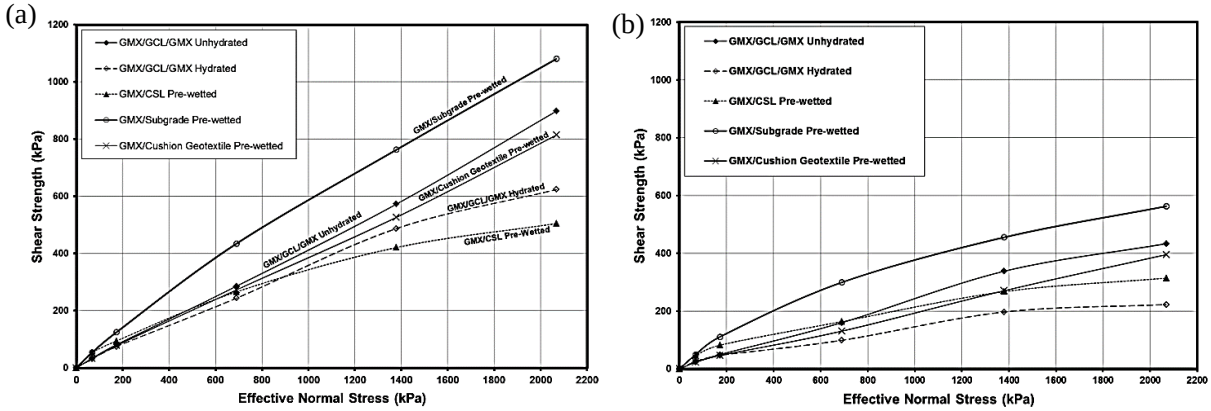

Figure 2-28: Peak and LD envelopes for single interfaces (after Stark, Niazi & Keuscher, 2015)

Another important observation by Stark, Niazi & Keuscher (2015) was that the un-hydrated critical interface determined after running multi-interface shear tests was stress-dependent, while the hydrated critical interface was not. This implied that under un-hydrated conditioning, the critical interface is highly likely to change from one interface to another during testing. This was evidenced by a change of critical interface from GTX-GMB pre-wetted to GMB-GCL un-hydrated, as seen in Table 2-5.

As Stark, Niazi & Keuscher (2015) predicted, the critical interface in the proposed lining system, as shown in Figure 2-26 (a), tested under both single and multi-interface configurations, remained GMB-GCL exposed to full hydration conditioning at peak and LD seen in Table 2-5. This observation confirms that tests conducted under the multi-interface arrangement are reliable and comparable to those tested under a single interface configuration. However, attention during the comparison process should be highly considered. In most cases, peak strengths of single interface configurations tend to be higher due to being tested in isolation and influenced by proper fixations, unlike in multi-interface testing. Conversely, multi-interface tests may yield higher LD shear strengths attributed to the shear displacements on the critical interfaces.

Table 2-5: Critical interfaces at different applied normal stresses for multi-interface (adapted from Stark, Niazi & Keuscher, 2015)

Normal stresses [kPa]	Test series	
	5 GMX-Black/Black-subgrade soil, un-hydrated	6 GMX-Black/Black- subgrade soil hydrated
70	Cushion geotextile/GMX-pre-wetted	GMX/GCL hydrated
170	Cushion geotextile/GMX-pre-wetted	GMX/GCL hydrated
690	Cushion geotextile/GMX-pre-wetted	GMX/GCL hydrated
1380	Cushion geotextile/GMX-pre-wetted	GMX/GCL hydrated
2070	GMX/GCL un-hydrated	GMX/GCL hydrated

Research conducted by Stark & Choi (2004) proposed that post-peak strength envelopes for the critical interface should be used in designing geosynthetic lined slopes. Additionally, in a study by Khilnani, Stark & Bahadori (2017), multi-interface tests emphasized the use of post-peak strengths developed from the critical interface of GMB-GC, which also yielded the same post-peak results as the single interface tests run on the same interface GMB-GC as seen in Figure 2-29. For this case, it is worth noting that the critical interface did not change with increasing normal stresses; if it, however, would have changed, then the critical interface would also change, according to Stark and Choi (2004). It should also be noted that when geosynthetics and soils used in testing were the actual ones used in construction, the interface GMB-GC would remain relevant. If that was not the case, then the lowest post-peak strength envelope and its critical interface would have to change, and additional testing would then be required. This testing set has shown that single interface testing produces similar results to multi-interface shear testing. Therefore, for a real project, multi-interface shear testing could be conducted and confirmed by at least one single interface shear testing, especially where the critical interface was observed.

In the different test series by Khilnani, Stark & Bahadori (2017) for the basal lining system, the GMB-GCL interface was observed to be critical under single interface shear testing; this was once again confirmed by the multi-interface shear testing, as seen in Figure 2-30. Additionally, the peak strengths were similar in both testing configurations, i.e., single and multi-interface testing. The transition of critical interface from GMB-GCL to GMB-Gravel was noticed in terms of peak strengths. This change in the critical interface was attributed to GMB, as gravel failed to fully embed into the HDPE GMB at low applied normal stresses. This criterion was another great importance of using multi-interface shear tests to confirm the critical interfaces. Like in the side-slope lining system, the interface GMB-GCL in the basal lining system produced post-peak shear strengths that exceeded the project specified strength. This observation confirmed that multi-interface shear strength testing could confirm the critical interface created in the single interface testing and vice versa would be true.

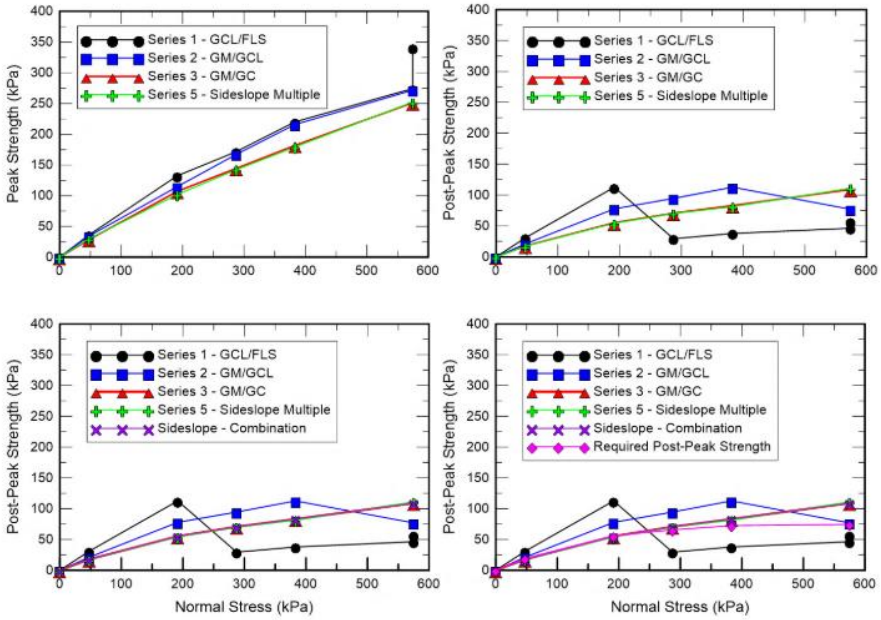

Figure 2-29: Peak strength for side slope liner system (after Khilnani, Stark & Bahadori, 2017)

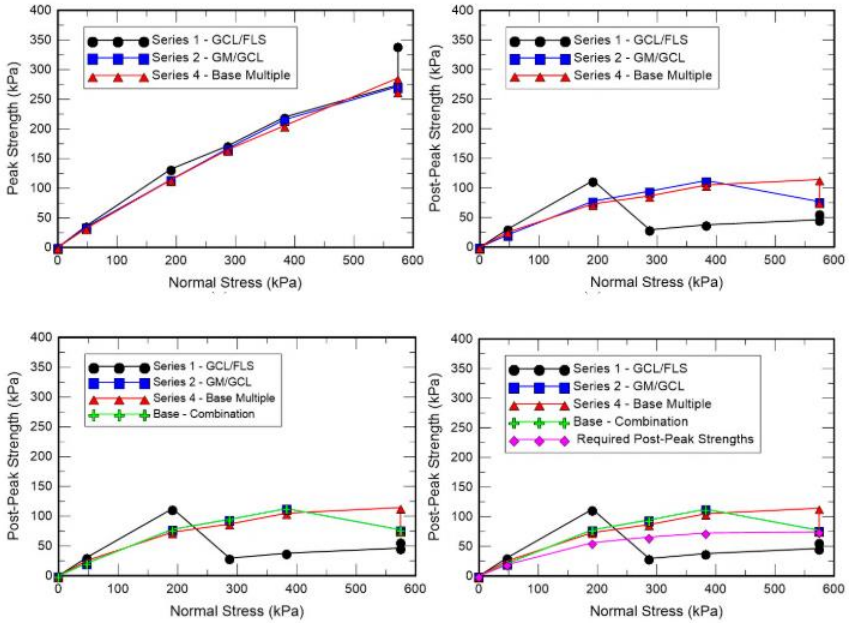

Figure 2-30: Peak strength for basal liner (after Khilnani, Stark & Bahadori, 2017)

Muluti (2021) pointed out that, as the applied normal stress was increased in the single interface shear testing, the weakest interface changed at peak and LD, as seen in Figure 2-31, with the GCL/SAND being the critical interface. For this same interface exposed to a double interface shear testing with an adjacent geosynthetic layer as is in the proposed lining system, i.e., GMB/GCL/SAND, the peak strength envelopes were similar in both testing configurations seen

in Figure 2-32. Interface shear strength parameters also proved to be relatively similar at peak as GCL/SAND interface obtained 22.9° interface friction angle and 25.9kPa apparent adhesion compared to those obtained by GMB/GCL/SAND interface of 23.9° and 24.7kPa, respectively. In contrast, at LD, interface shear strength parameters obtained were very dissimilar, with the single critical interface obtaining higher values than the critical double interface, as seen in Table 2-6.

Worthwhile noting, as more landfill linings were added into the testing configuration, i.e., multi-interface shear testing, the change of critical interface became more significant since the other lining components other than those in the critical interface were observed not to experience tension hence, resulting in difficulty in evaluating the correct weakest/critical interface.

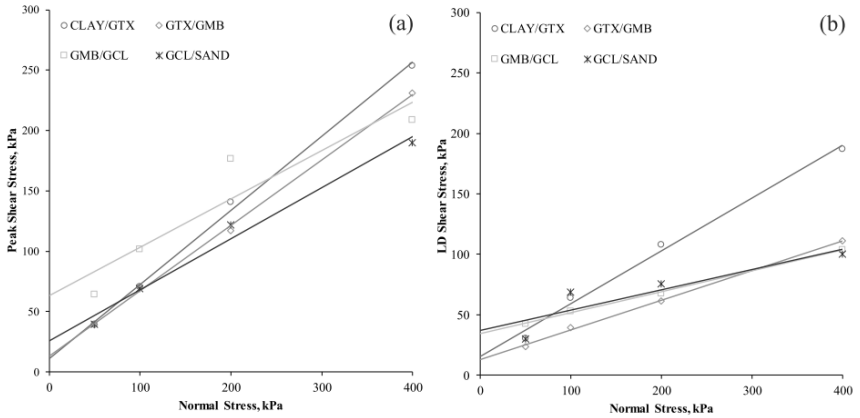

Figure 2-31: Mohr-Coulomb failure criteria for single interfaces (after Muluti, 2021)

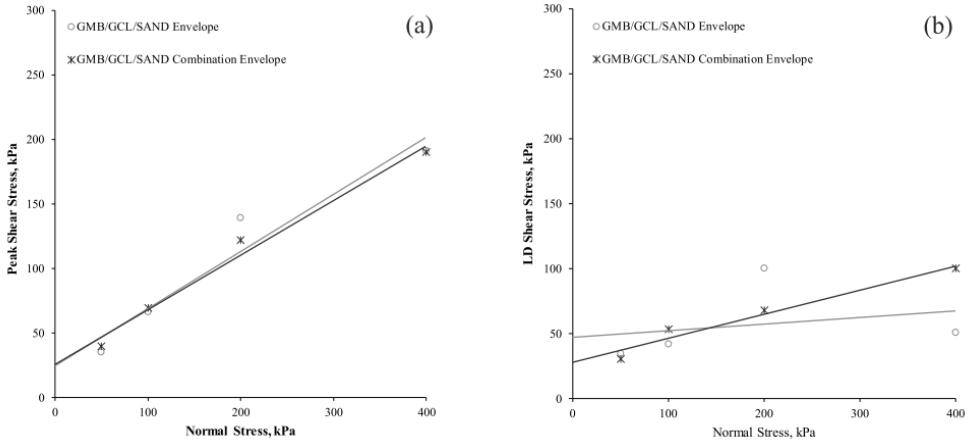

Figure 2-32: Mohr-Coulomb criteria for double-interfaces (after Muluti, 2021)

Table 2-6: Parameters for single and double interface shear testing (adapted from Muluti, 2021)

Interface Configuration		Strength Parameters			
		Peak		LD	
		δ_P [°]	$c_{\alpha\text{-}p}$ [kPa]	δ_{LD} [°]	$c_{\alpha\text{-}LD}$ [kPa]
Single -	CLAY/GTX	31.5	11.1	23.5	15.7
	GTX/GMB	28.4	13.0	13.8	12.8
	GMB/GCL	21.8	63.0	9.8	34.4
	GCL/SAND	22.9	25.9	9.5	37.2
Double -	CLAY/GTX/GMB	24.7	32.5	11.7	47.7
	GTX/GMB/GCL	28.0	0.8	13.2	3.8
	GMB/GCL/SAND	23.9	24.7	2.9	47.2
Notes: δ_P & δ_{LD} are interface friction angles, and $c_{\alpha\text{-}p}$ & $c_{\alpha\text{-}LD}$ are apparent adhesions					

2.6 Summary of Literature Review

This summary pinpoints key findings extracted from the literature on interface shear testing of landfill lining components. A focus was concentrated on specimen configuration in the LSA, which resulted in two key investigative areas, i.e., single and double interface shear tests.

- Currently, four laboratory methods are used in determining interface shear strength properties of soil-geosynthetic and geosynthetic-geosynthetic interactions. These include the direct shear test, torsional ring shear, inclined plane test, and pull-out test. The direct shear test method is highly preferred due to its ability to measure interface shear strengths of large soil-geosynthetic and geosynthetic specimens. Other capabilities offered by this test method include producing reliable shear results, especially when the applied normal stress exceeds 25kPa, as claimed by notable researchers.
- Despite the strengths, tests conducted in a 305mm×305mm LSA have been noted to sometimes not reach the residual condition due to the limitation of horizontal displacement offered by the machine. In most studies by prominent researchers, a condition known as large displacement (LD) or post-peak strength is normally reported, especially after the sheared specimens have undergone a strain-softening condition.
- Several factors have been noted to influence interface shear results, among which normal applied stresses and gripping specimen mechanisms have been noted to be crucial. As a result, therefore, critical interfaces are subject to changes in the level of applied normal stresses, as acclaimed by numerous researchers. Interestingly, the level of applied normal stress has also been critical for tests conducted under single interface configuration and those under multi-interface configuration. Additionally, according to a few studies reviewed, gripping surfaces have also impacted interface shear results.

- Interface shear tests of landfill lining components have traditionally been conducted based on single interface configurations. This testing configuration has also been adopted in testing standards such as ASTM due to a vast understanding of testing conditions with the LSA, the easiness of interpreting shear results, and limitations associated with the LSA, such as shear gap issues. Recently, multi-interface shear tests conducted by numerous scholars have also proven to produce comparable results; most works have been presented in Section 2.5. However, more research is still required to develop a large database. Due to project and site-specific testing, there are numerous landfill designs and countless types of geosynthetics in the industry. In addition, there is no specific standard guide that directs the conduction of multi-interface shear tests; as a result, inconsistent reported results have been noted among the reviewed studies.

In conclusion, further studies of multi-interface shear testing would ascertain the approach's appropriateness. Owing to its benefits, multi-interface shear testing would save time and money while rendering an understanding of how several lining components behave under shear failure. This study was thus, conducted to further understand the comparability of shear results between single and double interface shear tests by using the LSA subjected to the same conditioning of MSW landfill lining components of the proposed landfill cell in the Western Cape Province in South Africa.

3 Research Materials & Methodology

3.1 Introduction

This chapter gives an overview of the research materials, main testing apparatus, and experimental approach followed to achieve the objectives outlined in Chapter 1. In this work, several lining components that formed part of the basal lining system of a proposed landfill cell in the Western Cape Province, South Africa, were utilized. These included three types of nonwoven geotextiles, two smooth-sided geomembranes, synthetic cuspate drain (CD), sand, gravelly sand (GS) and leachate collection stone (LCS). Efforts were made to understand the mechanical and physical properties of the mentioned lining components, as shown in Section 3.3. The chapter concludes with a testing programme and an outline of the measures taken to ensure that the quality and consistency of results were achieved. In addition, a repeatability analysis of two sampled interface tests on single and double interface testing configurations is presented.

3.2 The Basal Lining System

According to DWAF (1998) & DEA (2013), the proposed landfill cell was classified as a general waste landfill with the potential to generate significant leachate. It was to be built on top of a pre-existing wastefill and consisted of multi-layered basal lining components, as shown in Figure 3-1. The basal lining system was mainly divided into four segments, including:

- The leachate collection layer which consisted of stones (LCS) and a porous nonwoven geotextile (GTX-1).
- The secondary leachate collection layer which comprised of gravelly sand (GS) and a porous, thick nonwoven protection geotextile (GTX-2). This layer also served as the primary protection to the hydraulic barriers.
- The leak detection layer included a sandwiched synthetic cuspate drain (CD) between two smooth-sided geomembranes, an HDPE geomembrane (GMB-1) on the top and an LLDPE geomembrane (GMB-2) on the bottom. This layer was intended to capture any leaking leachate and direct it to the leachate collection point for further treatment.
- Finally, a base preparation layer that consisted of sand and a highly reinforced and porous geotextile (GTX-3). The GTX-3 stabilized the basal foundation, underlain by the pre-existing wastefill. In addition, due to the porosity of this layer, it also acted as a gas escape layer for the underlying wastefill.

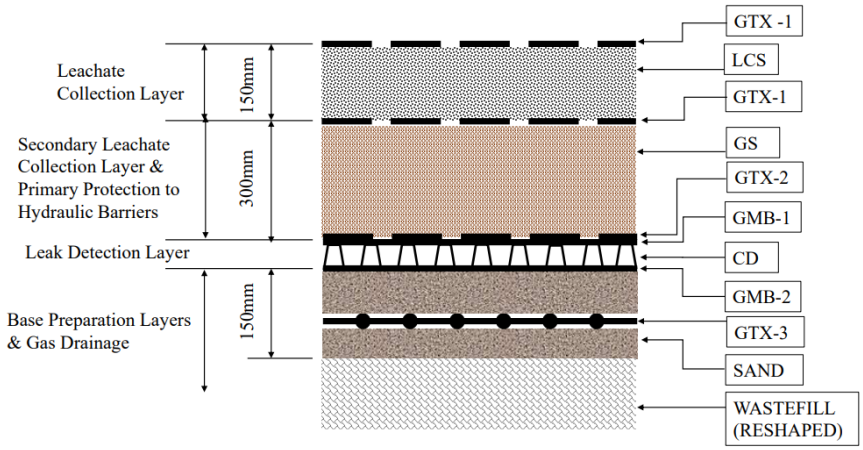

Figure 3-1: Basal Lining System for General Waste Landfill

3.3 Research Materials

3.3.1 Geosynthetics

3.3.1.1 Geotextiles

Three nonwoven geotextiles were used. These included bidim® A5 (GTX-1), bidim® A7 (GTX-2) and RockGrid®PC (GTX-3). Geotextiles perform several crucial functions in landfills, as was discussed in Section 2.3.2. Kaytech Engineered Fabrics Ltd manufactured all three geotextiles in Cape Town, South Africa. Therefore, these materials were readily and locally available. Table 3-1 shows the properties of GTX-1 & GTX-2, while Table 3-2 shows the properties of GTX-3.

Particularly for this study, GTX-1 performed a separation function between the new solid waste & the leachate collection stone (LCS) and between the LCS & gravelly sand (GS), as seen in Figure 3-1. GTX-2 fulfilled a protection function by offering cushioning to the geomembrane against the GS attributed to its thickness of 4.4mm tested under 2kPa load. In addition, both GTX-1 & GTX-2 permitted leachate filtration, allowing its easy collection and management. According to Kaytech Engineered Fabrics Ltd (2017), bidim® products, i.e., GTX-1 & GTX-2, were manufactured from 100% polyester, thereby resulting in high-performance nonwoven geotextiles whose continuous filaments were bonded by needle-punching. GTX-1 and GTX-2 were set to offer several advantages in the basal lining system, including better modulus deformation, better plastic yield stability, higher breaking strength, better resistance to high temperatures, and less sensitivity to ultraviolet (UV) light (Kaytech Engineered Fabrics Ltd, 2014). Additionally, properties such as high resistance to abrasion and piercing while retaining their thicknesses and high tensile strengths made GTX-1 and GTX-2 ideal to form part of the basal lining components as they offered the ideal cushioning protection. Moreover, their high in-plane drainage characteristics were ought to aid in dissipating the built-up pore water pressures beneath other lining components.

GTX-3 was used as a reinforcing lining component to the proposed landfill cell from the unstable pre-existing wastefill, as seen in Figure 3-1. GTX-3 was a high tensile composite reinforcing geotextile that offered characteristic performance between those of a geogrid and a woven geotextile in conjunction with hydraulic qualities of a nonwoven geotextile (Kaytech Engineered Fabrics Ltd, 2013). The nonwoven component of GTX-3 was strengthened with high tenacity multi-filament yarns, allowing the reinforcing elements to be protected during installation. GTX-3 offered an effective and lasting reinforcement effect when used in soft soils with low bearing capacities, such as the solid waste in the pre-existing wastefill where the proposed landfill cell was to be constructed (Kaytech Engineered Fabrics Ltd, 2017b).

Table 3-1: Properties of GTX-1 & GTX-2 (after Kaytech Engineered Fabrics Ltd, 2019)

Property		Units	Test Method	Geotextile Label	
				A5	A7
Material	Nonwoven, Needle-punched, Continuous Filament, Polyester Geotextile				
Mechanical Properties					
Thickness	Under 2kPa	mm	SANS 9863-1 / ISO 9863-1	2.6	4.4
Tensile Strength	Weaker Direction	kN/m	SANS 1525 / ISO 10319	17.2	35
	Elongation	%		50 - 70	
Static Puncture Strength	CBR	kN	SANS 12236 / ISO 12236	3.4	6.5
Puncture Resistance	Diameter of hole (max)	mm	SANS 13433 / ISO 13433	16	8
Trapezoidal Tear Strength	Weaker Direction	N	ASTM D4533	500	1050
Grab Strength	Weaker Direction	N	ASTM D4632	1100	2100
	Elongation	%		50 - 80	
Hydraulic Properties					
Normal Throughflow	50mm head	l/s/m^2	SANS 11058 / ISO 11058	80	45
Flow Velocity	Calculation based on throughflow & thickness	m/s		0.08	0.045
Permeability		$\times 10^{-3}$ m/s		4.2	4
In-plane Throughflow	20kPa load i=1.0	l/hr (per m width)	ISO 12958	50	80
Pore Size	$O_{95\,W}$	µm	SANS 12956 / ISO 12956	132	114

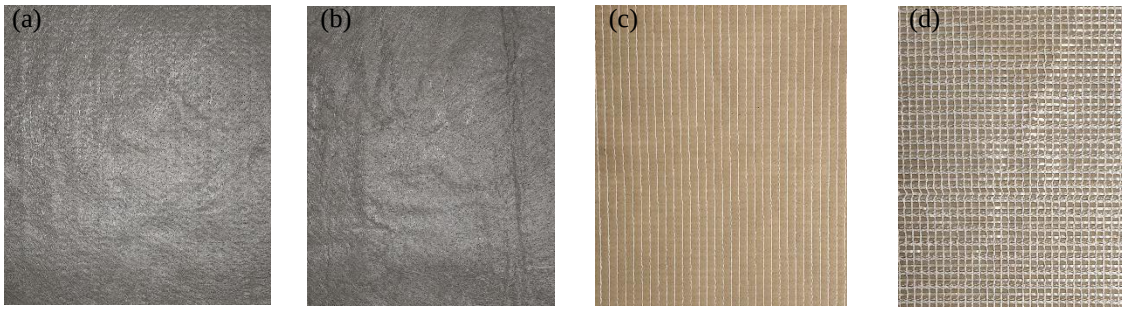

Figure 3-2: Geotextiles; (a) GTX-1, (b) GTX-2, (c) GTX-3S1 & (d) GTX-3S2

Table 3-2: Properties of GTX-3 (after Kaytech Engineered Fabrics Ltd, 2013)

Property		Units	Test Method	Values
Material	Polyester, staple fibre 150g/m^2 needle-punched, nonwoven & high strength polyester yarns			
Short Term Tensile Strength	Machine	kN/m	ISO 10319	100
	Across	kN/m		100
	Elongation	%		10
Long Term Design Strength (120years)		kN/m	ISO 10319	52
Creep Limited Strength (120years)		kN/m	ISO 13431	60
Water Flowrate	Normal to Plane	l/s/m^2	ISO 11058	150
	In Plane 20kPa	l/s/m/hr	ISO 12958	20

3.3.1.2 Geomembranes

This study utilized two smooth-sided geomembranes, i.e., 2.00mm thick HDPE geomembrane (GMB-1) and 1.5mm thick LLDPE geomembrane (GMB-2). The LLDPE geomembrane was more flexible than the HDPE geomembrane, which allowed for its easy placement and anchorage. Both geomembranes were manufactured by AKS Liner Systems (Pty) Ltd in Cape Town, South Africa.

According to AKS Lining Systems (Pty) Ltd (2015), geomembranes used in the proposed lining system were manufactured through a calendered flat-die extrusion process. Smooth geomembranes are usually deployed as containment barriers on gentle sloping containment facilities because of their weak interface shear strength properties compared to the single or double-sided textured geomembranes. Notably, when geomembranes are used adjacent to the geotextiles, a critical interface is introduced, as observed in numerous previous studies (Bacas, Cañizal & Konietzky, 2015; Qian & Koerner, 2015; Adeleke et al., 2021). The geomembranes utilized in this study formed part of the leak detection system together with the cuspate drain. In addition, due to their placement, as shown in Figure 3-1, a potentially weak shear interface was introduced. Table 3-3 summarises the properties of the geomembranes used in this study, and their surface image is shown in Figure 3-3.

Figure 3-3: Geomembranes 1 & 2 Surface Outlook

Table 3-3: Properties of Geomembranes (after AKS Lining Systems (Pty) Ltd, 2015)

Property	Units	Test Method	Min Average Values	
			GMB-2	GMB-1
Polymer Type			LLDPE	HDPE
Thickness	mm	ASTM D5199	1.5	2
Formulated Density	g/cm^3	ASTM D792 ASTM D1505	>0.94	
Carbon Black Content	%	ASTM D4218	2 to 3	2 to 3
Carbon Black Dispersion	category	ASTM D5596	cat 1 / cat 2	cat 1 / cat 2
Tensile Properties				
Yield Strength	kN/mm	ASTM D6693	22	29
Yield Elongation	%	Type IV	12	12
Break Strength	KN/m	Dogbone	40	53
Break Elongation	%		700	700
Tear Resistance	N	ASTM D1004	187	249
Puncture Resistance	N	ASTM D4833	480	640
Dimensional Stability	%	ASTM D1204	±2	
Rapid Tensile Test (300mm/min)	visual	ASTM D6693	No separation visible	
Oxidative Induction Time (OIT)				
Standard OIT	minutes	ASTM D3895	>100	
High Pressure OIT	minutes	ASTM D5885	>400	
Stress Crack Resistance (SP - NCTL)	hours	ASTM D5397 Appendix	500	
Oven Aging at 85C (retained after 90days) - ASTM D5721				
Standard OIT	%	ASTM D3895	55	
High Pressure OIT	%	ASTM D5885	80	
UV Resistance - % retained after 1600hrs - ASTM D7238				
High Pressure OIT	%	ASTM D5885	50	

3.3.1.3 Synthetic Cuspate Drain

According to Aquatan (Pty) Ltd (2017), synthetic cuspate drain (denoted as CD & trading as HI-DRAIN®) was a durable, heat-formed multiple-cuspated synthetic sheet that provided a high capacity and non-restricted drainage path that was compatible with GMB-1 & GMB-2. The cusps of the CD were symmetrical; hence they provided high resistance to crushing when exposed to heavy loads. Additionally, the synthetic cuspate drain was manufactured primarily from HDPE resins; as a result, it offered the same life expectancy as the HDPE geomembrane used (Aquatan (Pty) Ltd, 2017). The synthetic cuspate drain formed part of the leak detection layer for the basal lining system of the proposed landfill cell. The CD's properties are provided in Table 3-4, with images shown in Figure 3-4.

Table 3-4: Properties of Synthetic Cuspate Drain (after Aquatan (Pty) Ltd, 2017)

Property	Unit	Test Method	Values	
Classification	-	-	Hi-Drain 750	
Sheet thickness	mm	-	0.75	
Physical Properties				
Colour	-	-	Black	
Type	-	-	Cuspate, 7×7:4	
Material	-	-	HDPE	
Density	g/m^3	ASTM D792	>958	
Cuspate Height	mm	-	4	
Cuspate Centres	mm	-	6 to 7	
Carbon Black Content	%	ASTM D4218	1.5 to 2.6	
Mechanical Properties				
Strength at Yield	N/mm	-	MD 12.0 / TD 11.4	
Elongation at Yield	%	-	MD 15.0 / TD 15.0	
Strength at Break	N/mm	-	MD 13.0 / TD 12.1	
Elongation at Break	%	-	MD 300 / TD 300	
Puncture Resistance	N/mm	ASTM D4833	200	
Compressive Yield Strength	kPa	ASTM D1621	1200	
In-Plane Waterflow			HG=1	HG=0.1
At 200kPa	LPM/meter	ASTM D1621	65	18
At 500kPa	LPM/meter		60	17
At 1000kPa	LPM/meter		65	15
With hard contact surfaces to simulate structural drainage applications				
Compressive Creep Strain @ 500kPa/100years	%	ASTM D7361	12	
High Strength OIT	mm	ASTM D5885	200	
Resistance to microbes	-	-	No significant effect	
Compatibility with Geomembranes	-	-	Fully compatible	
Health, Safety, Environment	-	-	Inert	

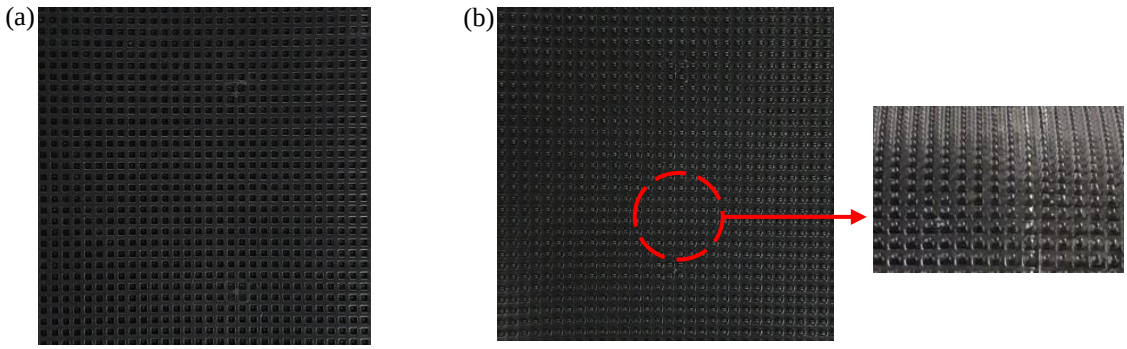

Figure 3-4: Synthetic Cuspate Drain (CD); (a) Smooth side & (b) Cusps side

3.3.2 Geomaterials

This study utilized three geomaterials: sand, gravelly sand (GS), and a stone layer referred to as leachate collection stone (LCS). Each geomaterial was delivered in excess of 150kg to cater for all the interface shear tests conducted. The gravelly sand and leachate collection stone were products of crushed building waste materials (also known as builder's rubble). They were readily available in the old section of the landfill where the builder's rubble was disposed of. The use of these geomaterials was motivated by their availability, the need to reuse building waste, and their high permeability, allowing easy leachate collection from the proposed landfill cell and easy landfill gas release from the pre-existing overlying wastefill. The mechanical properties for these geomaterials and the appropriate test methods used are presented in Table 3-5, and their images are shown in Figure 3-5. The mechanical properties presented in this study were all conducted in the Geotechnical Engineering Laboratory at the University of Cape Town.

According to the dry sieving results shown in Figure 3-6, the sand presented mainly medium particles at 49% and fine particles at 48%, while gravelly sand comprised 24% fine gravel, 11% coarse, 41% medium and 22% fine sands. According to the USCS, the sand was classified as Poorly graded Sand (SP), while the gravelly sand was classified as Poorly graded Sand with gravel (SP with Gravel). The leachate collection stones comprised coarse gravel at 100% with a USCS classification as Poorly graded Gravel (GP). These indicator properties confirmed that these geomaterials were highly permeable due to their particle size range and would therefore perform the intended functions as per the proposed landfill cell's requirements (DWAF, 1998; DEA, 2013).

In terms of dry density - optimum moisture relationships for the two soils, as shown in Figure 3-7, the sand presented a maximum dry density (MDD) of 1.77Mg/m^3 at an Optimum Moisture Content (OMC) of 3.8%. The gravelly sand (GS) presented an MDD of 2.12Mg/m^3 with an OMC of 7.6%, and no compaction test was conducted for the leachate collection stone (LCS).

Figure 3-5: Geomaterials; (a) Sand, (b) Gravelly Sand & (c) Leachate Collection Stone

Table 3-5: Mechanical properties of geomaterials

Property	Units	Test Method		Sand	GS	LCS
Specific Gravity, G_s	-	Small pycnometer	BS 1377: Part 2: 1990	2.67	2.64	-
Cohesion (c')	kPa	Direct Shear Test	ASTM D3080	0.0	0.0	-
The angle of Internal Friction (ϕ')	°			35.18	35.55	-
Optimum Moisture Content (OMC)	%	Standard Proctor	BS 1377: Part 4: 1990	3.8	7.6	-
Maximum Dry Density (MDD)	Mg/m^3			1.77	2.12	-
Particle Size Distribution						
Coarse Gravel (75 - 19 mm)	%	Dry Sieving	BS 1377: Part 2: 1990	0	0	100
Fine Gravel (19 - 4.75 mm)				0	24.78	0
Coarse Sand (2.00 - 4.75 mm)				1.93	11.31	0
Medium sand (0.425 - 2.00 mm)				49.26	41.27	0
Fine Sand (0.075 - 0.425 mm)				48.75	22.62	0
Silt (0.002 - 0.075 mm)				0.06	0.04	0
Clay (<0.002 mm)				0	0	0
Coefficient of Uniformity (C_u)				2.13	4.67	1.03
Coefficient of Curvature (C_c)				1.09	0.60	1.00
USCS Classification			ASTM D2487	SP	SP with Gravel	GP

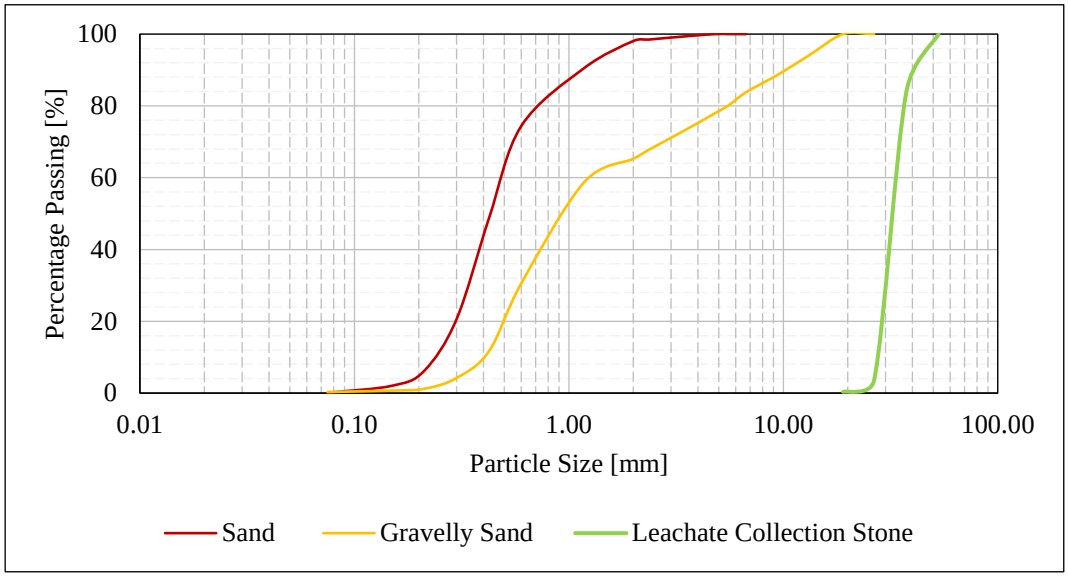

Figure 3-6: Grain size distribution

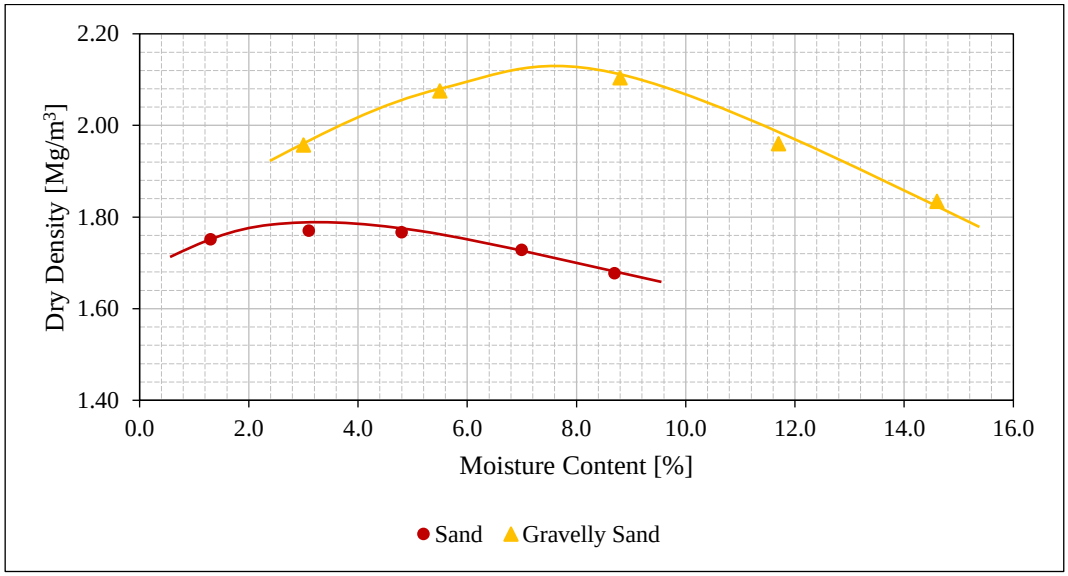

Figure 3-7: Dry density – moisture content relationship for Sand & Gravelly Sand

3.4 Testing Apparatus & Equipment

3.4.1 *ShearTrac-III* Large Shear Apparatus

The equipment used to conduct all interface shear tests in this research was *ShearTrac-III* Large Shear Apparatus (LSA). This equipment was designed and manufactured by Geocomp Corporation from the USA and was assembled in the Geotechnical Engineering Laboratory at the University of Cape Town. The device was fully automated and could conduct consolidated

drained direct shear tests for soils and interface shear tests for soil-geosynthetic and geosynthetic-geosynthetic interactions. It was also able of conducting internal shear strength tests of GCLs. According to Geocomp (2018), the equipment conducted tests according to standards such as AASHTO T236, BS 1377-7 and ASTM D3080, D5321 & D6243.

ShearTrac-III LSA consisted of mainly two shear boxes: the upper static shear box with dimensions 305mm×305mm×100mm and the lower movable shear box with dimensions 460mm×355mm×100mm. The lower box was loaded in a water bath box primarily for the hydration of samples during testing. The equipment also contained two load cells, i.e., horizontal for shear and vertical for normal forces with their displacement transducers. The *ShearTrac-III* LSA was complemented by a computer unit that hosted similar equipment controls as the machine itself and showed the progress of the test in real-time using graphical displays. According to Geocomp (2018), the equipment had a loading capacity of up to 160kN vertically and 115kN horizontally. Its displacement transducers could measure up to ±45mm range with a 0.002mm resolution and produced accurate displacement rates from 0.00003mm/min to 7.5mm/min (Geocomp, 2018).

Consequently, the *ShearTrac-III* LSA fulfilled all the minimum requirements stipulated in the ASTM D5321 & D6243 standards for soil-geosynthetic interface shear strength assessments geosynthetic-geosynthetic interactions. Moreover, this equipment has been used previously by scholars such as Buthelezi (2017), Sikwanda (2018), Adeleke (2020) and Muluti (2021), who all produced reliable interface shear results in their works. Figure 3-8 shows the 305mm×305mm×205mm *ShearTrac-III* Large Shear Apparatus used.

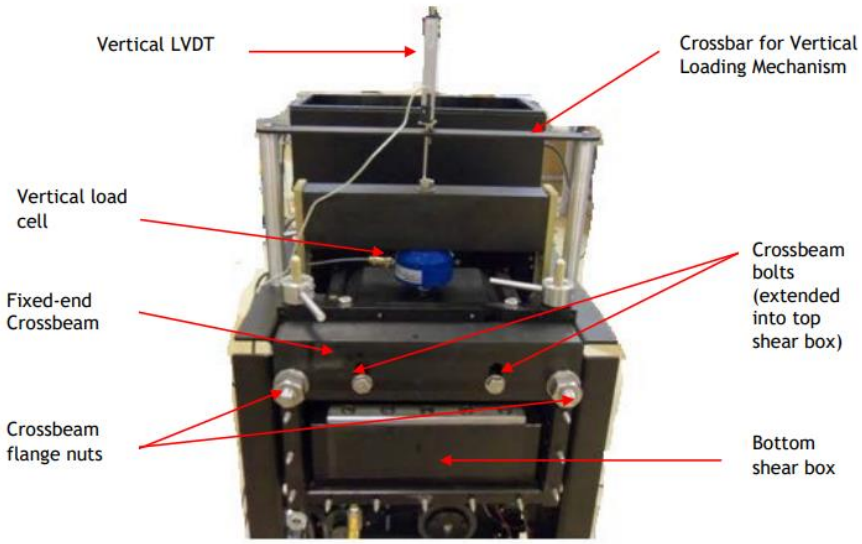

Figure 3-8: *ShearTrac-III* Large Shear Apparatus (after Geocomp, 2018)

3.5 Test Preparations

3.5.1 Specimen Preparation

3.5.1.1 Geosynthetics

In this study, geosynthetic samples were prepared with the aid of the following tools, also shown in Figure 3-9:

- A pair of scissors for cutting all geotextile specimens to their required dimensions.
- Mechanical saw machine for cutting geomembrane and synthetic cuspate drain specimens to their required dimensions. The motivation for using a mechanical saw machine was due to the high tear resistances offered by the specimens.
- A hammer & 6.36mm puncher for making clamping holes in the geosynthetic specimens.
- A rachet for fixing geosynthetic specimens in either lower or upper shear box using bolts and clamps.

Figure 3-9: Geosynthetic preparation tools; (a)A pair of scissors, (b) Hammer and puncher, (c) Rachet, & (d) Mechanical saw machine

For geosynthetics such as geotextiles, geomembranes and synthetic cuspate drain, preparations followed instructions from the ASTM D5321. All geosynthetic specimens used in this study were cut from the supplied geosynthetic rolls and dimensioned to the sizes applicable in the LSA, i.e.,

300mm×420mm for the upper shear box and 300mm×520mm for the lower shear box. The accuracy of ±0.5mm was aimed for during this exercise. This ensured sufficient area coverage in the shear boxes; as a result, no area correction was necessary during the processing of results. Additionally, specimens with excessive wrinkles or any serious damage for the case of geotextiles were eliminated and thus, were never used in any interface tests. For geomembranes, special care was taken during sample preparation to minimize the effects of creating surface irregularities or abrasions. All specimens were labelled for easy identification before and after the interface shear tests.

Depending on the testing configuration and whether a geosynthetic specimen was to be clamped on the LSA, five 10mm diameter holes were created. These holes were created at 30mm from the short edge of the geosynthetic with a spacing of 60mm centre to centre. Tools such as the hammer and puncher were used for this purpose. The holes were primarily to enable the clamping of geosynthetic specimens onto the LSA, as shown in Figure 3-10. The clamping of geosynthetics on the LSA replicated an anchorage condition in the field and ensured that failure occurred at the intended predetermined weaker surface. Furthermore, to ensure field placement conditions of the geosynthetics were replicated, machine direction (MD) was used as the direction of shearing.

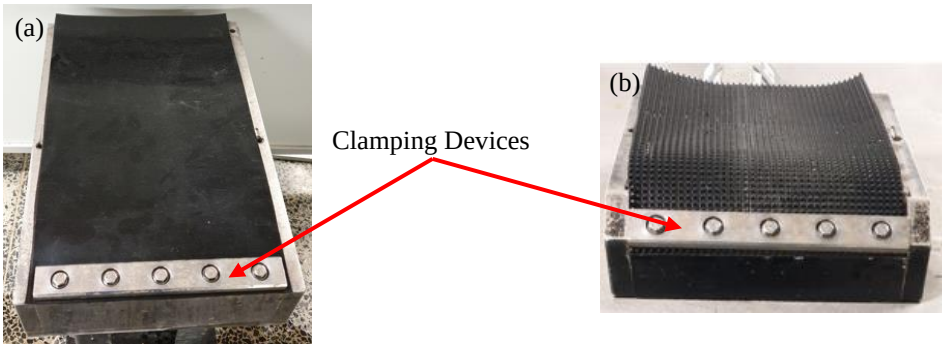

Figure 3-10: Clamping Mechanism in (a) Lower Shear Box & (b) Upper Shear Box

3.5.1.2 Geomaterials

This study's geomaterials were prepared following the ASTM D5321 standard. Representative samples from the field were first oven-dried at 110°C for a minimum of 16hrs since they were coarse-grained soils and contained no clay particles. They were then left to cool for about 2hrs. A weighing scale was used to measure the required masses in the ranges of 2.8 to 4 kgs for the three layers that were to be compacted in the shear boxes, depending on the target density required. These three soil samples were then thoroughly mixed with fresh tap water using a mechanical mixer. The soils were poured into the top shear box for single interface configurations and compacted to the required density. Consequently, for some double interface tests, the soils were placed either on top and bottom shear boxes or just on the top shear box, after which they were well compacted to their target densities. For the LCS, no compaction was conducted; however, to achieve the maximum possible density, the placement of stones in the shear boxes ensured that minimal gaps were present.

A 20mm thick solid steel plate (300mm×300mm) with a hand tamper and a drop weight of 4kg at the height of 300mm, was used for soils compaction purposes in this study. Figure 3-11 shows the compacting tool used.

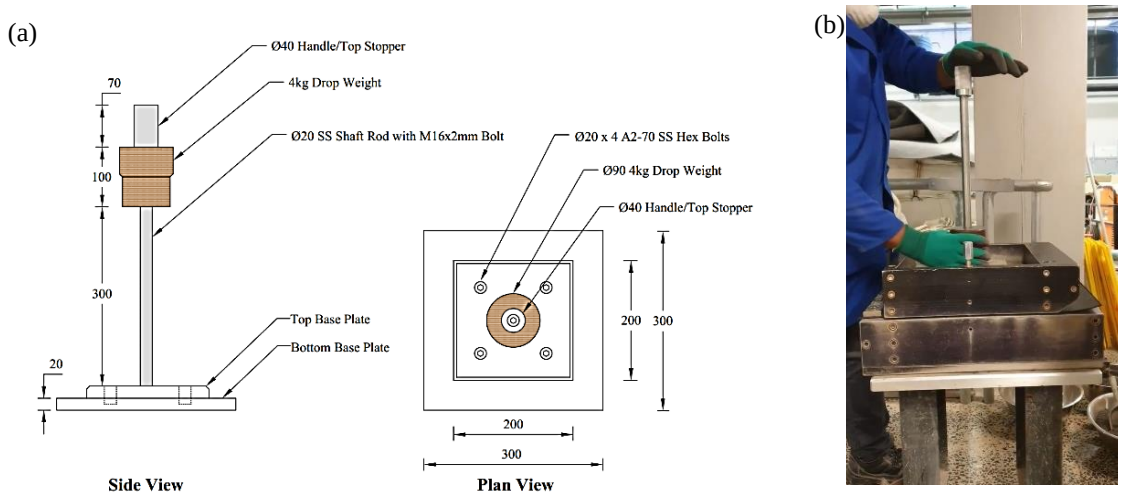

Figure 3-11: Hand Tamper Compactor (after Muluti, 2021)

3.5.2 Testing Configurations

3.5.2.1 Single Interface Configuration

Two scenarios existed in the single interface configuration: soil-geosynthetic and geosynthetic-geosynthetic interface testing. Table 3-6 summarises the specimen setups for single interface shear tests

As illustrated in Figure 3-12, the geosynthetic component was clamped on the lower shear box for soil-geosynthetic interface testing. In addition, the soil was compacted to the target density in the upper shear box after its alignment with the bottom shear box using alignment screws. The soil placement in the upper shear box is followed in Section 3.5.1.2.

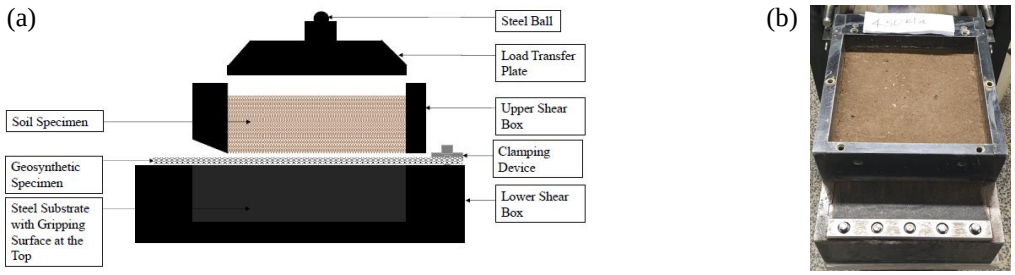

Figure 3-12: Soil-Geosynthetic Testing Configuration

In the case of geosynthetic-geosynthetic interface shear testing, as shown in Figure 3-13, the prepared geosynthetic samples for the respective interface test were clamped on the upper and lower shear boxes. A geosynthetic specimen with dimensions 300mm×520mm was placed and

clamped on the lower box, while that of dimensions 300mm×420mm was placed and clamped on the upper shear box.

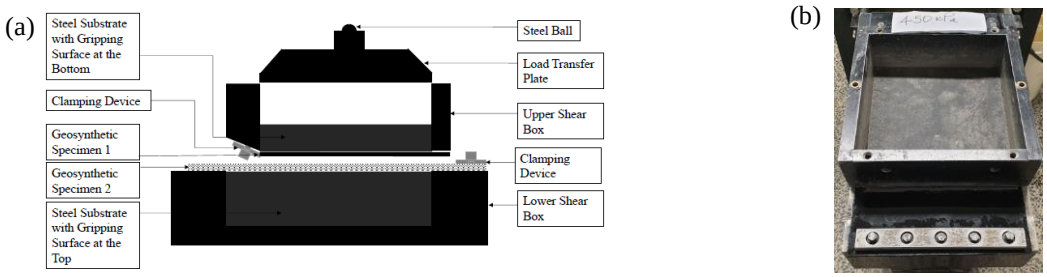

Figure 3-13: Geosynthetic-Geosynthetic Testing Configuration

Table 3-6: Summary of single interface testing arrangement

Type	Lining Component			
	Upper Shear Box		Lower Shear Box	
	Name	Dimensions [mm]	Name	Dimensions [mm]
Basal	LCS	n/a	GTX-1	300 × 520
	GTX-1	300 × 420	GS	n/a
	GS	n/a	GTX-2	300 × 520
	GTX-2	300 × 420	GMB-1	300 × 520
	GMB-1	300 × 420	CD	300 × 520
	CD	300 × 420	GMB-2	300 × 520
	GMB-2	300 × 420	SAND	n/a
	SAND	n/a	GTX-3S1	300 × 520
	GTX-3S2	300 × 420	SAND	n/a

3.5.2.2 Double Interface Configuration

Three scenarios existed in the double interface testing configuration: soil-geosynthetic-soil, soil-geosynthetic-geosynthetic and geosynthetic-geosynthetic-geosynthetic, as summarized in Table 3-7. Notably, specimen preparation and methodology for double interface configuration were similar to those used in the single interface configuration. The only modification was the addition of one specimen to the setup. The primary purpose of adding a third lining component in the test setup was to allow failure to occur at the weakest interface of the two interfaces and fulfil the objectives set out for this study. The three specimens did not require a significantly large shear gap between the two boxes compared to if it could have been a multi-layered interface shear test. This provided a clear and correct observation of multi-layer interface shear testing through a double interface configuration.

In soil-geosynthetic-soil interface testing, as illustrated in Figure 3-14, the individual soil specimen was first placed in the lower shear box and compacted to the target density following procedures in Section 3.5.1.2, with the final level exceeding the shear box by 1mm to allow for consolidation during the test. The geosynthetic specimen with dimensions 300mm×420mm was then gently placed on top of the lower box without any clamping mechanisms. Finally, the upper shear box was attached to the lower box using alignment screws, after which the respective soil/stone was placed and compacted to the target density as well. The loading transfer plate was then placed, and an assemblage of the whole equipment subsequently followed.

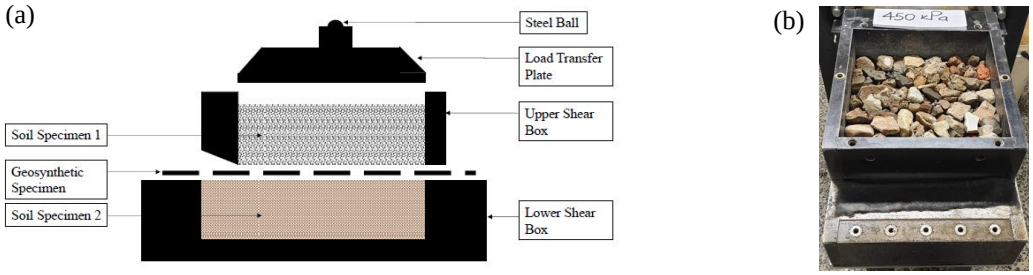

Figure 3-14: Soil-Geosynthetic-Soil Testing Configuration

A similar approach was used for the soil-geosynthetic-geosynthetic interface testing, as seen in Figure 3-15, except a geosynthetic was placed on top of the lower box to replace the soil. The geosynthetic sat on top of sandpaper attached to a heavy-duty steel plate substrate and was clamped on one end using bolts and a clamping device. The middle geosynthetic was placed freely, while the soil in the upper shear box was compacted to its target density.

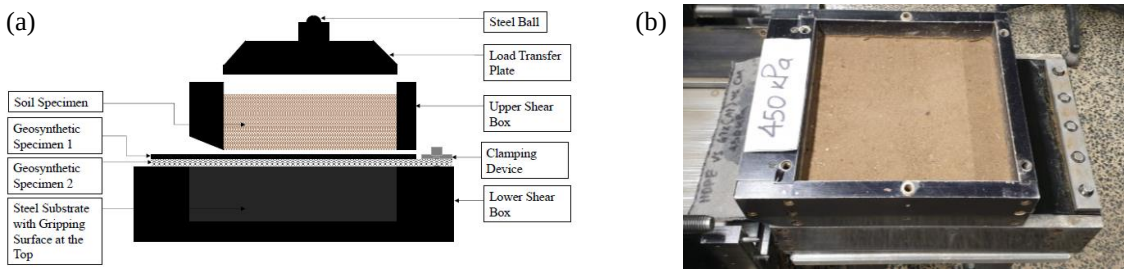

Figure 3-15: Soil-Geosynthetic-Geosynthetic Testing Configuration

For a geosynthetic-geosynthetic-geosynthetic interface testing, as seen in Figure 3-16, two geosynthetics were placed and clamped on one of the ends of the upper and lower shear boxes. In addition, one geosynthetic was placed freely in the middle. The bottom geosynthetic sat on top of the sandpaper, and a steel plate covered the top geosynthetic with sandpaper attached to it. This was crucial as it limited specimens' slippage against the steel plates, allowing failure to occur at either interface with the weakest friction properties.

(a)

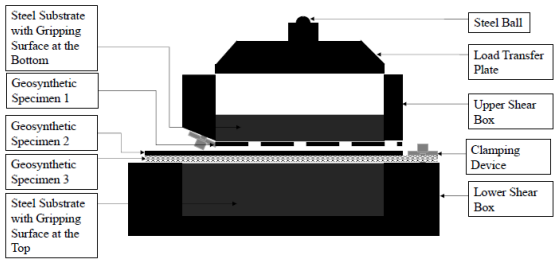

(b)

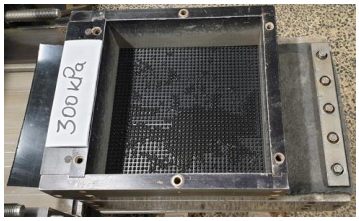

Figure 3-16: Geosynthetic-Geosynthetic-Geosynthetic Testing Configuration

Table 3-7: Summary of double interface testing arrangement

Type	Lining Components					
	Upper Shear Box		Middle		Lower Shear Box	
	Name	Dimensions [mm]	Name	Dimensions [mm]	Name	Dimensions [mm]
Basal	LCS	n/a	GTX-1	300 × 420	GS	n/a
	GS	n/a	GTX-2	300 × 420	GMB-1	300 × 520
	GTX-2	300 × 420	GMB-1	300 × 420	CD	300 × 520
	GMB-1	300 × 420	CD	300 × 420	GMB-2	300 × 520
	CD	300 × 420	GMB-2	300 × 420	SAND	n/a
	SAND	n/a	GTX-3	300 × 420	SAND	n/a

3.5.3 Final Assemblance

Once the setup was completed, the final assemblage was conducted before initiating the tests. This involved covering the top shear box with a 300mm×300m×22mm 10kg steel plate, which distributed the normal loading received through a 26.6mm diameter ball mass of 79g from the *ShearTrac-III* loading frame. The assembly ensured that the two shear boxes were properly transferred to the *ShearTrac-III* mainframe and fixed using two steel reaction beams to limit horizontal and vertical movement, as shown in Figure 3-17. These beams would hold the upper shear box during the shearing phase and ensure that the lower bottom box's movement was orchestrated. The vertical loading cell was then lowered until it just touched a load-bearing ball present on the shear box cover, after which two aligning screws that held the two shear boxes together to prevent any slippage during assemblage were removed.

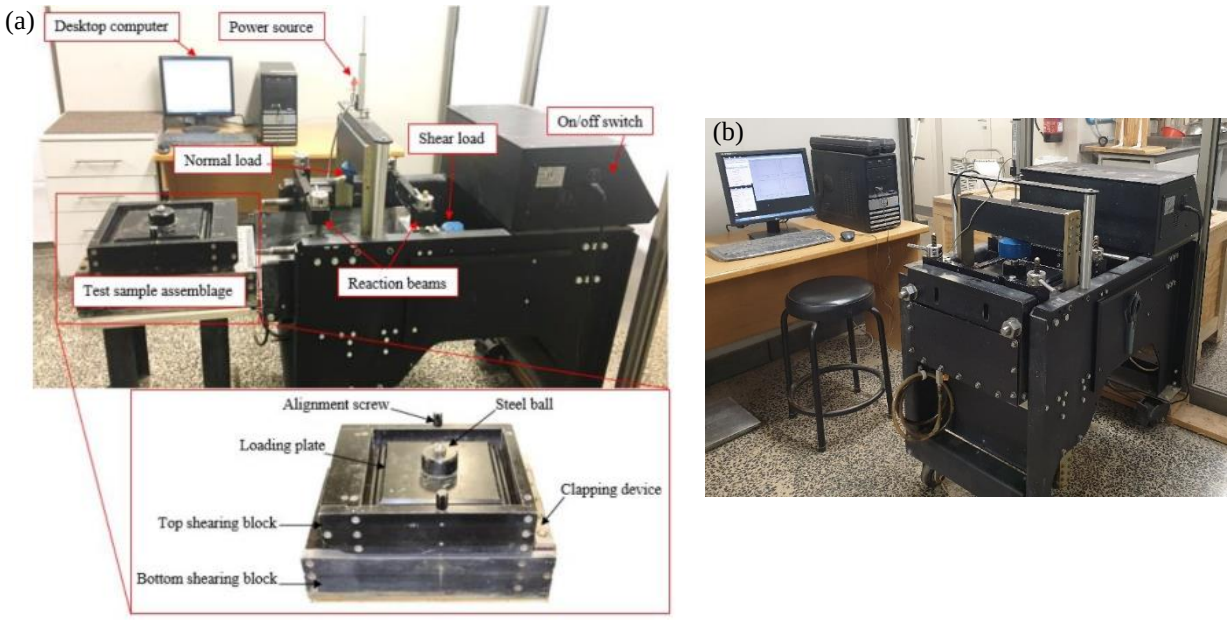

Figure 3-17: Assemblage of *ShearTrac-III* Large Shear Apparatus (after Sikwanda, 2018)

3.6 Testing Procedures

After the sample had been loaded onto the *ShearTrac-III* Large Shear Apparatus housing unit, the complementary software in the computer unit known as the DS program was opened. The conditions for the tests were then inserted. These conditions included the amount of normal stress, the shearing displacement rate, maximum horizontal displacement, and consolidation times of the tested specimens. Finally, the system monitor window was opened along with the calibration summary window. The vertical and horizontal load cells were correlated by copying the system monitor offset values to the calibration summary.

Tests were run for the basal lining components at normal stresses of 150, 300 and 450 kPa following the anticipated field loading conditions from the proposed landfill cell. The choice of the normal stresses also conformed to the ASTM D5321 standard, which stated that a minimum of three normal pressure must be used to establish a Mohr-Coulomb failure criterion. Additionally, a faster shearing rate of 1.0mm/min was used for all the basal lining components as they did not incorporate any clay or GCL material. Moreover, the choice of the shearing rate followed the recommendations in the previously mentioned ASTM standards, ensuring that any excess pore pressure build-ups that would interfere with the interface shear results were nullified.

The shearing displacement of 75mm was used for all interface shear tests in this study. The maximum horizontal displacement of 75mm that the *ShearTrac-III* LSA could offer was interpreted as large displacement (LD) shear strengths. In addition, the transducers (vertical and horizontal) were correlated for every test conducted to produce consistency in the measured

values. The manufacturer conducted the calibration of the entire *ShearTrac-III* equipment before testing had begun. Therefore, it was established that the measured values were acceptable according to the capability of the equipment.

A 30minutes consolidation time was adopted in this study for the basal lining components (Geocomp, 2018; Muluti, 2021). This time was also sufficient to allow specimens and gripping surfaces to engage fully and establish an intimate interaction (Stark, Niazi & Keuscher, 2015). Additionally, this time catered for the expulsion of any built-up pore pressures before the shearing phase could begin. Concurrently, fresh tap water was added to the basin within the LSA equipment to hydrate samples. For all the basal lining components, a hydration time of 30minutes was adopted to simulate full hydration conditions in the field. The hydration of all specimens was implemented at their respective normal stresses.

After completing the consolidation and hydration phases, the shearing phase began. A gap of approximately 1mm to 3mm was created between the upper and lower shear boxes by raising the reaction beams. This was necessary to prevent the resulting friction between the two shear boxes and allowed the measured frictional properties to be at the intended surfaces (Geocomp, 2018). While the applied normal force remained constant, the shear force was applied through a horizontal load cell on the lower shear box to establish shear stress. This enabled the lower shear box to move horizontally relative to the upper shear box at a 1.0mm/min specified shearing rate. The DS software embedded in the computer unit recorded all crucial results, such as the vertical displacements, horizontal displacements, normal forces, and shear forces against time. All interface shear tests were automatically terminated when the horizontal displacement of 75mm was reached.

3.7 Testing Program

A total of 51 single and double interface shear tests were conducted to achieve the objectives of this study. The tests encapsulated the basal lining system for the proposed landfill cell in the Western Cape Province, South Africa. Table 3-8 summarises all lining components tested with the respective conditions followed.

Table 3-8: Testing Schedule

Type	Interface Configuration		Testing Conditions				No.
			Hydration & Consolidation Phase		Shearing Phase		
			Duration [mins]	Normal Pressure [kPa]	Shearing Rate [mm/min]	Duration [mins]	
Basal	Single-	LCS | GTX-1	60	150 | 300 | 450	1	75	3
		GTX-1 | GS	60	150 | 300 | 450	1	75	3
		GS | GTX-2	60	150 | 300 | 450	1	75	3
		GTX-2 | GMB-1	60	150 | 300 | 450	1	75	3
		GMB-1 | CD	60	150 | 300 | 450	1	75	3
		CD | GMB-2	60	150 | 300 | 450	1	75	3
		GMB-2 | SAND	60	150 | 300 | 450	1	75	6
		SAND | GTX-3S1	60	150 | 300 | 450	1	75	3
		GTX-3S2 | SAND	60	150 | 300 | 450	1	75	3
	Double-	LCS | GTX-1 | GS	60	150 | 300 | 450	1	75	3
		GS | GTX-2 | GMB-1	60	150 | 300 | 450	1	75	6
		GTX-2 | GMB-1 | CD	60	150 | 300 | 450	1	75	3
		GMB-1 | CD | GMB-2	60	150 | 300 | 450	1	75	3
		CD | GMB-2 | SAND	60	150 | 300 | 450	1	75	3
		SAND | GTX-3 | SAND	60	150 | 300 | 450	1	75	3
						Tests	**51**

3.8 Data Processing

3.8.1 Shear Results Processing

After completing the interface shear tests, the results recorded by the computer unit using the DS software were exported to a Microsoft Excel file with a similar template for further analysis. The analysis included interpreting results by plotting vertical displacement graphs against time, shear stress against horizontal displacement, and shear stress against normal stress to establish failure envelopes. Ultimately, interface shear strength parameters were derived.

3.8.2 Failure Envelope Criterion

For this study, Mohr-Coulomb failure criteria were developed from plots of shear-normal stress relationships. Peak and large displacement (LD) shear strength values and their respective normal stresses were used to determine peak and LD shear strength parameters. A linear envelope related to Equation 3-1 was utilized. However, if the coefficient of regression (R^2 value) was lower than 0.98, then a curvilinear failure envelope was adopted and was related to a hyperbolic function represented by Equation 3-2.

$$\tau = c_a + \sigma_a \tan\delta \quad \textbf{Equation 3-1}$$

$$\tau = a\sigma_n^2 + b\sigma_n + c_a \quad \textbf{Equation 3-2}$$

Where:

τ = Peak or LD shear strength

c_a = Apparent adhesion

σ_n = Applied normal pressure

δ = Interface friction angle

a & b = Hyperbolic functions

The adoption of a curvilinear or non-linear approach was motivated by other studies, such as those by Bacas, Cañizal & Konietzky (2015) & Muluti (2021), who observed that linear failure envelopes do not explicitly apply to some soil-geosynthetic interface tests and thus strengths determined could not be used to define the interface shear strength parameters. Through Equation 3-2, interface shear strength parameters may be determined using a linear approximation where; a straight tangent line was drawn at a normal stress of interest to obtain the interface shear strength parameters. In this case, a y-axis intercept would still represent an apparent adhesion, while the tangent's angle to the horizontal would represent an interface angle of friction. The average of all interface shear strengths at normal stress levels of interest was conducted to obtain the overall interface shear strength parameters (Adeleke, 2020).

3.9 Quality Assurance

3.9.1 Actions Implemented

To minimize experimental errors and ensure the quality of results obtained in this study, the following actions were taken during all interface shear tests conducted:

i Test preparations, setups and procedures described in Section 3.5 were consistently followed for each interface test conducted to ensure coherence and repeatability of results.

ii For each interface test conducted, new geosynthetic specimens were used. The preparation of these geosynthetics ensured that they conform to the machine direction (MD) and this study's descriptions. All interface shear tests were conducted according to ASTM D5321.

iii For soil specimens, maximum quality control was ensured through using clean containers during sample preparations after being oven-dried at 110°C in the ovens for at least 16hrs. The moisture content required to achieve the soil's target densities was accurately measured, and mixing was consistent throughout the tests.

iv According to proposed landfill cell requirements, the stone sizes for the LCS layer were continuously monitored by conducting sieve analysis before test setup to ensure that only the specified sizes, i.e., 38 to 50 mm, were used in the LSA.

v Fresh tap water from the geotechnical engineering laboratory at a normal temperature of 23.5°C was used for each interface test. No recirculation of tap water was done to ensure that effects resulting from hydration were similar throughout all experiments. Before hydration, the water basin in the lower shear box was thoroughly cleaned.

vi According to ASTM D5321, all interface tests were conducted under similar physical conditions, i.e., the temperature in the laboratory was retained at 22°C, and consistent humidity levels ranged from 50% to 70%.

vii To ensure that reliable results were produced, the routine calibration of the *ShearTrac-III* LSA was conducted by Geocomp Corporation personnel, while routine correlation of software values to match the machine values was continuously done at the beginning of each interface test.

3.9.2 Repeatability of Results

A repeatability assessment to ensure the coherence and consistency of the measured results for single and double interface shear tests was conducted for this study. It involved repeating similar tests under the same testing conditions to establish the differences due to human error or equipment. For this study, the repeated tests were those of GMB-2 | SAND interface for single interface configuration and GS | GTX-2 | GMB-1 interface for double interface configuration. Figure 3-18 represents the shear stress against horizontal displacement for these interfaces. These interfaces (single & double) exhibited similar shear stress responses. Additionally, a further assessment to establish percentage differences was conducted as presented in Table 3-9 for verification purposes.

A percentage difference (%D) assessment of the mobilized peak and LD shear strengths, herewith implemented using Equation 3-3 according to Adeleke (2020) & Muluti (2021), was capped at 10% as an upper limit. This meant that for an interface shear test result to be valid, the percentage difference had to be lower than 10%.

$$\text{Percentage Difference (\%D)} = \frac{(E_1 - E_2)}{\left(\frac{E_1 + E_2}{2}\right)} \qquad \textbf{Equation 3-3}$$

Where:

E_1 = First experimental measured value

E_2 = Second experimental measured value

As shown in Table 3-9, the minimum and maximum percentage differences in the peak interface shear results were 1.2% and 9.3%, respectively, while those for the LD interface shear strengths were 0% and 5.2%. Since the percentage differences for the sampled tests were all under 10%, it was deemed that the experimental procedure was reproducible and repeatable. For other non-sampled tests, this meant that the interface shear tests conducted will likely be within the maximum allowable percentage deviation from the mean value and will contain minimal errors unless the experimental procedure is negligently not kept consistent.

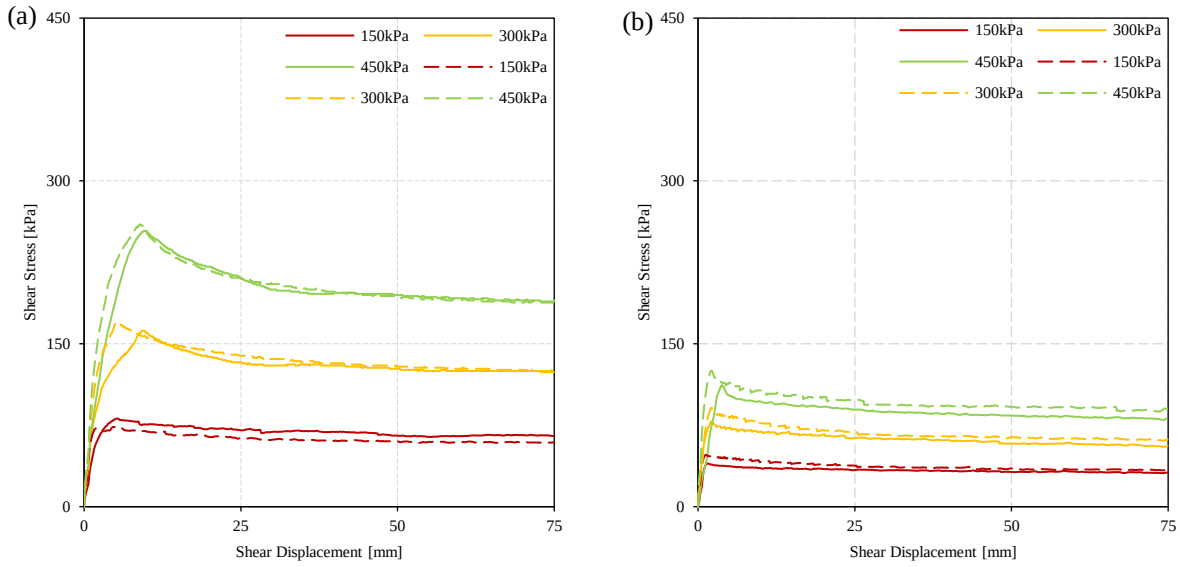

Figure 3-18: Shear stress - horizontal displacement relationships for: (a) Single interface (SAND | GMB-2) & (b) Double interface (GS | GTX-2 | GMB-1)

Table 3-9: Repeatability analysis of selected interface shear tests

Interface Configuration		Applied Normal Stress	Peak Shear Stress	Mean Peak Shear Stress	Deviation from Mean Peak Shear Stress		LD Shear Stress	Mean LD Shear Stress	Deviation from Mean LD Shear Stress	
		kPa	kPa	kPa	kPa	%	kPa	kPa	kPa	%
Single-	SAND | GMB-2	150	81.1	77.4	-3.8	4.8	65.0	62.1	-2.9	4.7
			73.6		3.8	4.8	59.2		2.9	4.7
		300	162.0	166.0	4.0	2.4	124.0	124.0	0.0	0.0
			170.0		-4.0	2.4	124.0		0.0	0.0
		450	254.0	257.0	3.0	1.2	190.0	189.5	-0.5	0.3
			260.0		-3.0	1.2	189.0		0.5	0.3
Double-	GS | GTX-2 | GMB-1	150	39.7	43.8	4.1	9.3	31.7	33.2	1.5	4.4
			47.8		-4.1	9.3	34.6		-1.5	4.4
		300	78.6	84.9	6.3	7.4	55.9	59.0	3.1	5.2
			91.1		-6.3	7.4	62.0		-3.1	5.2
		450	112.0	118.5	6.5	5.5	81.2	85.5	4.3	5.0
			125.0		-6.5	5.5	89.8		-4.3	5.0

4 Results & Discussion

4.1 Introduction

This chapter presents all the results of the interface shear tests conducted through single and double interface configurations for the basal lining system of the proposed MSW landfill cell. The presentation begins with the shear stress - horizontal displacement relationships, critically examined through peak and large displacement (LD) strength developments. After testing, specimens' assessment seconded these examinations and the variation of dry densities before and after the test, vertical displacements - time relationships of soils and integration of previous similar works by other scholars. The peak and LD interface shear strengths were further assessed with the applied normal stresses through shear - normal stress relationships, also called failure envelopes. As a result, these enabled the determination of the interface shear strength parameters from the two testing configurations. Finally, a critical interface that essentially governed the design of side-slopes in MSW landfills was assessed.

4.2 Shear Stress - Horizontal Displacement Relationships

4.2.1 Introduction

This section exhibits all the shear stress - horizontal displacement relationships for interface shear tests conducted in this study for both single and double interface configurations. All interface shear tests were performed using the *ShearTrac-III* large shear apparatus (LSA) at applied normal pressures of 150, 300 & 450 kPa. Other testing conditions included; submergence of all lining components in fresh tap water during the duration of the test and a shearing rate of 1mm/min to allow expulsion of any developed excess pore pressures (ASTM, 2020a,b). Furthermore, 1hour hydration and consolidation period was used as it was deemed sufficient to engage the lining components before shearing (Stark & Choi, 2004).

The results are presented under their respective interfaces to observe the differences in the two testing configurations. Additionally, other testing parameters, including vertical displacement - time relationships, especially for tests involving soils, and density changes before and after the interface shear tests, are included to explain the scenarios better. A quantitative summary of the peak and LD strengths at their respective horizontal displacements is also included in a tabular format.

4.2.2 Basal Lining System Assessment

4.2.2.1 LCS | GTX-1 | GS Interface

Three lining components were utilised in this interface shear set. These included leachate collection stone (LCS) comprising of mixed builder’s rubble stones of between 38 to 50 mm

particle size range; protection geotextile type 1 (GTX-1) in the form of nonwoven needle-punched geotextile with a nominal thickness of 1.425mm (as measured in the lab) made from primarily recycled polyester (PET); and crushed gravelly sand material (GS) with D_{50}=0.85mm, obtained from recycled crushed building waste material. In terms of the test setup, single interface configurations included the LCS (lightly compacted in the upper shear box) sheared against GTX-1 (clamped on the lower shear box) and GTX-1 (secured once again on the lower shear box) sheared against GS (compacted to 95%MDD in the upper shear box). For the double interface configuration, GS (compacted to 95% MDD in the lower shear box), GTX-1 (freely sitting on top of GS) and LCS (lightly compacted & levelled in the upper shear box) were sheared concurrently. The placement of GS in the lower shear box instead of a heavy-duty steel substrate was for practical purposes following the arrangement of lining components in the proposed landfill cell. Other scholars, such as Lopes & Silvano (2010), deemed the method to be acceptable.

In the single interface configuration, the development of peak shear stresses was observed to be more prevalent, notably, in Figure 4-1 (a) & (b), than in the double interface configuration, as seen in Figure 4-1 (c). For the case of the LCS | GTX-1 interface, for example, peak shear stresses were mobilised at relatively lower horizontal displacements of <30mm, while the GTX-1 | GS interface mobilised peak shear stresses at somewhat higher horizontal displacements, as vividly seen in Table 4-1. Contrary to single interfaces, double interface configuration of similar lining components in this set, mobilised peak shear stresses at higher horizontal displacements exceeding 70mm which were relatively closer to the maximum horizontal displacement accommodated by the LSA. Commonly to all interface configurations, the mobilised peak shear stresses were higher than the strengths developed at LD.

The dry densities were observed to increase with increasing applied normal pressure for single and double interface configurations, as seen in the Appendices for a GS compacted to 95%MDD (2.014Mg/m^3) before testing. Additionally, the stones were subsequently crushed for tests involving LCS as the test progressed. The extent of crushing the stones in the upper shear box depended on the amount of applied normal pressures, as the higher the applied normal force, the more crushing took place.

The effects resulting from changes in dry densities were directly linked with the extent of vertical displacement of soil/stone layers, which were evaluated through a series of vertical displacement - time relationships as seen in Figure 4-2. In part (a) of Figure 4-2, the vertical displacement increased because of more crushed stones from the LCS layer as the applied normal pressure increased. This phenomenon, however, stabilised 20minutes after the shearing test had begun. The particle sizes also influenced the crushing of the stones in the LCS layer. Given its range as specified by project requirements, i.e., 38 to 50 mm, there were more pore spaces for the crushed particles to fill in, thereby facilitating more crushing. However, this observation was not present with the GTX-1 | GS interface, where the crushed gravelly sand material was well compacted.

Even though vertical displacement was observed for the three applied normal pressure, the change was not as extreme as Figure 4-2 (b) confirmed.

For the double interface (LCS | GTX-1 | GS), a drastic vertical displacement - time relationship was observed consistently at all three applied normal pressures, as seen in Figure 4-2 (c). It is worth noting that the equilibrium of vertical displacement was observed a few minutes after the test had started, i.e., <10minutes for the applied normal pressure of 150kPa, and this was not the case at higher applied normal pressures. The extent of soil ploughing, as described by Stark, Niazi & Keuscher (2015) or soil blistering, as explained by Lopes & Silvano (2010) in the lower shear box, was observed to increase with increasing applied normal pressures. In addition, this scenario progressed throughout the entire test duration. According to Lopes & Silvano (2010), this scenario happens when soil is placed in the lower shear box, similar to soil failure under a conventional footing. In this study, soil ploughing/blistering could be defined as the escaping of soil mass through a frontal gap (100mm) of the LSA between the upper (300mm×300mm) and lower (300mm×400mm) shear boxes during the shearing phase due to constant application of vertical pressure. This observation was also supported by the fact that vertical displacement at higher applied normal pressures did not reach equilibrium even up to the maximum horizontal displacement of 75mm accommodated by the LSA. This scenario, therefore, would explain why peak stresses for the double interface configuration were only mobilised at higher horizontal displacements even though minor crushing of stone and an increase in the density of the CM were observed.

In summary, the mobilised peak and LD shear stresses registered by the double interface configuration were higher than those observed in both of the single interface configurations, as seen in Table 4-1. However, the horizontal displacements at which the peak shear stresses were mobilised were higher and closer to the maximum horizontal displacement offered by the LSA.

Table 4-1: Peak and LD strengths obtained for LCS | GTX-1 | GS interface

Applied Normal Stress [kPa]	Interface Configuration											
	LCS | GTX-1				GTX-1 | GS				LCS | GTX-1 | GS			
	τ_p [kPa]	Δ_{s-p} [mm]	τ_{LD} [kPa]	Δ_{s-LD} [mm]	τ_p [kPa]	Δ_{s-p} [mm]	τ_{LD} [kPa]	Δ_{s-LD} [mm]	τ_p [kPa]	Δ_{s-p} [mm]	τ_{LD} [kPa]	Δ_{s-LD} [mm]
150	103.0	30.2	49.5	75.0	120.0	62.2	115.0	74.9	152.0	74.7	152.0	74.8
300	177.0	19.1	105.0	75.1	241.0	34.3	235.0	74.9	329.0	72.0	306.0	74.8
450	195.0	12.0	107.0	75.1	316.0	23.5	180.0	74.9	423.0	70.4	421.0	74.8

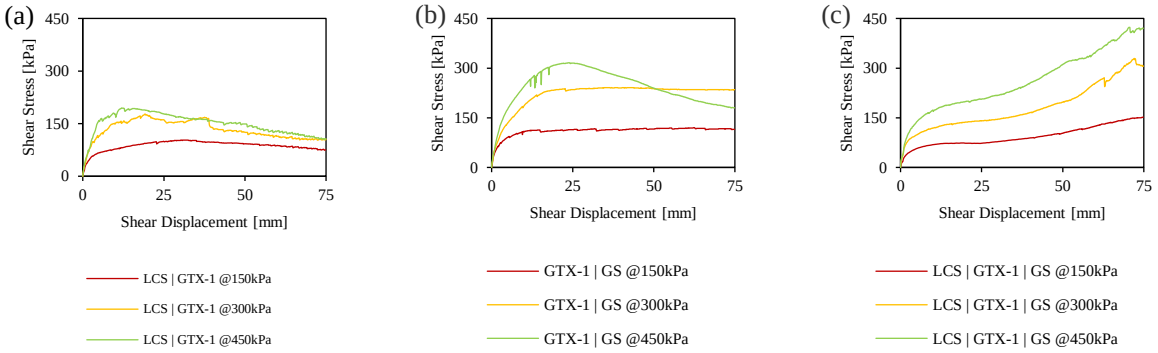

Figure 4-1: Shear stress - horizontal displacement relationships for: (a) LCS | GTX-1; (b) GTX-1 | GS & (c) LCS | GTX-1 | GS interfaces

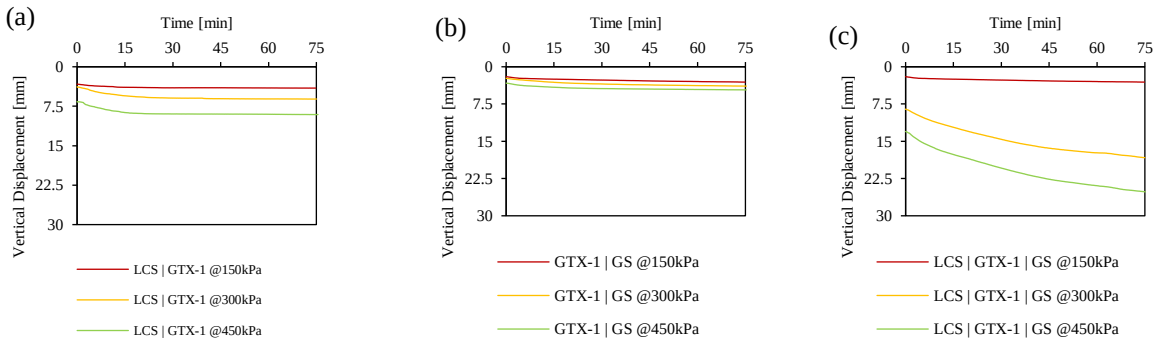

Figure 4-2: Vertical displacement - time relationships for: (a) LCS | GTX-1; (b) GTX-1 | GS & (c) LCS | GTX-1 | GS interface

4.2.2.2 GS | GTX-2 | GMB-1 Interface

Three lining components were used in the interface shear testing for this set. These included crushed gravelly sand material (GS), protection geotextile type 2 (GTX-2) made from similar materials as GTX-1 but with an average nominal thickness of 3.285mm (as measured in the lab) and a smooth HDPE geomembrane (GMB-1) with an average nominal thickness of 2.12mm (as measured in the lab). The interface shear setups comprised of single interface configurations, with GTX-2 (clamped on the lower shear box) sheared against GS (compacted to 95%MDD in the upper shear box) and GMB-1 (clamped on the lower shear box) sheared against GTX-2 (clamped on the upper shear box). The double interface configuration involved shearing of all three lining components with GMB-1 (clamped on the lower shear box), GTX-2 (placed freely on top of GMB-1) and GS (compacted to 95%MDD in the upper shear box).

Peak shear stresses were mobilised at very low horizontal displacements ~2mm for the GTX-2 | GMB-1 interface. The frictional resistance offered by the two materials was low, also evidenced by low peak shear stress values seen in Table 4-2. From Figure 4-3 (b), it can be observed that

this interface made a sharp increase in the shear stress for all applied normal pressures immediately after the shearing phase was initiated. However, this peak subsequently declined after a small horizontal displacement to a residual condition indicating the strain-softening phenomenon. The observations in this interface agreed with those of other scholars such as Cen, Wang & Sun (2018) & Adeleke, Kalumba & Oriokot (2019).

Additionally, the GS | GTX-2 interface mobilised peak shear stresses at higher horizontal displacements, especially for the applied normal pressures of 300 & 450 kPa. This interface's friction behaviour was driven mainly by the crushed gravelly sand material. Even though it was compacted to 95% MDD, its particle size distribution comprising 25% fine gravel and Figure 4-3 (a) suggest that a sample may have been contractive. The fine gravels penetrated the protection geotextile in all applied normal pressures, causing minor interlocks that shattered the fibres in the shear direction. This action increased the mobilised shear stress and its subsequent horizontal displacement at which it would be achieved. The peak shear stresses mobilised by both single interface configurations were generally higher than those mobilised at LD; however, not by significant magnitudes as seen in Table 4-2.

For the double interface configuration, i.e., GS | GTX-2 | GMB-1 interface, peak shear stresses with definitive peaks, as seen in Figure 4-3 (c), were mobilised at low horizontal displacements, as seen in Table 4-2. Also, notably in Figure 4-3, the peak shear stresses of a double interface were seen to be closer to those of the GTX-2 | GMB-1 interface and significantly lower than those of the GS | GTX-2 interface. This observation suggested that failure within the double interface occurred along the GTX-2 | GMB-1 interface attributed to its low frictional properties offered by the two lining components. Upon specimen assessment after the test, it was observed that the GS persistently ruptured the GTX-2 fibres in the direction of shear; however, this effect did not proceed to the GMB-1 surface. This scenario confirmed that the GTX-2's thickness was sufficient to protect the GMB-1 against possible holes formation from the fine gravels contained in the GS.

The dry densities for the crushed gravelly sand material (GS) placed in the upper shear box and compacted to 95% MDD (2.014Mg/m^3) were generally seen to increase as the test progressed, also presented in the Appendices. Interestingly, the vertical displacement - time relationships for the single interface configurations turned out to be similar, as seen in Figure 4-4 (a) & (b). This observation was primarily due to a well compacted GS layer that achieved the equilibrium of vertical displacement in less than 15minutes after the test was initiated. The geotextile developed a minimal compression attributed to its thickness as assessed after the test. For the double interface configuration, all the vertical displacements seemed to have reached equilibrium at ~45minutes; however, minor vertical indentations were observed as the test progressed, also seen in Figure 4-4 (c). This observation complements the minor differences observed in the mobilised peak shear stresses obtained by the double interface GS | GTX-2 | GMB-1 compared to those obtained by the single interface GTX-2 | GMB-1, even though the failure of a double interface occurred along the planes of this single interface.

Table 4-2: Peak and LD strengths obtained for GS | GTX-2 | GMB-1 interface

Applied Normal Stress [kPa]	Interface Configuration											
	GS | GTX-2				GTX-2 | GMB-1				GS | GTX-2 | GMB-1			
	τ_p [kPa]	Δ_{s-p} [mm]	τ_{LD} [kPa]	Δ_{s-LD} [mm]	τ_p [kPa]	Δ_{s-p} [mm]	τ_{LD} [kPa]	Δ_{s-LD} [mm]	τ_p [kPa]	Δ_{s-p} [mm]	τ_{LD} [kPa]	Δ_{s-LD} [mm]
150	129.0	11.6	120.0	74.9	34.0	2.1	29.9	74.9	39.7	1.5	31.7	75.0
300	252.0	74.2	252.0	74.8	64.5	2.2	55.8	74.8	78.6	2.1	55.9	74.9
450	364.0	65.3	334.0	74.9	93.8	2.0	84.1	74.9	112.0	3.8	81.2	74.8

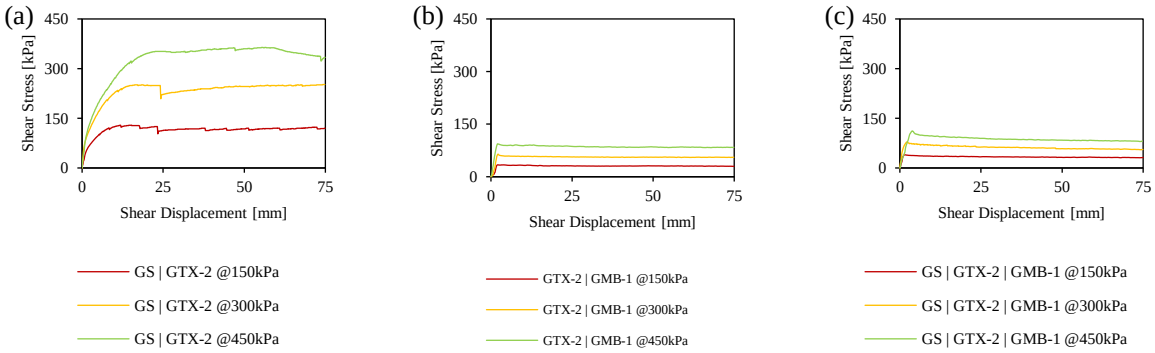

Figure 4-3: Shear stress - horizontal displacement relationships for: (a) GS | GTX-2; (b) GTX-2 | GMB-1 & (c) GS | GTX-2 | GMB-1 interfaces

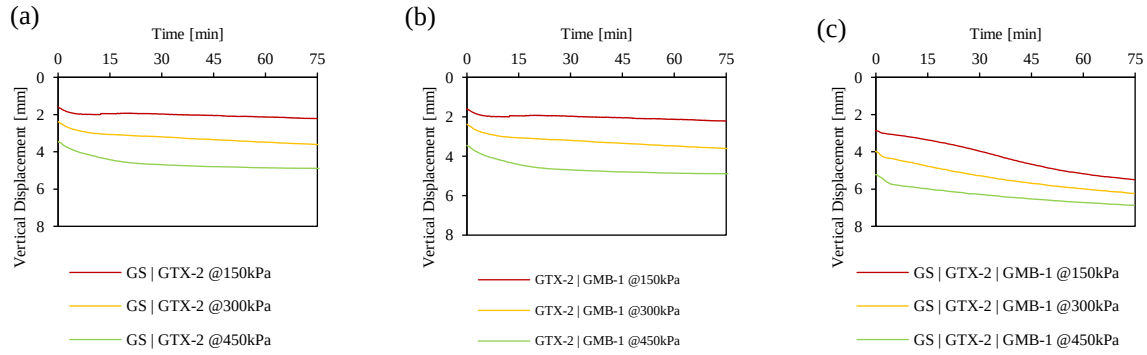

Figure 4-4: Vertical displacement - time relationships for: (a) GS | GTX-2; (b) GTX-2 | GMB-1 & (c) GS | GTX-2 | GMB-1 interfaces

4.2.2.3 GTX-2 | GMB-1 | CD Interface

This set of lining components involved interface shearing of the protection geotextile type 2 (GTX-2) against smooth HDPE geomembrane (GMB-1), similar to those described in Section 4.2.2.2 and GMB-1 sheared against the smooth side of the synthetic cuspate drain (CD) for single interface configuration tests. Consequently, for a double interface configuration, all the three

lining components were sheared concurrently with a setup that had GTX-2 (clamped on the lower shear box), GMB-1 (placed freely on top of GTX-2) and CD (secured on the upper shear box while its smooth face directly on top of GMB-1). The CD had an average nominal thickness of 5mm, where 1mm was the base layer and 4mm was the trapezoidal cusps, rectangularly spaced across the entire CD sheet.

Peak shear stresses mobilised by the GMB-1 | CD interface were higher than those mobilised by its single counterpart interface (GTX-2 | GMB-1). For instance, at an applied normal pressure of 450kPa, the former mobilised a peak shear stress of 158kPa compared to 93.8kPa mobilised by the latter interface. GTX-2 | GMB-1 interface mobilised peak shear stresses at very low horizontal displacements (<2.5mm). This led to development of standard peak curves, as shown in Figure 4-5 (a). Conversely, the GMB-1 | CD interface mobilised its peak strengths at higher horizontal displacements closer to the maximum horizontal displacement accommodated by the LSA (i.e., 75mm), thereby making this interface not have definitive peaks as seen in Figure 4-5 (b). Notably, in Table 4-3, this interface achieved similar strengths at LD, unlike the GTX-2 | GMB-1 interface, whose LD strengths were relatively lower than those obtained at peak.

The peak strengths for the double interface (GTX-2 | GMB-1 | CD) were mobilised at lower horizontal displacements, most especially for the applied normal pressures of 300 & 450 kPa. The horizontal displacements at which peak shear stresses were mobilised were similar to those of the GTX-2 | GMB-1, indicating that failure within the double interface configuration occurred on the GTX-2 | GMB-1 interface. As seen in Table 4-3, the peak strengths observed were between the two single interface configurations. All lining components tested contributed to the strengths obtained under this configuration with no significant predominance by a specific interface. The lower peak stresses obtained for both testing configurations indicated that the three lining components exhibited low frictional and interface shear properties. After the interface shear testing of all the lining components, specimen assessment suggested that no damage was done to the specimens except compression of the GTX-2 at higher applied normal pressures attributed to its thickness.

Table 4-3: Peak and LD strengths obtained for GTX-2 | GMB-1 | CD interface

Applied Normal Stress [kPa]	Interface Configuration											
	GTX-2 | GMB-1				GMB-1 | CD				GTX-2 | GMB-1 | CD			
	τ_p [kPa]	Δ_{s-p} [mm]	τ_{LD} [kPa]	Δ_{s-LD} [mm]	τ_p [kPa]	Δ_{s-p} [mm]	τ_{LD} [kPa]	Δ_{s-LD} [mm]	τ_p [kPa]	Δ_{s-p} [mm]	τ_{LD} [kPa]	Δ_{s-LD} [mm]
150	34.0	2.1	29.9	74.9	46.6	71.9	46.4	74.9	50.5	23.7	32.4	74.9
300	64.5	2.2	55.8	74.9	90.1	74.9	90.1	74.9	86.4	3.8	58.4	74.9
450	93.8	2.0	84.1	74.9	158.0	68.1	158.0	74.9	122.0	2.6	81.6	74.9

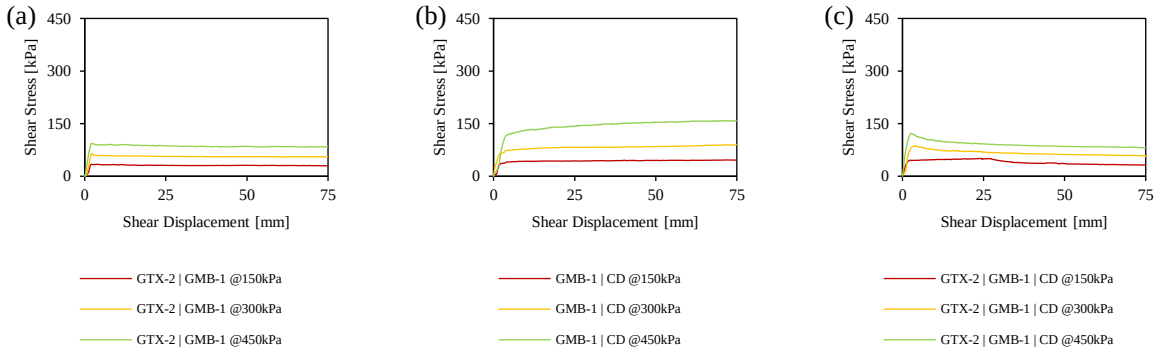

Figure 4-5: Shear stress – horizontal displacement relationships for : (a) GTX-2 | GMB-1; (b) GMB-1 | CD & (c) GTX-2 | GMB-1 | CD interfaces

4.2.2.4 GMB-1 | CD | GMB-2 Interface

Three lining components were used for this set. These included GMB-1 sheared against the smooth face of CD as described in Section 4.2.2.3 and the smooth LLDPE geomembrane (GMB-2) with an average nominal thickness of 1.735mm (as measured in the lab) sheared against the cusps of the CD for single interface configuration. For the double interface configuration, all three lining components were sheared simultaneously with GMB-1 (clamped on the lower shear box), CD (placed freely in the middle with the smooth side facing GMB-1 while the cusps facing GMB-2) and GMB-2 (clamped on the upper shear box). Other shear testing conditions remained similar to those of previous tests described in earlier sections.

CD | GMB-2 interface mobilised higher peak shear stresses than GMB-1 | CD interface, although both interfaces mobilised these peak shear stresses at higher horizontal displacements, as shown in Table 4-4. The surfaces of the two geomembranes were similar, i.e., smooth geomembranes described in Chapter 3; therefore, the only difference that resulted in the observed difference in mobilised shear stresses lies with the CD material. As described earlier, the cusps of the CD interfaced with the GMB-2 while its smooth side interfaced with GMB-1. This was the primary difference, apart from GMB-1 being an HDPE material (stiff) while GMB-2 being an LLDPE material (flexible). For both single interface configurations, mobilised peak shear strengths were similar to the strengths obtained at LD; this is confirmed by Figure 4-6 (a) & (b), which presented the undefined peaks.

The double interface (GMB-1 | CD | GMB-2) mobilised peak shear strengths between the two single interface configurations, as shown in Table 4-4, indicating that all lining components contributed to the observed strengths with no single interface being predominant. Despite this, CD | GMB-2 proved to be the most robust interface and possibly contributed more to the peak shear strengths. The horizontal displacements at which the peak strengths were mobilised for the double interface configuration were higher than those of the single interface configurations, except for the GMB-1 | CD interface at 150 & 300 kPa. The behaviour of the lining components through double interface shear testing was still similar to those of single interfaces as in no

definitive peaks were observed from the shear stress - horizontal displacement relationships, as seen in Figure 4-6 (c).

Table 4-4: Peak and LD strengths obtained for GMB-1 | CD | GMB-2 interface

Applied Normal Stress [kPa]	Interface Configuration											
	GMB-1 | CD				CD | GMB-2				GMB-1 | CD | GMB-2			
	τ_p [kPa]	Δ_{s-p} [mm]	τ_{LD} [kPa]	Δ_{s-LD} [mm]	τ_p [kPa]	Δ_{s-p} [mm]	τ_{LD} [kPa]	Δ_{s-LD} [mm]	τ_p [kPa]	Δ_{s-p} [mm]	τ_{LD} [kPa]	Δ_{s-LD} [mm]
150	46.6	71.9	46.4	74.9	75.2	44.5	74.5	75.0	65.0	59.8	60.6	75.1
300	90.1	74.9	90.1	74.9	145.0	69.1	143.0	75.0	122.0	57.5	119.0	75.0
450	158.0	68.1	158.0	74.9	209.0	73.3	208.0	75.0	176.0	73.4	173.0	75.0

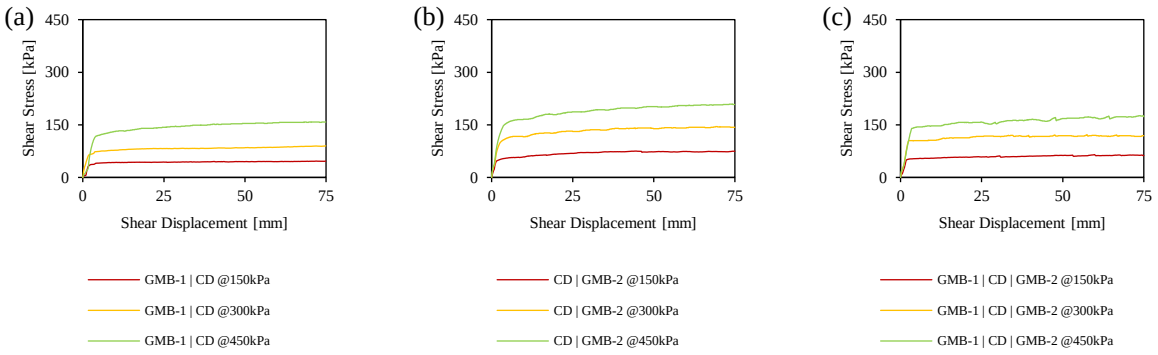

Figure 4-6: Shear stress - horizontal displacement relationships for: (a) GMB-1 | CD; (b) CD | GMB-2 & (c) GMB-1 | CD | GMB-2 interfaces

4.2.2.5 CD | GMB-2 | SAND Interface

This series of interface shear tests involved three lining components, including the synthetic cuspate drain (CD), which was sheared against the smooth LLDPE geomembrane (GMB-2) as described in Section 4.2.2.4; and GMB-2, which was sheared against a sand sample (compacted to 95% MDD in the upper shear box) for single interface testing. CD (clamped on the lower shear box with cusps facing upwards), GMB-2 (placed in the middle without any clamping) and sand sample (compacted to 95% MDD in the upper shear box) were sheared simultaneously for a double interface configuration. Similar shearing conditions as previously outlined were followed.

For single interface configurations, GMB-2 | SAND interface mobilised higher shear strengths at low horizontal displacements <10mm than CD | GMB-2 interface, which mobilised its peak strengths at higher horizontal displacements, as can be seen in Table 4-5. This resulted in the GMB-2 | SAND interface having definitive peaks, as shown in Figure 4-7 (b), especially for the applied normal pressures of 300 & 450 kPa. The higher peak strengths obtained from this interface were attributed to the sandy soil, which developed a relatively more assertive frictional behaviour by polishing the GMB-2 and creating minor grooves. This observation was in

agreement with that of other scholars such as Choudhary & Krishna (2016) and Cen, Wang & Sun (2018), who described that the shear behaviour of smooth geomembranes against soil relied on the particle sizes and gradation of soils. In their studies, large and angular soils resulted in higher strengths due to inter-locking mechanisms with the geomembrane. Additionally, the LD strengths of the GMB-2 | SAND interface were low compared to the LD strengths of the CD | GMB-2 interface due to a consistent decline of strengths, also known as strain-softening on the GMB-2 | SAND interface after achieving a peak condition.

For the double interface configuration of the three lining components, the peak shear strengths were mobilised at relatively higher horizontal displacements than those of the GMB-2 | SAND interface but lower than those of the CD | GMB-2 interface. The shear stress - horizontal displacement relationships were similar to those of the single weak interface (CD | GMB-2), confirmed by Figure 4-7 (c). Interestingly, however, the determined peak shear strengths were lower than both single interfaces but within a tolerable differential limit of 5% to those obtained on the CD | GMB-2 interface. This indicated that failure within the double interface occurred on the CD | GMB-2 interface. Moreover, this observation was consistent with Shi et al. (2020), who conducted a double interface study on three lining materials: the geomembrane, geocomposite and sand. It was shown that shear displacement occurred mainly along the geomembrane-geocomposite interface, thereby confirming that failure within a double interface occurred there.

Table 4-5: Peak and LD strengths obtained for CD | GMB-2 | SAND interface

Applied Normal Stress [kPa]	Interface Configuration											
	CD | GMB-2				GMB-2 | SAND				CD | GMB-2 | SAND			
	τ_p [kPa]	Δ_{s-p} [mm]	τ_{LD} [kPa]	Δ_{s-LD} [mm]	τ_p [kPa]	Δ_{s-p} [mm]	τ_{LD} [kPa]	Δ_{s-LD} [mm]	τ_p [kPa]	Δ_{s-p} [mm]	τ_{LD} [kPa]	Δ_{s-LD} [mm]
150	75.2	44.5	74.5	75.0	81.1	5.2	65.0	75.0	60.4	38.6	59.8	74.8
300	145.0	69.1	143.0	75.0	162.0	9.2	124.0	75.0	144.0	46.7	139.0	74.8
450	209.0	73.3	208.0	75.0	254.0	9.5	189.0	75.0	203.0	46.9	199.0	74.8

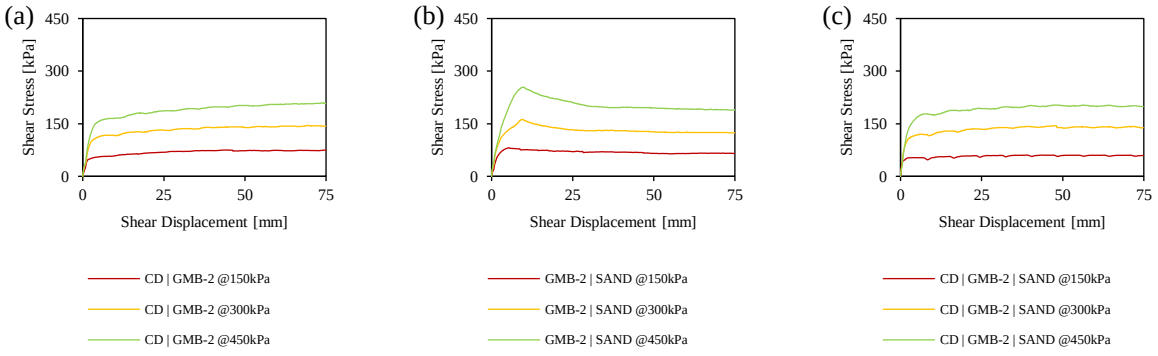

Figure 4-7: Shear stress - horizontal displacement relationships for: (a) CD | GMB-2; (b) GMB-2 | SAND & (c) CD | GMB-2 | SAND interfaces

4.2.2.6 SAND | GTX-3 | SAND Interface

For this set of lining components, nine interface shear tests were conducted. They included a sand sample (compacted to 95% MDD in the upper shear box) sheared against firstly the rough surface of the reinforcing geotextile - GTX-3S1 (which was clamped on the lower shear box) and later with its smooth face (GTX-3S2) for single interface configuration. For the double interface shear testing, three lining components were sheared against each other concurrently, i.e., sand sample (compacted to 95% MDD in the lower shear box), GTX-3 (placed freely in between the two shear boxes) and a similar sand sample (compacted to 95% MDD in the upper shear box). As mentioned earlier and detailed in Chapter 3, the reinforcing geotextile had two distinct surfaces. A smooth and rough surface (due to high strength fibres). GTX-3 had a nominal thickness of 1.58mm (as measured in the lab).

The peak shear stresses for both single interface configurations were mobilised at randomly distributed higher horizontal displacements, i.e., there was no consistent trend that can be deduced from the results. For example, at an applied normal pressure of 150kPa, the sand | GTX-3S1 interface mobilised peak shear stress at a horizontal displacement of 43.91mm. In contrast, its counterpart SAND | GTX-3S2 interface mobilised peak shear stress at a horizontal displacement of 74.91mm, which is a large displacement (LD). Notably, on both interfaces, the peak shear stress mobilised was either similar to or slightly higher than the shear stress mobilised at LD, as shown in Table 4-6. A unique trend was evidenced on the SAND | GTX-3S2 (smooth side of the reinforcing geotextile). As the normal applied pressure increased, the mobilised peak shear stress increased, and the horizontal displacements at which the mobilised peak shear stress increased. However, this trend had a minimal impact on the strengths obtained at LD, except for the applied normal pressure of 450kPa, where the specimen was worn-out after reaching the peak, consequently decreasing its strength, as seen in Figure 4-8 (b).

The double interface configuration for these lining components mobilised peak shear stresses similar to those at LD, as seen in Figure 4-8 (c). Additionally, these mobilised strengths at peak and LD were higher than those mobilised by the single interfaces. However, there was evidence of soil ploughing through the gap between the upper and lower shear boxes during the double interface testing, similar to that explained in Section 4.2.2.1. It is worth noting that the gap between shear boxes was necessary for allowing the sheared materials to slide against each other for the intended horizontal displacement. For instance, 75mm, as offered by the LSA, was used in this study, so it was essentially unavoidable.

The dry densities of the sand sample were observed to consistently decline after the test; this was primarily due to the sand's high permeability, which allowed the specimen to absorb high moisture contents, as seen in the Appendices. However, this moisture absorption by the sand sample during the test did not influence the vertical displacement by a significant magnitude, as can be seen in Figure 4-9. The vertical displacement - time relationships were almost similar for single interfaces, i.e., Figure 4-9 (a) & (b). The equilibrium in the vertical displacements was not

reached during the test even though minimal depressions were observed and persisted throughout the test duration. For the double interface, equilibrium of the vertical displacement was reached at <45minutes for the three applied normal pressures, as shown in Figure 4-9 (c).

Furthermore, large vertical displacements were observed for the double interface compared to both single interfaces. This could have resulted from soil ploughing since soils in all configurations were similar and compacted to the same level, i.e., 95%MDD before the test. This reason could be the one that influenced the shear behaviour, as observed in Figure 4-8 (c), where peak shear stresses mobilised were higher and were achieved at large horizontal displacements. Additionally, during the test, it was also observed that the soil sample placed in the bottom box absorbed more amounts of moisture than that in the top shear box. However, this had a negligible impact on changing the testing conditions as the LSA was designed to accommodate the escaping water through the small holes on its bottom shear box, thereby preventing pore water pressure build-ups.

Table 4-6: Peak and LD strengths obtained for SAND | GTX-3 | SAND interface

Applied Normal Stress [kPa]	Interface Configuration											
	SAND | GTX-3S1				SAND | GTX-3S2				SAND | GTX-3 | SAND			
	τ_p [kPa]	Δ_{s-p} [mm]	τ_{LD} [kPa]	Δ_{s-LD} [mm]	τ_p [kPa]	Δ_{s-p} [mm]	τ_{LD} [kPa]	Δ_{s-LD} [mm]	τ_p [kPa]	Δ_{s-p} [mm]	τ_{LD} [kPa]	Δ_{s-LD} [mm]
150	135.0	43.9	129.0	75.0	140.0	74.9	140.0	74.9	182.0	74.9	182.0	74.9
300	268.0	74.7	268.0	75.0	233.0	36.3	233.0	74.9	255.0	74.8	255.0	74.9
450	367.0	46.9	355.0	75.0	329.0	25.0	209.0	74.9	363.0	74.9	363.0	74.9

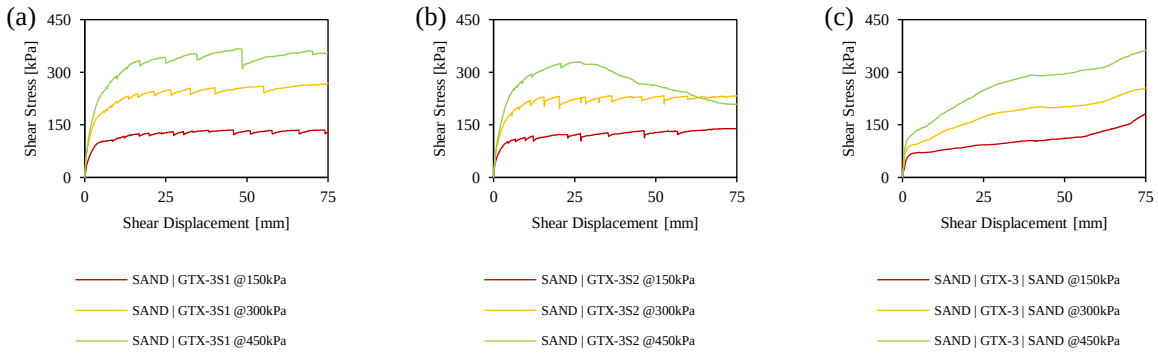

Figure 4-8: Shear stress - horizontal displacement relationships for : (a) SAND | GTX-3S1 (b) SAND | GTX-3S2 & (c) SAND | GTX-3 | SAND interfaces

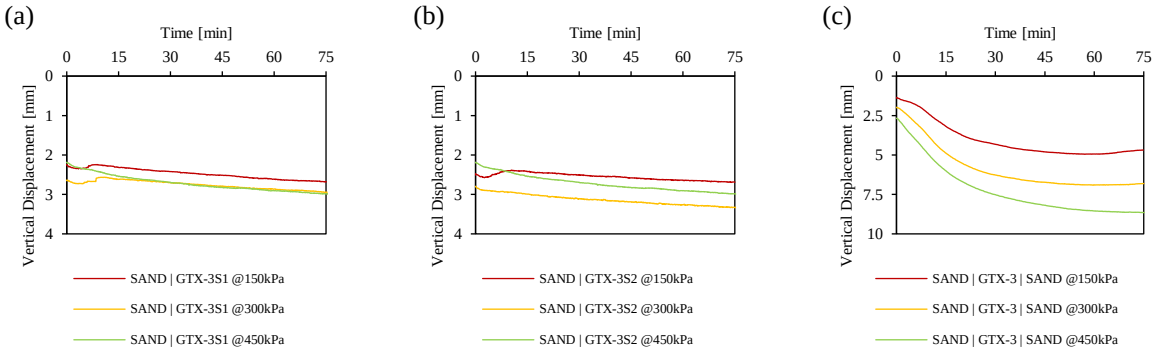

Figure 4-9: Vertical displacement - time relationships for : (a) SAND | GTX-3S1; (b) SAND | GTX-3S2 & (c) SAND | GTX-3 | SAND interfaces

4.3 Shear - Normal Stress Relationships

4.3.1 Introduction

As stipulated in the ASTM D5321, a minimum of three applied normal pressures is required to establish a Mohr-Coulomb failure envelope, enabling the determination of shear strength parameters for soil-geosynthetic and geosynthetic-geosynthetic interactions (ASTM, 2020a,b). The choice of these applied normal pressures is imperative and should cater to the field's anticipated conditions. For instance, the basal lining system would experience more stress than the cover lining system. So, this must be reflected in the choice of applied normal pressures at which interface shear tests are conducted. This study utilized three applied normal pressures, i.e., 150, 300 & 450 kPa, for the basal lining system to conduct single and double interface direct shear tests.

4.3.2 Development of Failure Envelopes

Mohr-Coulomb failure envelopes were developed using best-fit linear regression and non-linear/curvilinear analyses for those that did not conform well to the best-fit line. This was conducted for both testing configurations, i.e., single and double interfaces at peak and large displacements (LD). The realisation of whether a particular failure envelope depicted a linear or non-linear relationship was derived using the best-fit linear regression approach with which the R^2 value was assessed.

Coefficient of Regression (R^2) has been used by scholars such as Esterhuizen, Filz & Michael Duncan (2001) & Muluti (2021) to suitably understand the best way of plotting failure envelopes and consequently determining the appropriate interface shear strength parameters. In addition, according to Fox & Stark (2015), non-linear/curvilinear failure envelopes produce a sudden change in friction's interfacial angles, a behaviour that could replicate field conditions.

According to Adeleke (2020) & Muluti (2021), all best-fit lines depicting the R^2 values of less than 0.98 need to be replaced by either bilinear or non-linear/curvilinear analyses to accurately represent the shear - normal stress relationships of the respective lining components under stipulated testing conditions. If the R^2 value for a specific line/curve is closer to 1, this line/curve touches most of the plotted points and is therefore deemed sufficient as a Mohr-Coulomb failure envelope for a particular interface.

A tangent line was drawn closer to the applied normal stress of interest to determine interface shear strength parameters from a non-linear/curvilinear analysis recommended by Chiu & Fox (2004) and Fox & Stark (2015). The inclination of this tangential line produced an angle of interface friction, while its intercept with the y-axis produced an apparent adhesion value. The mean/average was then taken to obtain the overall interface shear strength parameters for the Mohr-Coulomb failure envelope(s) (Adeleke, 2020).

4.3.3 Failure Envelopes of the Basal Lining System

4.3.3.1 LCS | GTX-1 | GS Interface

For the peak shear strength assessment using best-fit linear regression as seen with dotted lines in Figure 4-10 (a) & (b) and using non-linear fit as seen on the similar figures with solid lines, a single interface involving LCS against GTX-1 was shown to be the weakest. As seen in Table 4-1 for this interface, the shear stress values were low by 14, 27 & 38 % at all tested applied normal pressures of 150, 300 & 450 kPa, respectively, compared to the subsequent single interface involved GTX-1 against GS. Furthermore, compared to the double interface that combined the three lining components, LCS | GTX-1 interface had low shear stress values of 32, 46 & 54 % at the three tested applied normal pressures.

The double interface (LCS | GTX-1 | GS) achieved maximum shear stress values, producing higher interface shear strength parameters as seen in Table 4-7 & Table 4-8. This was attributed to the fact that the LCS developed a sufficient intimate interaction with the GS by embedding the GTX-1, resulting in high interface friction angles. This intimate interaction could only be achieved through the double interface shear testing configuration due to replacing the heavy-duty rigid steel substrate from the lower shear box with a well compacted GS. Additionally, this set of interfaces highlighted the importance of allowing the lining materials to develop intimate interaction before the shearing phase. This would enable the tested soil-geosynthetic specimens to distribute/transfer the applied normal pressure uniformly along the shearing planes. Moreover, the double configuration setup would avoid underestimating interface shear strengths when gravelly materials are involved since they produce a minimal shear contact area due to their particle sizes.

Another important observation was that with the best-fit linear regression analyses, shear strength parameters, specifically the interfacial friction angles, increased significantly for the linear with zero intercepts than for its counterpart with non-zero intercepts. The Coefficient of Regression

(R^2) also increased for the linear with zero intercept analysis, indicating that the plotted points are very close to the trendline. While the apparent adhesion value difference was not of concern, the interface friction values increased significantly, as shown in Table 4-7.

Table 4-7: Peak & LD strength parameters for LCS | GTX-1 | GS Interface

Strength Type	Interface Configuration		Failure Envelopes					
			Linear (non-zero intercept)			Linear (zero intercept)		
			R^2	δ [°]	c_α [kPa]	R^2	δ [°]	c_α [kPa]
Peak	Single -	LCS | GTX-1	0.8903	17.05	66.42	0.9698	26.40	0.00
		GTX-1 | GS	0.9820	33.16	29.66	0.9958	36.43	0.00
	Double -	LCS | GTX-1 | GS	0.9697	42.11	30.50	0.9950	44.74	0.00
LD	Single -	LCS | GTX-1	0.7764	10.85	29.71	0.9657	15.46	0.00
		GTX-1 | GS	0.2928	12.23	111.66	0.8964	28.18	0.00
	Double -	LCS | GTX-1 | GS	0.9931	41.90	24.17	0.9983	44.02	0.00

For this set of interfaces at peak, the best-fit linear regression did not seem to exactly replicate the shear behaviour of the lining materials even though it gave interface shear strength parameters as summarized in Table 4-7. Therefore, a non-linear analysis was adopted to pin the differences in the shear strength parameters obtained from a similar test as seen in Figure 4-10 (a) & (b).

As seen in Table 4-8, both testing configurations produced R^2 value closer to 1.0, and the interface shear strength parameters have been summarised therein. For the range of applied normal pressures tested, the LCS | GTX-1 single interface has been shown to exhibit lower shear stresses, resulting in a flatter curve compared to other interfaces. The flatter curve observed on this interface has produced low interface shear strength parameters, making this interface the weakest/critical. Furthermore, the double interface's shear strength parameters have been the highest compared to both single interface configurations. This could mean that single interfaces underestimate the shear strength properties of the concerned lining components.

Table 4-8: Peak & LD strength parameters for LCS | GTX-1 | GS interface

Strength Type	Interface Configuration		Failure Envelopes					
			Non-linear (non-zero intercept)			Non-linear (zero intercept)		
			R^2	δ [°]	c_α [kPa]	R^2	δ [°]	c_α [kPa]
Peak	Single -	LCS | GTX-1	1.0000	5.83	110.00	0.9948	6.67	106.67
		GTX-1 | GS	1.0000	12.83	75.00	0.9950	13.83	78.33
	Double -	LCS | GTX-1 | GS	1.0000	16.17	103.33	0.9865	18.83	78.33
LD	Single -	LCS | GTX-1	1.0000	3.50	71.67	0.9403	3.33	75.00
		GTX-1 | GS	1.0000	3.33	210.00	0.9563	2.50	205.00
	Double -	LCS | GTX-1 | GS	1.0000	17.00	55.00	0.9980	19.67	56.67

At large displacement (LD), shear stress values of a double interface (LCS | GTX-1 | GS) were the highest compared to both single interfaces, as seen in Table 4-7. Interface shear strength parameters were determined through best-fit linear and non-linear/curvilinear analyses as seen in Figure 4-10 (c) & (d). LCS | GTX-1 interface was still the weakest interface, similar to what was observed at its peak. Additionally, it was noted that every interface had a preferred Mohr-Coulomb failure envelope. For example, the GTX-1 | GS interface was well analysed using a curvilinear approach that produced an R^2 value of 0.9563 compared to the best-fit linear path, which had a significantly lower R^2 value of 0.2928 and 0.8964 for non-zero and zero intercepts, respectively, as seen in Table 4-8.

The weakest interface, i.e., LCS | GTX-1, recorded shear stress values lower by 57%, 55% & 41% compared to its subsequent single interface (GTX-1 | GS). Double interface (LCS | GTX-1 | GS) produced the highest shear stress values, which led to higher interface shear strength parameters. Furthermore, the double interface analysed with both linear and non-linear regressions produced almost equal values of R^2 closer to 1. However, the interface shear strength parameters were significantly different, as shown in Table 4-7 & Table 4-8.

4.3.3.2 GS | GTX-2 | GMB-1 Interface

As discussed in Section 4.2.2.2, the peaks of a single interface GTX-2 | GMB-1 and those of a double interface GS | GTX-2 | GMB-1 were reached at minimal horizontal displacements <10mm, while the peaks of the single interface GS | GTX-2 were achieved at relatively higher horizontal displacements for the three applied normal pressures. Figure 4-11 (a) & (b) depict the relationships of peak shear stress against normal stresses for all the tested interfaces, and their interface shear strength parameters have been determined for both zero and non-zero intercepts.

Single interface GTX-2 | GMB-1 was found to be the weakest interface with the interfacial angle of friction of 11.27° and an apparent adhesion value of 4.30kPa, and this was in line with the results obtained by other scholars such as Akpinar & Benson (2005); Bacas, Cañizal & Konietzky (2015); Buthelezi (2017); Cen, Wang & Sun (2018) and Adeleke (2020). In their studies, a smooth geomembrane directly sheared against a geotextile was the weakest interface compared to the textured geomembrane, which provided an excellent interlocking (hook & loop) mechanism at the geotextile interface under similar testing conditions.

The double interface GS | GTX-2 | GMB-1 was observed to have interface shear strength parameters closer to the single interface GTX-2 | GMB-1, constituting an interfacial angle of friction of 13.55° and an apparent adhesion of 4.46kPa. This indicated that failure occurred along the GTX-2 | GMB-1 interface on a double interface testing configuration. However, the slightly higher angle of interfacial friction was attributed to the presence of crushed gravelly sand material (GS) interfacing with the geotextile, which transferred some of the shear resistance effects to the geomembrane. The values of shear stress for the two interfaces have been summarised in Table 4-2, with a double interface GS | GTX-2 | GMB-1 having slightly higher shear stresses with a maximum percentage difference of 18% when compared to the single

interface GTX-2 | GMB-1 for the range of the applied normal stresses. This further highlighted the role played by the compacted crushed gravelly sand material (GS) in the double interface setup.

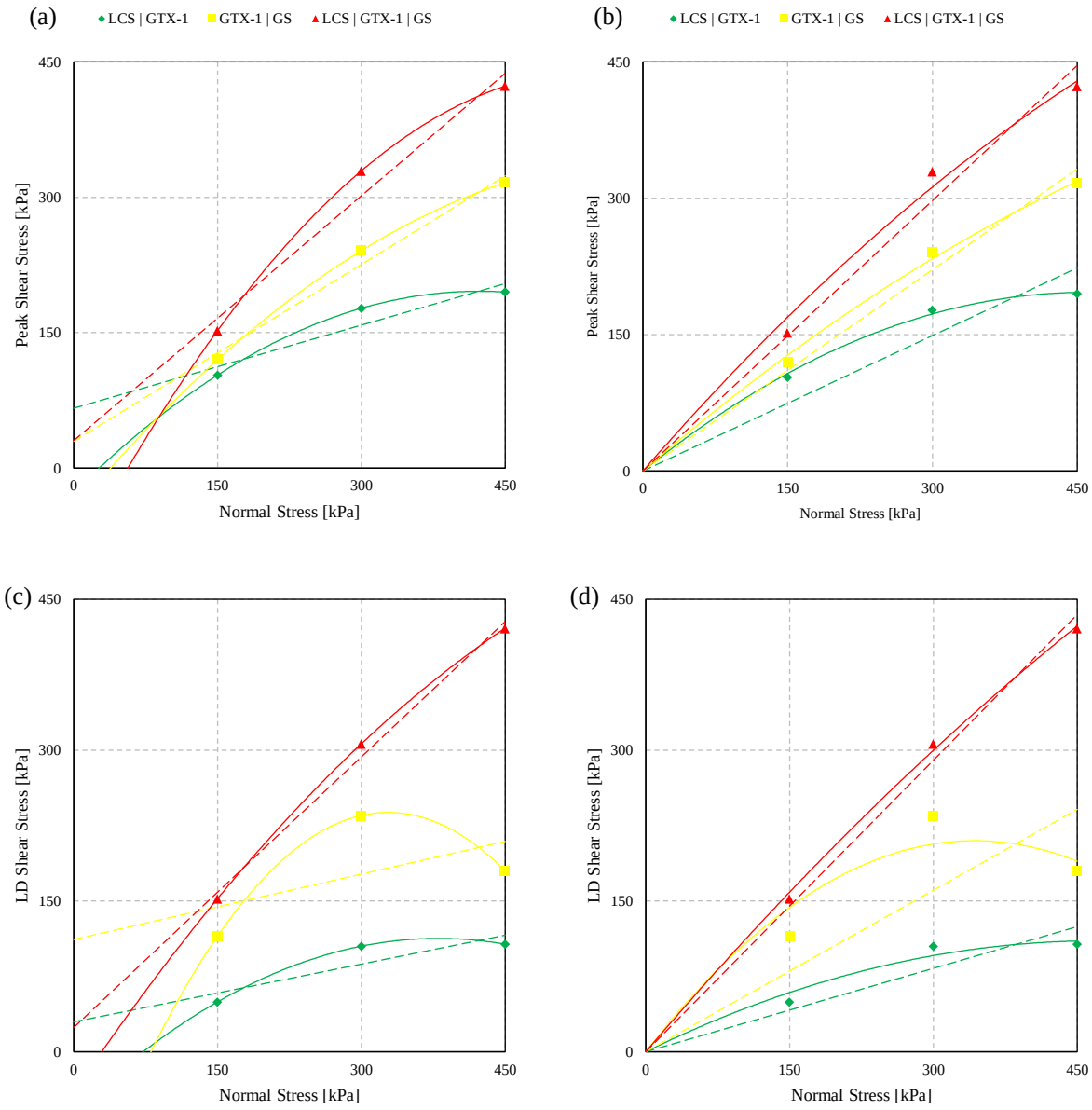

Figure 4-10: Shear stresses against normal stresses for LCS | GTX-1 | GS Interface: (a) & (b) At peak and (c) & (d) At LD

GS | GTX-2 interface exhibited the highest interface shear strength parameters with an interfacial friction angle of 38.08° and an apparent adhesion of 13,32kPa. The highest interfacial friction angle was attributed to the compacted crushed gravelly sand material (GS), which polished geotextile fibres in the shear direction and got embedded onto the geotextile surface. The apparent adhesion value achieved was attributed to the confinement of the tested lining materials.

When the relationship of peak shear stresses against normal stresses for both single and double interfaces was analysed with the zero-intercept best-fit linear regression approach, the interfacial angle of friction values were observed to increase by a small margin of 6%, as seen in Table 4-9. The significance of zero-intercept best-fit analysis was to understand the effects of neglecting the apparent adhesion value in the side-slope stability analyses. With the range of applied normal stresses used, which recorded a regression coefficient exceeding 0.98, other failure envelopes such as bilinear and non-linear/curvilinear were not observed in this interface.

As with the peak strengths, the large displacement (LD) strengths for the single interfaces and a double interface investigated depicted similar trends. The single interface GTX-2 | GMB-1 remained the weakest, while a double interface GS | GTX-2 | GMB-1 remained the strongest. The magnitudes of the LD interface shear strength parameters were lower than those at the peak. From Table 4-9, the values of LD shear stresses of the weakest interface (GTX-2 | GMB-1) when compared to the strongest interface (GS | GTX-2) had a minimum difference of 78%, and when compared to the double interface GS | GTX-2 | GMB-1 a maximum difference of 6% was noted.

At LD, as seen in Figure 4-11 (c) & (d), the weakest single interface (GTX-2 | GMB-1) was observed to have a similar shear-normal stress relationship as the double interface (GS | GTX-2 | GMB-1); this confirmed that failure in the double interface still occurred on the weakest GTX-2 | GMB-1 interface. No significant difference in the shear strength parameters, precisely the interfacial angle of friction, was observed when the analysis was done with a zero-intercept best-fit linear analysis, as shown in Table 4-9. Notably, in Figure 4-11 (c) & (d), no overlap of the shear - normal stress relationship was observed for the three tests at LD; therefore, the weakest and strongest interfaces experienced no interface changes/transitions as the tests progressed.

Table 4-9: Peak & LD shear strength parameters for GS | GTX-2 | GMB-1 interface

Strength Type	Interface Configuration		Failure Envelopes					
			Linear (non-zero intercept)			Linear (zero intercept)		
			R^2	δ [°]	c_α [kPa]	R^2	δ [°]	c_α [kPa]
Peak	Single -	GS | GTX-2	0.9993	38.08	13.32	0.9995	39.40	0.00
		GTX-2 | GMB-1	0.9999	11.27	4.30	0.9994	11.95	0.00
	Double -	GS | GTX-2 | GMB-1	0.9981	13.55	4.46	0.9993	14.24	0.00
LD	Single -	GS | GTX-2	0.9821	35.50	21.32	0.9968	37.75	0.00
		GTX-2 | GMB-1	0.9993	9.37	2.40	0.9997	10.62	0.00
	Double -	GS | GTX-2 | GMB-1	0.9998	10.24	6.77	0.9982	10.44	0.00

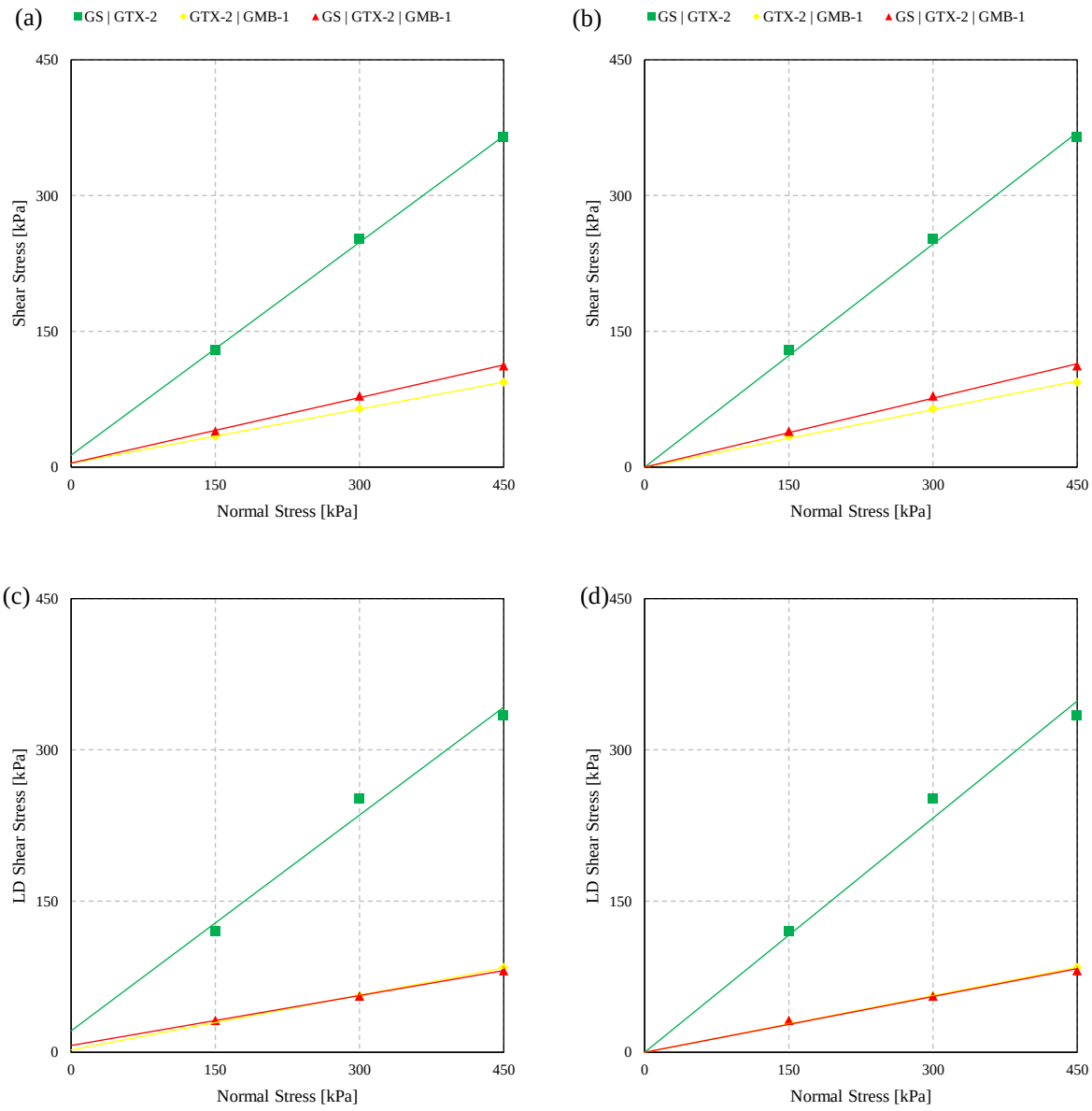

Figure 4-11: Shear stresses against normal stresses for GS | GTX-2 | GMB-1 Interface: (a) & (b) At peak and (c) & (d) At LD

4.3.3.3 GTX-2 | GMB-1 | CD Interface

Peak shear stresses of the single interfaces and a double interface were plotted against normal stresses, as seen in Figure 4-12 for zero and non-zero vertical intercepts. Maximum shear stress of 158kPa was obtained from the interface tests by GMB-1 | CD interface at an applied normal pressure of 450kPa. This indicated that the tested lining materials were weak in shear, as evidenced by the low shear strength. Furthermore, the weakest interface at the peak was GTX-2 | GMB-1 with an interface friction angle of 11.27° and an apparent adhesion of 4.30kPa, attributed to the smoothness of the geomembrane, i.e., not being co-extruded. Additionally, the

strongest interface was observed to cut across the weakest interface at an applied normal stress of <50kPa and the double interface at an applied normal stress 150kPa, as seen in Figure 4-12 (a) & (b). In terms of interface shear strength parameters, the strongest interface (GMB-1 | CD) recorded an interface friction angle of 18.45° with no apparent adhesion, while the weakest recorded 11.27° and 4.30kPa the angle of interface friction and an apparent adhesion, respectively. The difference in the interface angles obtained was marginally attributed to the nature of the faces of the lining materials being almost similar, as detailed in Chapter 3.

The double interface GTX-2 | GMB-1 | CD recorded an interface friction angle of 13.40°, which lies between the two interfaces, as seen in Table 4-10, and the highest apparent adhesion was 14.80kPa. Additionally, shear stress values recorded by the double interface for the range of applied normal stresses were consistently higher than those of the single interfaces, with a maximum percentage difference of 33%.

In terms of zero intercepts best-fit linear regression analysis, the interface friction angles observed were similar to those of non-zero intercept linear regression analysis with R^2>0.98. However, the exception was recognised on the double interface GTX-2 | GMB-1 | CD whose interface friction angle increased to 15.67° from 13.40°.

At large displacements (LD), the tested shear-normal stress relationships of the three sets of interfaces were plotted and analysed using the best-fit linear regression approach with zero-intercept. This was because the lining components exhibited negligible apparent adhesion values. The double interface GTX-2 | GMB-1 | CD and single interface GTX-2 | GMB-1 were equally depicted as the weakest interfaces, as seen in Figure 4-12 (c), while a single interface GMB-1 | CD was observed to be the strongest. The weakest interfaces had equal interface friction angles of ~10.50°, as seen in Table 4-10, while the strongest interface exhibited an interface friction angle of ~18.50°. This further highlighted that failure at LD within a double interface GTX-2 | GMB-1 | CD occurred on the weakest single interface GTX-2 | GMB-1.

Table 4-10: Peak & LD strength parameters for GTX-2 | GMB-1 | CD Interface

Strength Type	Interface Configuration		Failure Envelopes					
			Linear (non-zero intercept)			Linear (zero intercept)		
			R^2	δ [°]	c_α [kPa]	R^2	δ [°]	c_α [kPa]
Peak	Single -	GTX-2 | GMB-1	0.9999	11.27	4.30	0.9994	11.95	0.00
		GMB-1 | CD	0.9951	18.45	0.00	0.9951	18.45	0.00
	Double -	GTX-2 | GMB-1 | CD	1.0000	13.40	14.80	0.9962	15.67	0.00
LD	Single -	GTX-2 | GMB-1	-	-	-	0.9997	10.62	0.00
		GMB-1 | CD	-	-	-	0.9950	18.45	0.00
	Double -	GTX-2 | GMB-1 | CD	-	-	-	0.9972	10.59	0.00

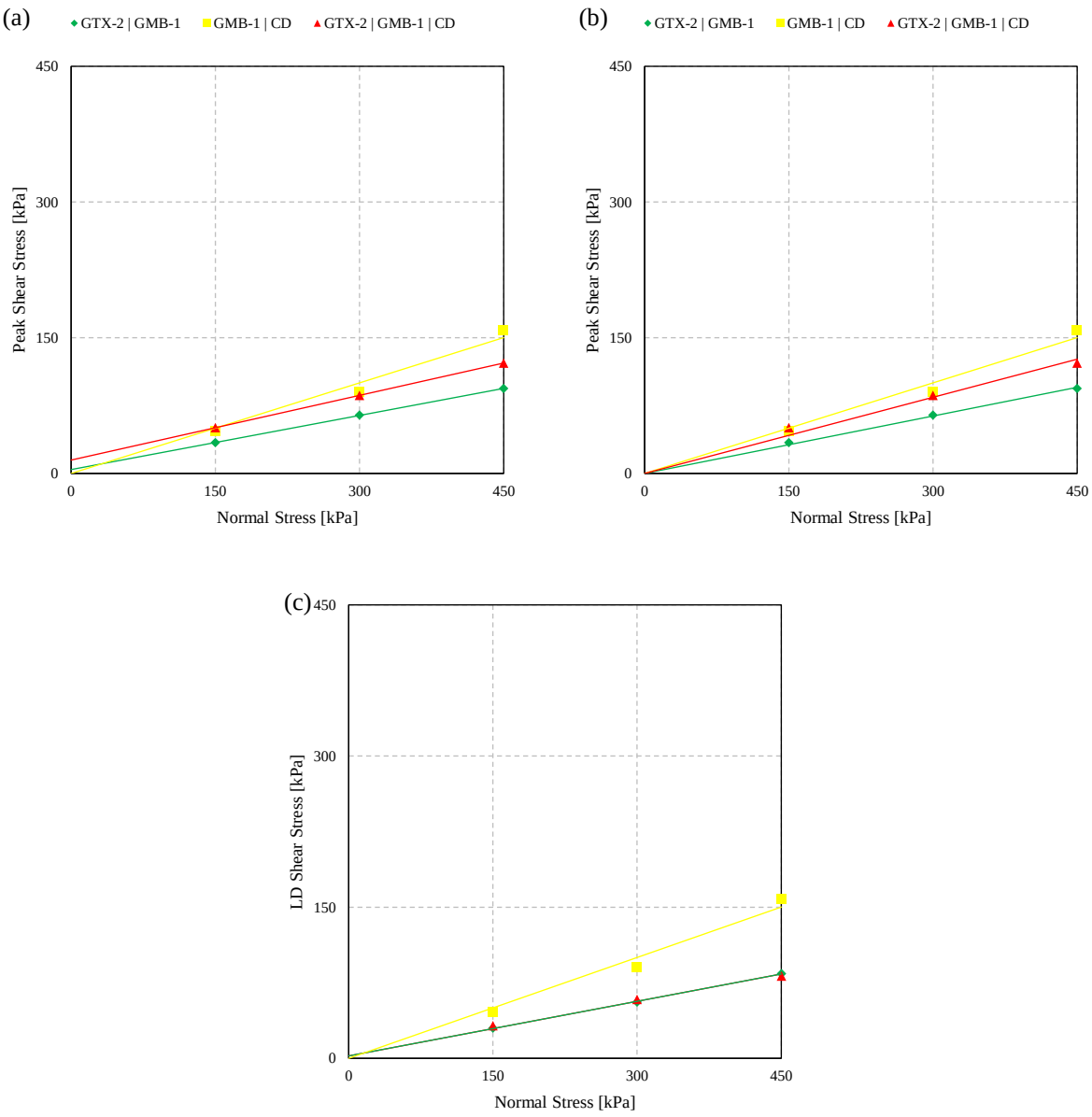

Figure 4-12: Shear stresses against normal stresses for GTX-2 | GMB-1 | CD Interface: (a) & (b) At peak and (c) At LD

4.3.3.4 GMB-1 | CD | GMB-2 Interface

At peak, the strongest interface was observed to be one of the single interfaces, i.e., the CD | GMB-2 interface; this was because the surface of a CD facing GMB-2 was box-textured, as seen in Chapter 3. GMB-2 surface was identical to that of GMB-1, the difference being the raw materials used to manufacture these geomembranes, i.e., HDPE for GMB-1 & LLDPE for GMB-2, attributed to their flexible nature. This meant that the contributing factor to the high interface friction angle was the presence of this box-textured CD material on the face of GMB-2. The strongest interface exhibited an interface friction angle of 24.04° with a maximum shear stress

of 209kPa recorded at an applied normal pressure of 450kPa, as shown in Table 4-4. The weakest interface at the peak was GMB-1 | CD, and it exhibited an interface friction angle of 18.45° with a peak shear stress of 158kPa recorded at an applied normal pressure 450kPa. This peak shear stress was a 24 & 10 % decline compared to the strongest interface (CD | GMB-2) and a double interface GMB-1 | CD | GMB-2.

The failure plane of a double interface GMB-1 | CD | GMB-2 was observed to lie between the two single interfaces, as seen in Figure 4-13 (a) & (b), with an interface friction angle of 20.30° and maximum shear stress of 176kPa that occurred at an applied normal pressure of 450kPa. The double interface's failure plane highlighted all the three lining components that contributed to the shear stresses experienced on the interfaces. When analysed using a zero intercept best-fit linear regression analysis, the interface shear strength parameters, specifically the angles of interface friction, were comparable to those obtained from non-zero linear regression analyses, as seen in Table 4-11. This indicated that the contribution of an apparent adhesion was almost negligible to the changes in interface friction angles for these specific lining components. Worth noting, however, a maximum apparent adhesion of 10kPa was recorded by the CD | GMB-2 and a double interface GMB-1 | CD | GMB-2, as can be seen in Table 4-11, possibly because of the confinement that existed between the box-textured CD and the GMB-2 which ensured a maximum contact area between the lining components.

As seen in section 4.2.2.4, the plots of shear stress against horizontal displacement for all the nine interface shear tests showed that the shear stresses consistently increased up to the horizontal displacement of 75mm, with no residual or large displacement (LD) strengths were observed. This meant that the LD strengths for this set of interfaces were similar to the peak strengths.

Table 4-11: Peak & LD strength parameters for GMB-1 | CD | GMB-2 interface

Strength Type	Interface Configuration		Failure Envelopes					
			Linear (non-zero intercept)			Linear (zero intercept)		
			R^2	δ [°]	c_α [kPa]	R^2	δ [°]	c_α [kPa]
Peak/ LD	Single -	GMB-1 | CD	0.9951	18.45	0.00	0.9951	18.45	0.00
		CD | GMB-2	0.9994	24.04	9.27	0.9994	25.29	0.00
	Double -	GMB-1 | CD | GMB-2	0.9998	20.30	10.00	0.9991	21.48	0.00

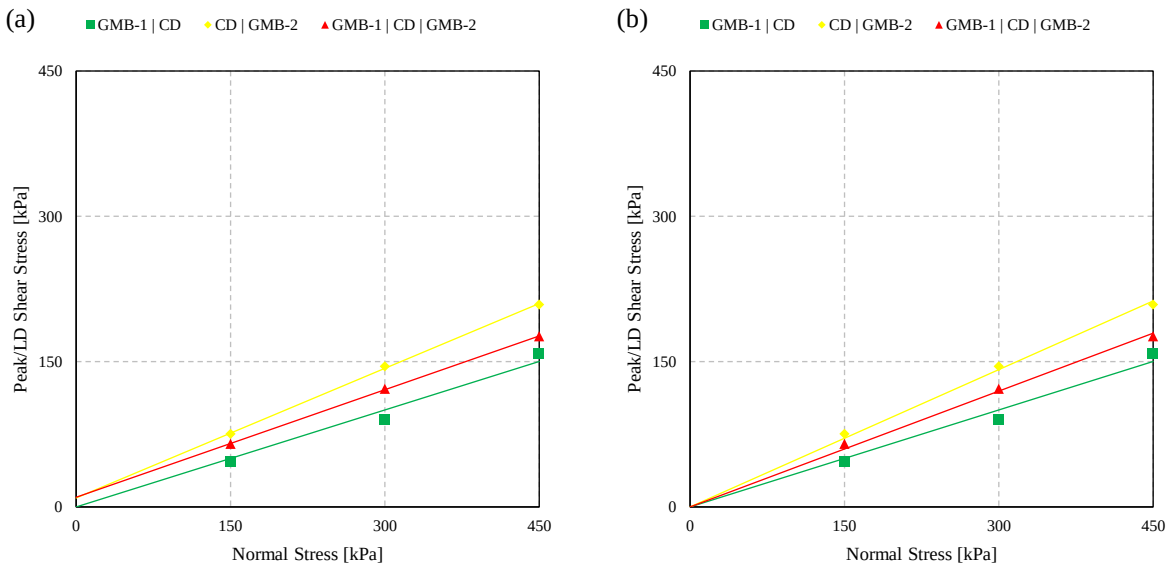

Figure 4-13: Shear stresses against normal stresses for GMB-1 | CD | GMB-2 Interface: (a) & (b) At peak and at LD

4.3.3.5 CD | GMB-2 | SAND Interface

At peak, single interface GMB-2 | SAND achieved maximum shear stress of 254kPa at an applied normal pressure of 450kPa. In contrast, the double interface CD | GMB-2 | SAND achieved minimum shear stress of ~60kPa at an applied normal pressure of 150kPa, as shown in Table 4-5. Generally, shear stresses increased with the increasing applied normal pressures. GMB-2 | SAND interface was the strongest interface, as seen in Figure 4-14 (a) & (b), with an interface friction angle of 29.07° and a negligible apparent adhesion. These results agreed with those determined by Cen, Wang & Sun (2018), where interface friction angles of 28.96° & 30.62° with negligible apparent adhesions were observed for smooth geomembranes sheared against fine and gravelly sands, respectively. It was also noted that sandy particles created minor grooves on the smooth geomembrane surface through polishing, thereby increasing the interface friction properties; this observation was in line with Vangla & Latha (2015). The groove depths mainly depended on the contact area between sand particles and the geomembrane surface.

In contrast, other factors such as particle sizes, angularity, roughness, and hardness of the sand particles remained equally important. In the study by Vangla & Latha (2015), medium sand with D_{50}=0.87 was observed to have the highest peak interface friction angle of 19.04° when tested against a smooth HDPE geomembrane at applied normal pressures of 21, 37 & 53 kPa. In this study, however, the peak interface friction angle was higher due to the sand sample tested against an LLDPE geomembrane (GMB-2) being a mix of fine and medium-sized particles. This allowed sand particles to develop impressions of ploughing and wearing on the geomembrane surface, thereby increasing friction properties.

The results of the GMB-2 | SAND interface at peak also aligned with the results obtained by Bacas, Cañizal & Konietzky (2015), who investigated the frictional behaviour of critical interfaces of a landfill's lining system. In their study, two textured geomembranes were tested against sand under dry conditions at applied normal pressures of 100, 300 & 500 kPa. The failure mechanisms in their study predominantly took place along the internal soil layers and at the superficial level of the asperities interacting with sand (Bacas, Cañizal & Konietzky, 2015). The failure mechanisms were contrary to those observed in this study, where a smooth geomembrane developed micro grooves and polishing by sand particles. Additionally, the interface frictional angle of 29° was recorded by a geomembrane with an average asperity height of 1.3mm, and 31° was recorded by a geomembrane with 0.5mm asperity height interfaced against the sand with 90% fines and 10% coarse particle sizes. Even though the testing conditions in their study were different from this study, it is worth noting that the peak interface angles of friction are almost similar.

The weakest interface in this set was a double interface CD | GMB-2 | SAND. However, with negligible apparent adhesion, it achieved an interface friction angle of 24.51°, a 16% decline from the strongest single interface. CD | GMB-2 interface obtained an interface friction angle of 24.04°, a 2% difference from the weakest interface and an apparent adhesion of 9.27kPa. This highlighted that the failure of the double interface CD | GMB-2 | SAND occurred on the CD | GMB-2 interface. The difference in the interface shear strength parameters was attributed to the effective normal stress transfer among the three lining components due to contact area maximization in the double interface configuration. Furthermore, when analysed using the best-fit linear regression analysis with zero vertical intercepts, the CD | GMB-2 interface recorded a percentage increase of 5% between the interface friction angles measured, as shown in Table 4-12.

At large displacements (LD), the weakest interface was GMB-2 | SAND, and it exhibited an interface friction angle of 22.74°. Compared to an interface angle of friction of 24.04° with an apparent adhesion of 8.33kPa & 25.12° with no apparent adhesion, which was recorded by the strongest interface (CD | GMB-2) as seen in Table 4-12. The double interface CD | GMB-2 | SAND exhibited no apparent adhesion; however, an interface friction angle of 23.99°, a percentage difference of 4.5% and 5.2% compared to the strongest and weakest interfaces, respectively recorded. This indicated that failure within the double interface occurred concurrently at the two interfaces, and the contribution towards the interface friction angle was attributed to all the lining components. In terms of shear stresses, the highest value of 208kPa was recorded by the CD | GMB-2 interface at an applied normal pressure of 450kPa, followed by 199kPa by the double interface CD | GMB-2 | SAND and 189kPa by GMB-2 | SAND interface, both recorded at the same applied normal pressure of 450kPa. The ranges of LD shear stresses and that of the interface angles of friction confirm that the failure within the double interface configuration was a contribution from the three lining elements and that there was a possibility of shear transfer among the components, as can be seen in Figure 4-14 (c) & (d).

Table 4-12: Peak & LD strength parameters for CD | GMB-2 | SAND interface

Strength Type	Interface Configuration		Failure Envelopes					
			Linear (with non-zero intercept)			Linear (with zero intercept)		
			R^2	δ [°]	c_α [kPa]	R^2	δ [°]	c_α [kPa]
Peak	Single -	CD | GMB-2	0.9994	24.04	9.27	0.9994	25.29	0.00
		GMB-2 | SAND	-	-	-	0.9996	29.07	0.00
	Double -	CD | GMB-2 | SAND	-	-	-	0.9982	24.51	0.00
LD	Single -	CD | GMB-2	0.9998	24.04	8.33	0.9995	25.12	0.00
		GMB-2 | SAND	-	-	-	0.9999	22.74	0.00
	Double -	CD | GMB-2 | SAND	-	-	-	0.9987	23.99	0.00

4.3.3.6 SAND | GTX-3 | SAND interface

At peak, maximum shear stress achieved by the SAND | GTX-3S1 interface was 367kPa at an applied normal pressure of 450kPa, while that of the SAND | GTX-3S2 interface was 329kPa. A double interface SAND | GTX-3 | SAND achieved shear stress of 363kPa at the same applied normal pressure as shown in Table 4-6. Regarding percentage differences in shear stresses, the SAND | GTX-3S1 interface recorded a 1% higher and SAND | GTX-3S2 exhibited a 9% lower when compared to the double interface SAND | GTX-3 | SAND. This illustrated that failure in the double interface configuration mainly occurred between the SAND | GTX-3S2 interface and partially on the GTX-3S1.

Contrary to the shear stresses at peak, the interface shear strength parameters obtained from the SAND | GTX-3S2 interface were an interface friction angle of 32.21° and an apparent adhesion value of 44.99kPa. A double interface SAND | GTX-3 | SAND recorded 31.11° and 85.71kPa, respectively. This indicated that the failure envelopes of SAND | GTX-3S2 and a double interface were coherent with a percentage difference of only 3% in the angles of interface friction obtained. Failure envelope overlap was noticed at two distinct points, as seen in Figure 4-15 (a), where SAND | GTX-3S1 interface intercepted SAND | GTX-3S2 interface at an applied normal pressure of ~150kPa, it also intercepted SAND | GTX-3 | SAND interface at an applied pressure of ~350kPa. This overlap transition indicated a change in failure planes for the single interfaces at normal stresses below and above intercepted. When analysed using the best-fit linear regression approach with a zero vertical intercept, i.e., zero apparent adhesion, the SAND | GTX-3S2 interface recorded an interface friction angle of 37.18°. This was lower than its adjacent interface of SAND | GTX-3S1 and the double interface, which recorded a similar interface friction angle of ~40°.

Nonetheless, the R^2 value for the SAND | GTX-3S2 interface with zero-intercept was deficient (~0.75) of the required >0.98. This indicated that the failure envelope for this interface with zero

apparent adhesion was not linear. A further curvilinear regression analysis was conducted for this interface, as seen in Figure 4-15 (b), where the R^2 improved from 0.75 to 0.9939. The recorded average interface shear strength parameters were 13.5° and 73.33kPa for interface friction angle and apparent adhesion, respectively, as seen in Table 4-13. The SAND | GTX-3S2 interface was then identified as the weakest interface for this set, while the SAND | GTX-3S1 interface was the strongest.

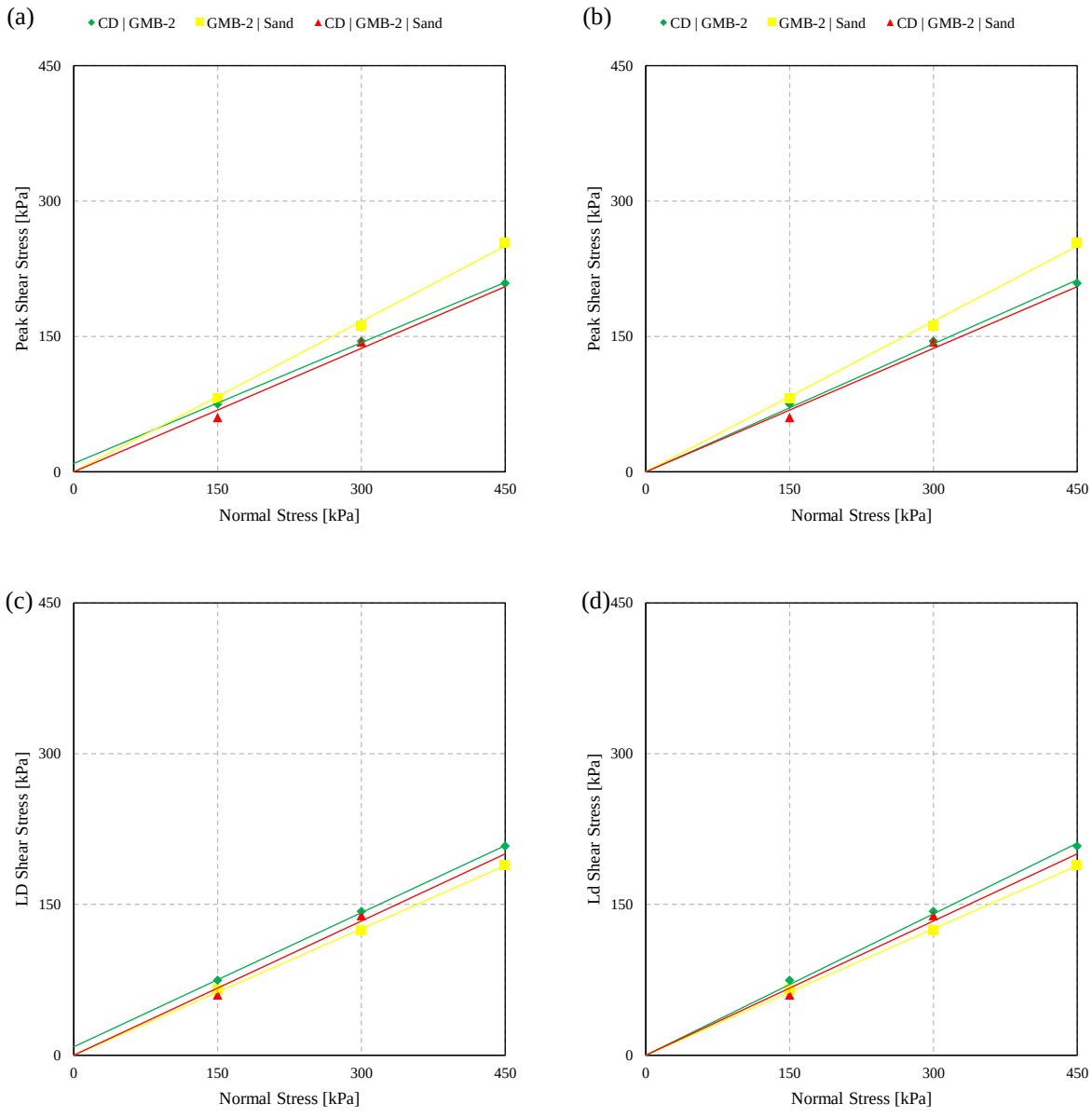

Figure 4-14: Shear stresses against normal stresses for CD | GMB-2 | Sand Interface: (a) & (b) At peak and (c) & (d) At LD

At large displacements (LD), the SAND | GTX-3S1 interface recorded the maximum shear stress as 355kPa at an applied normal pressure of 450kPa, while the SAND | GTX-3S2 interface was

recorded at 209kPa. The double interface SAND | GTX-3 | SAND did not achieve a residual or LD condition as the peak shear stresses were similar to those recorded at a maximum horizontal displacement of 75mm. The SAND | GTX-3S1 interface recorded the highest angle of interface friction of 36.99°. In comparison, its single interface counterpart recorded a lower angle of 12.95°, but with an R^2 value of ~0.50 for linear regression analysis. Also, the adhesion values of 24.66kPa and 124.99kPa were recorded by the SAND | GTX-3S1 and SAND | GTX-3S2 interfaces, respectively. When interpreted using best-fit linear regression analysis at zero apparent adhesion, the SAND | GTX-3S1 interface recorded an interface friction angle of 39.48°, while its single interface counterpart recorded an angle of 30.42°. This highlighted that the different surface outlook of the GTX-3 on either side contributed to the values of interface strength parameters obtained. Additionally, the double interface recorded an interface angle of friction of 31.11° with the adhesion of 85.71kPa, and an interface friction angle of 40.31° when analysed at zero apparent adhesion. These interface strength parameters for a double interface are comparable to those of the SAND | GTX-3S1 interface, highlighting that failure in the dual interface could have occurred on this interface.

The non-linear/curvilinear regression analysis was conducted for the SAND | GTX-3S2 interface to understand further the changes in the interface shear strength parameters for when R^2>0.98. The interface angles of friction were similar at 4.67° when analysed with non-zero and zero vertical intercepts, whilst the apparent adhesion values were 195kPa and 206.67kPa, respectively, as seen in Table 4-14. According to Figure 4-15 (c) & (d), coupled with regression analyses, the double interface SAND | GTX-3 | SAND was depicted as the strongest interface, while the SAND | GTX-3S2 interface was shown to be the weakest for this set.

Table 4-13: Peak & LD strength parameters for SAND | GTX-3 | SAND interface

Strength Type	Interface Configuration		Failure Envelopes					
			Linear (non-zero intercept)			Linear (zero intercept)		
			R^2	δ [°]	c_α [kPa]	R^2	δ [°]	c_α [kPa]
Peak	Single -	SAND | GTX-3S1	0.9929	37.71	24.66	0.9980	40.16	0.00
		SAND | GTX-3S2	0.9999	32.21	44.99	0.7585	37.18	0.00
	Double -	SAND | GTX-3 | SAND	0.9877	31.11	85.71	0.9885	40.31	0.00
LD	Single -	SAND | GTX-3S1	0.9826	36.99	24.66	0.9967	39.48	0.00
		SAND | GTX-3S2	0.5107	12.95	124.99	0.9237	30.42	0.00
	Double -	SAND | GTX-3 | SAND	0.9877	31.11	85.71	0.9854	40.31	0.00

Table 4-14: Peak & LD strength parameters for SAND | GTX-3 | SAND interface

Strength Type	Interface Configuration		Failure Envelopes					
			Non-linear (non-zero intercept)			Non-linear (zero intercept)		
			R^2	δ [°]	c_α [kPa]	R^2	δ [°]	c_α [kPa]
Peak	Single -	SAND | GTX-3S1	-	-	-	-	-	-
		SAND | GTX-3S2	-	-	-	0.9939	13.50	73.33
	Double -	SAND | GTX-3 | SAND	-	-	-	-	-	-
LD	Single -	SAND | GTX-3S1	0.9934	14.17	70.00	1.0000	16.33	56.67
		SAND | GTX-3S2	0.9830	4.67	195.00	1.0000	4.67	206.67
	Double -	SAND | GTX-3 | SAND	-	-	-	-	-	-

4.4 Basal Lining Critical Interface Assessment

4.4.1 Introduction

In both interface direct shear testing configurations, i.e., single and double, the objective was to determine the weakest soil-geosynthetic and geosynthetic-geosynthetic interface through shear-normal stress relationships as presented in Section 4.3. The determination of a critical interface within a multi-layered soil-geosynthetic system is crucial in the design and analysis of side-slope stability of structures where these materials are utilised, for example, in MSW landfills (Bacas, Cañizal & Konietzky, 2015; Khilnani, Stark & Bahadori, 2017). An interface bearing the minimum shear resistance is usually considered a critical interface. It has a high chance of facilitating a structural failure if the generated shear stresses are more than the shear resistances the material components can offer (Stark, Niazi & Keuscher, 2015). According to many design guidelines involving the design of soil-geosynthetic interactions on side-slopes, the critical interface must be identified as this governs the design (Muluti, 2021).

The previous section presented the shear-normal stress relationships and showed that shear resistance depended on normal stress. Thus, any change to the applied normal stress would result in a change in the shear failure. This fact aligned with the findings of other scholars such as Yamsani, Sreedeep & Rakesh (2016). As a result, the critical interface was also analysed depending on the normal stress range anticipated in the field and tested in the laboratory since the critical interface could change abruptly as normal stress changed (Khilnani, Stark & Bahadori, 2017).

This section presents a critical interface assessment for both interface testing configurations at peak and LD for the basal lining system. A comparative evaluation was also conducted to identify the similarities and dissimilarities between critical interfaces obtained from single and double

interface configurations. The assessments presented in this section follow those in Section 4.3. The failure envelopes were provided, and only those with a coefficient of regression (R^2) exceeding 0.98 were considered.

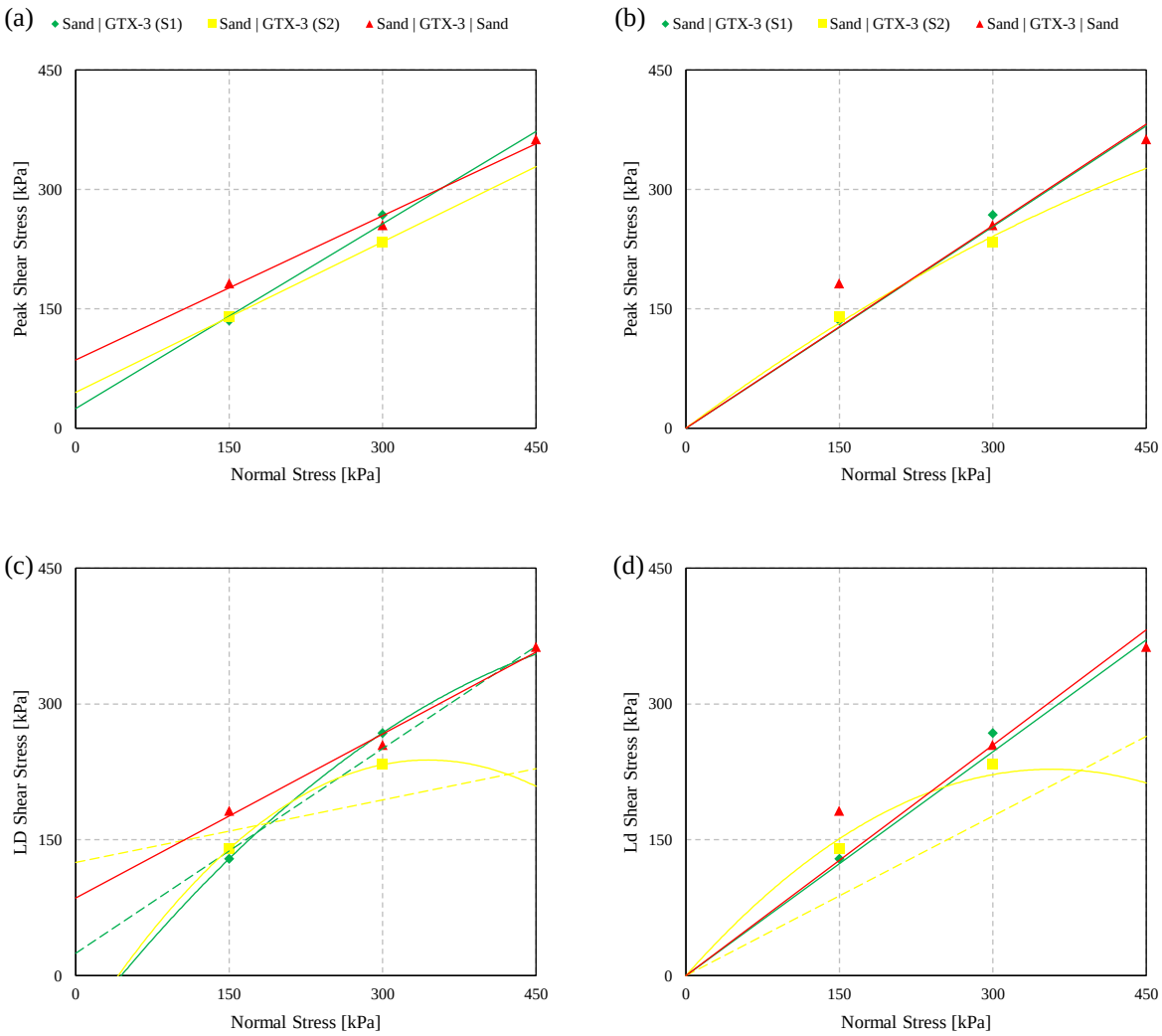

Figure 4-15: Shear stresses against normal stresses for SAND | GTX-3 | SAND Interface: (a) & (b) At peak and (c) & (d) At LD

4.4.2 Peak Strengths

4.4.2.1 Single Interfaces

A summary of soil-geosynthetic and geosynthetic-geosynthetic interfaces tested under a single interface configuration obtained at peak for the range of applied normal stresses is presented in Figure 4-16 (a). The top and bottom shear - normal stress relationships represent the strongest and weakest/critical interfaces. The SAND | GTX-3S1 interface was the strongest interface for

the applied normal pressures exceeding 150kPa. In contrast, its counterpart, i.e., the SAND | GTX-3S2 interface, was the strongest at lower applied normal stresses.

The GTX-2 | GMB-1 interface was the critical interface in this basal lining suite for the whole range of applied normal stresses. Since there was no change in the failure envelope of the weakest/critical interface, a combination failure envelope was deemed unnecessary, as recommended by Stark, Niazi & Keuscher (2015) and Khilnani, Stark & Bahadori (2017). The interface shear strength parameters for both strong and critical interfaces at the peak are presented in Table 4-15.

4.4.2.2 Double Interfaces

The peak strengths for the double interface testing configurations are as seen in Figure 4-16 (b). The double interface arrangement involved testing three lining components, as described in Chapter 3. The LCS | GTX-1 | GS interface was strongest for the applied normal stresses beyond 160kPa, while the SAND | GTX-3 | SAND interface was observed to be the strongest for lower applied normal stresses. The latter observation was in line with what was observed in the single interface testing configuration, where both SAND | GTX-3S1 and SAND | GTX-3S2 interfaces were strong for this basal lining suite. The former, i.e., LCS | GTX-1 | GS interface, however, was observed to produce high shear resistances due to minimal crushing of the LCS layer, which comprised of stones in the top shear box of the LSA. This action enabled the development of a solid intimate/embedment interaction of the LCS with GS layers through the protection geotextile (GTX-1). Additionally, the presence of a GS layer instead of a heavy-duty rigid steel substrate (as is the case of a single interface configuration) in the lower shear box maximised the contact area between the LCS and the protection geotextile, thereby allowing sufficient transfer of applied normal stresses among the lining components.

The GS | GTX-2 | GMB-1 interface was weakest under this testing configuration. As explained in Section 4.3.3.2, failure within this lining set occurred on the GTX-2 | GMB-1 interface, which was also the critical interface under a single interface testing configuration. This observation agreed with other scholars' findings, such as Khilnani, Stark & Bahadori (2017), who established that critical interfaces for the side-slope and basal lining systems were similar for the materials tested under single and multi-layer testing configurations. Additionally, these results for the critical interface were also in line with findings by firstly, Bacas, Cañizal & Konietzky (2015), who identified geomembrane-geotextile combinations as the possible critical interface. And secondly, Adeleke (2020) who observed that a smooth geomembrane produced the least shear resistances compared to a textured geomembrane among the lining components.

Conversely, it was noted that the interface shear strength parameters for the same lining components between the two testing configurations were different. The double interface was observed to have higher shear strength parameters due to a GS layer which increased the shear resistances attributed to its particle sizes polishing on the protection geotextile surface. Table 4-15 presents these interface shear strength parameters.

4.4.3 Large Displacement (LD) Strengths

4.4.3.1 Single Interfaces

Generally, the SAND | GTX-3S1 interface was observed to be the strongest interface at LD for the range of applied normal stresses, as seen in Figure 4-16 (c). An intersection with two curvilinear failure envelopes, i.e., SAND | GTX-3S2 and GTX-1 | GS interfaces, was observed at applied normal stresses between 50 to 225 kPa and 150 to 300 kPa, respectively. This disruption, however, did not affect the interface shear strength parameters of the strongest interface, especially the angle of interface friction, since the curvilinear failure envelopes produced relatively low parameters, as seen in Table 4-15.

The GTX-2 | GMB-1 interface was the weakest single interface at LD, having generated the lowest interface shear resistances at all applied normal stress ranges. This was consistent with what was observed as the weakest/critical interface at peak strengths for single interface configurations. The interface shear strength parameters at LD for this weakest interface are presented in Table 4-15.

4.4.3.2 Double Interfaces

As seen in Figure 4-16 (d), the strongest interface was initially SAND | GTX-3 | SAND interface up to applied normal stress of 200kPa, after which the strongest interface became LCS | GTX-1 | GS. These two strongest double interfaces observed at LD were similar to those observed under peak strengths.

Two interfaces, i.e., CM | GTX-2 | GMB-1 interface and GTX-2 | GMB-1 | CD interface, were observed to be the weakest interfaces, and these produced similar shear resistances at LD conditions as seen in Figure 4-16. As observed in the single interface configurations at peak in Section 4.4.3.1, it was emphasised through the observed shear-normal stress relationship that failure within these two interfaces took place along the GTX-2 | GMB-1 interface. As a result, the combination post-peak/large displacement (LD) strength envelope would coincide with the critical interface as sliding occurred on this interface. Additionally, the interface shear strength parameters for the two double interfaces at LD conditions were similar with interface friction angles at 10.24° & 10.59° for GS | GTX-2 | GMB-1 and GTX-2 | GMB-1 | CD, respectively, as seen in Table 4-15.

4.4.4 Summary of Critical Interface Assessment

This study's critical interface assessment revealed that failure within soil-geosynthetic and geosynthetic-geosynthetic lining components would likely occur at the same interface(s) regardless of the testing configuration. However, the quality of testing conditions remained imperative to ensure that the results obtained were not significantly different (Sikwanda, Kalumba & Nolutshungu, 2019; Muluti, 2021). The study conducted by Stark, Niazi & Keuscher (2015) suggested similar outcomes, where multi-layered interface tests yielded similar

weakest/critical interface in terms of peak strengths as single interface tests. In this study, for both testing configurations, any arrangement of lining components in the LSA that involved the GTX-2 & GMB-1 combination resulted in weaker shear resistances. This was due to the geomembrane not being co-extruded, i.e., smooth on both sides, thereby producing weaker shear resistances as confirmed in other studies by scholars such as Bacas, Cañizal & Konietzky (2015); Buthelezi (2017) & Adeleke (2020).

Peak strengths of the critical interface have been higher for double interface configurations, while LD strengths have yielded either equal or lesser strengths for single interface configurations. This observation aligned with the study's outcome conducted by Stark, Niazi & Keuscher (2015), who found that the peak strengths for single interfaces were lower at higher normal stresses attributed to the testing configuration, which isolated the lining components from the influence of others. In terms of interface shear strength parameters, as summarized in Table 4-15, it was observed that the GTX-2 | GMB-1 interface at LD conditions yielded an angle of interface friction of 9.37° and an apparent adhesion of 3.40kPa, thereby being the critical interface for all single interface configurated tests. While for double interface configurated tests, GTX-2 | GMB-1 | CD interface was the weakest of all, with an angle of interface friction of 10.59° and no apparent adhesion. These critical interfaces for both testing configurations control the design of the proposed MSW landfill cell's side-slope and basal lining structures.

Table 4-15: Summary of strong and weak interface parameters for single & double interface configurations

Strength Type	Configuration	Category	Condition	Interface	δ_p [°]	c_{α}- [kPa]
Peak	Single	Strongest	Normal stresses > 150kPa	SAND | GTX-3S1	37.71	24.66
			Normal stresses < 150kPa	SAND | GTX-3S2	32.21	44.99
		Critical	n/a	GTX-2 | GMB-1	11.27	4.30
	Double	Strongest	Normal stresses > 160kPa	LCS | GTX-1 | GS	44.74	0.00
			Normal stresses < 160kPa	SAND | GTX-3 | SAND	31.11	85.71
		Critical	n/a	GS | GTX-2 | GMB-1	13.55	4.46
LD	Single	Strongest	n/a	SAND | GTX-3S1	36.99	24.66
			Curves seen at applied normal stresses up to 300kPa	SAND | GTX-3S2	4.67	206.67
				GTX-1 | GS	3.33	210.00
		Critical	n/a	GTX-2 | GMB-1	9.37	2.40
	Double	Strongest	Normal stresses > 200kPa	LCS | GTX-1 | GS	41.90	24.17
			Normal stresses < 200kPa	SAND | GTX-3 | SAND	31.11	85.71
		Critical	n/a	GS | GTX-2 | GMB-1	10.24	6.77
				GTX-2 | GMB-1 | CD	10.59	0.00

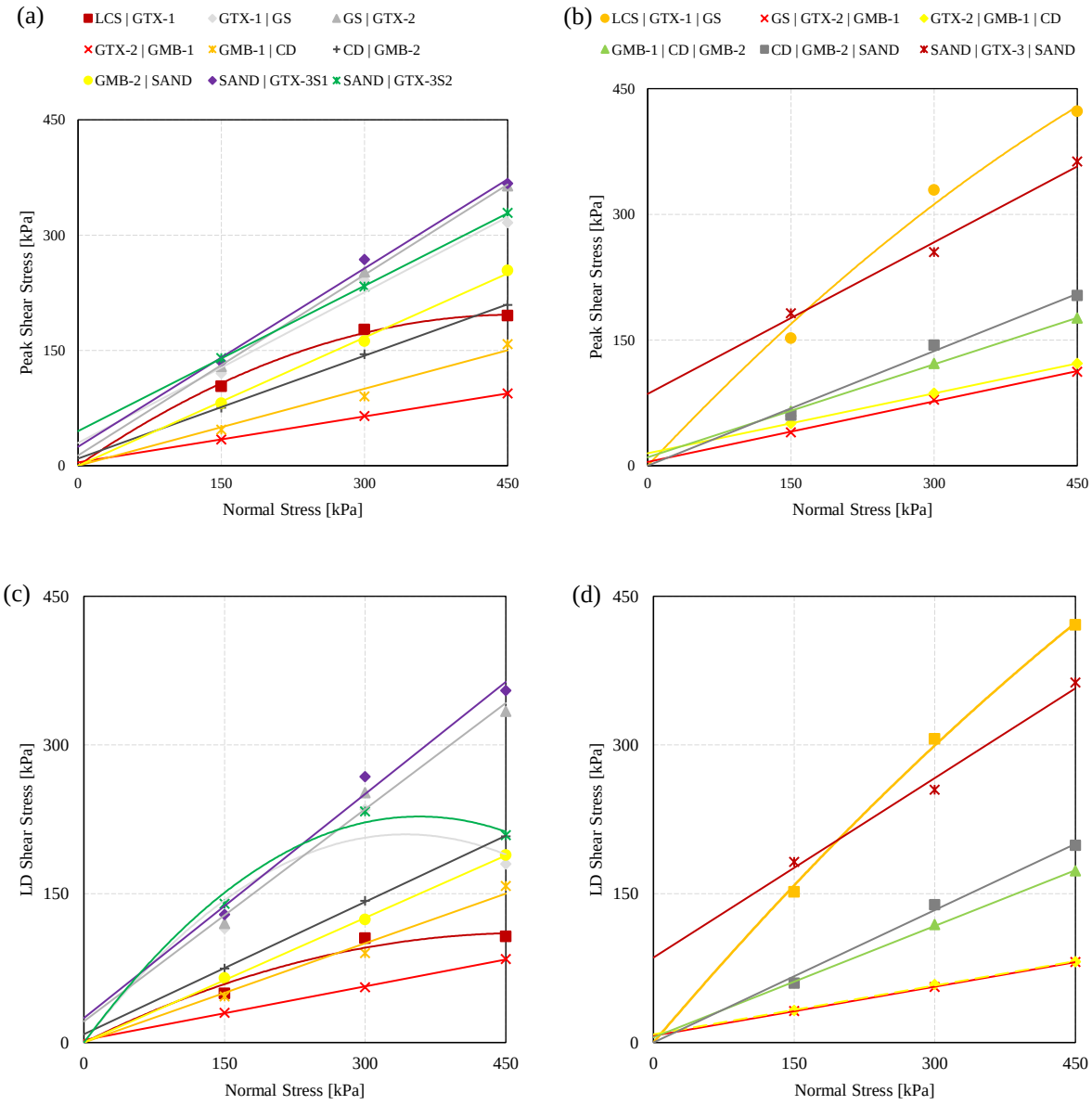

Figure 4-16: Critical Interface Assessment: At peak (a) Single interfaces & (b) Double interfaces and At LD (c) Single interfaces & (d) Double interfaces

5 Design Application

5.1 Introduction

This chapter assesses the obtained interface shear strength results in Chapter 4 on a practical MSW landfill design application by determining the basal lining system's factors of safety (FS). This assessment aimed to critically evaluate similarities and dissimilarities of the calculated minimum and maximum FS from single and double interface configuration shear testing results. The design application assessment implemented in this chapter is for the basal lining system, which contains multi-layered soil-geosynthetic and geosynthetic-geosynthetic interfaces.

Engineered landfills have played a crucial role in protecting both human health and the environment; however, inadequate design of these landfills has resulted in significant failures, which have been well documented by several scholars, including Chang, Mitchell & Seed (1999), Qian (2006), Koda et al. (2019) and Ansari & Daigavane (2021). In their studies, it was commonly found that failure within engineered landfills mainly took place along the liner's base and side-slopes or through landfill subgrades/foundations and through the waste mass itself. Therefore, it became imperative for landfill designers to understand all the failure dynamics and mechanisms before landfills are constructed and commissioned for operations. Two specific failure mechanisms have generally been critical in engineered landfills, i.e., the basal lining system's translational failure and rotational failure, whose analysis is normally implemented through the limit equilibrium method (LEM) and finite element method (FEM), respectively.

For this study, only a translational failure mechanism that assesses the internal stability of the MSW landfill's lining system was considered.

5.2 Design Method

Internal stability of the MSW landfill focuses on the integrity of materials and waste interaction from the subgrade, the linings, and the solid waste. This study implemented the internal stability analysis of the side-slope and base of the proposed MSW landfill cell using the limit equilibrium method (LEM). This method was adopted from a translational failure of a two-part wedge system as presented by Qian, Koerner & Gray (2003); and further modified to include the effect of apparent cohesion and adhesion by Qian & Koerner (2004). Translational failure mechanisms in MSW landfills can occur in two forms: failure of solid waste sliding immediately above or directly beneath the waste mass's basal lining system, as illustrated in Figure 5-1.

The LEM approach offered several benefits over other analytical techniques. It aimed to understand failure mechanisms in the side-slopes, bases, and covers of lining systems utilising soil-geosynthetic and geosynthetic-geosynthetic interface characteristics. The benefits included the ability to determine the magnitude and direction of the inter-wedge forces and the

determination of upper bound (maximum FS) and lower bound (minimum FS) solutions of the landfill stability (Qian & Koerner, 2015). The ultimate solution offered by the LEM approach ensures that the waste strength is not exceeded at any one point in the landfill's lining structure.

Furthermore, this approach incorporated the apparent cohesion/adhesion of lining components. It is worth noting that some lining materials were highly reinforced and exhibited high apparent cohesion/adhesion values to the extent that these cannot simply be ignored in the assessment of FS. Qian & Koerner (2004) argued that excluding apparent cohesion/adhesion could lead to unconservative FS results. Additionally, converting apparent cohesion/adhesion values to an equivalent friction angle could lead to inadequate designs, especially if the tests' parameters were not correctly obtained (Qian & Koerner, 2015). Therefore, the selection of the LEM approach suited this study, as the interface frictional properties obtained from testing using the LSA revealed the presence of apparent adhesions for some of the lining components.

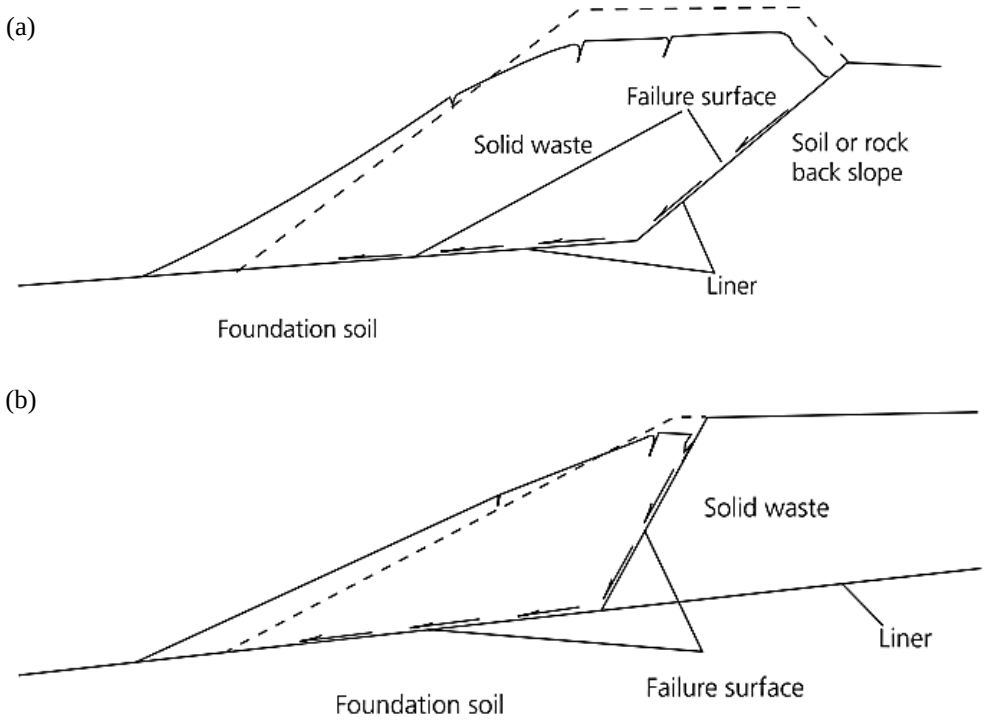

Figure 5-1: Translational failure: (a) completely along (or within) the liner system (b) along (or within) the base liner through waste mass (after Qian & Koerner, 2015)

To suitably estimate FS, a two-part wedge analysis was implemented and consisted of pre-determined sliding failure surfaces which reflected a translational failure mode as adopted from Qian & Koerner (2015) and shown in Figure 5-2. Within the waste mass; there existed a two-part wedge system which included active and passive wedges. An active wedge caused failure on the back-slope, which could be lined or placed over the existing waste mass. However, a passive wedge was on either the foundation subgrade or the basal lining system and was ought

to overcome the instability by providing resistance. The primary assumption of this approach, which greatly met the shear failure criteria, was that the average shear stress on the interface between active and passive wedges should not exceed the average shear strength available (Qian, Koerner & Gray, 2003).

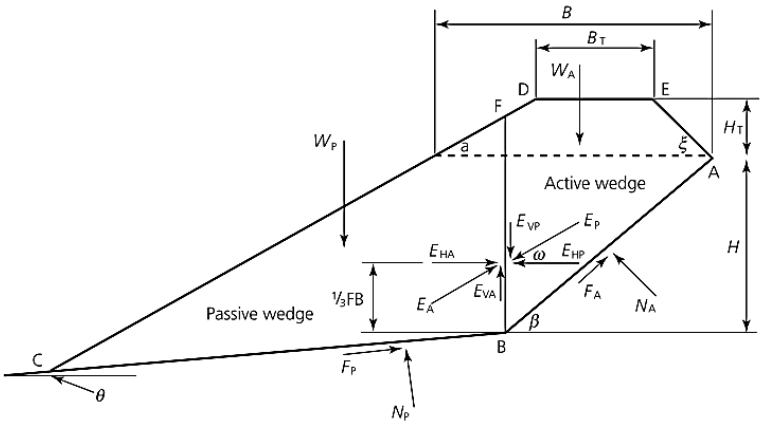

Figure 5-2: Acting forces within waste mass in a landfill cell (after Qian & Koerner, 2015)

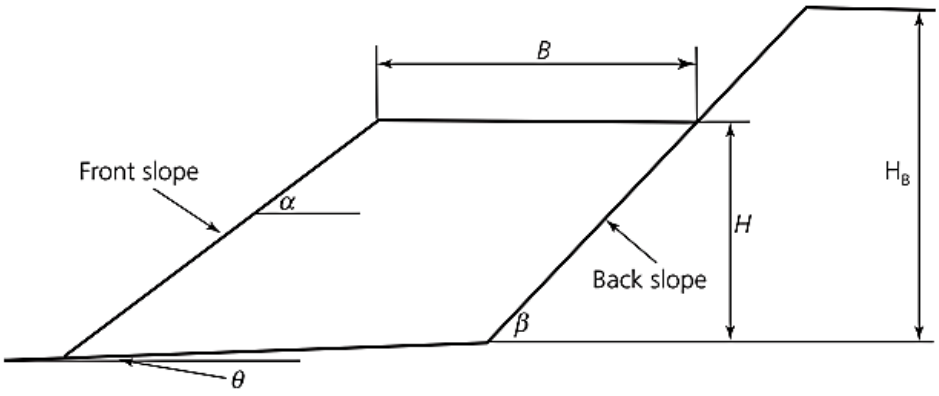

Figure 5-3: Waste filling condition within the landfill cell

The following equations were used to determine the factor of safety (FS) for the basal lining system in this study using a translational failure mode with a two-part wedge system as discussed in detail in studies by Qian, Koerner & Gray (2003), Qian & Koerner (2004, 2015), Qian (2006) and Shi et al. (2020).

$$\text{Factor of Safety (FS)} = \frac{-b \pm \sqrt{b^2 - 4ac}}{2a} \qquad \textbf{Equation 5-1}$$

Where:

$$a = W_T \sin\beta \sin\theta m_{SW} + W_A \sin\beta \cos\theta + W_P \cos\beta \sin\theta - \sin(\beta - \theta) n_{SW}$$

$$b = -\{W_T(\sin\beta\cos\theta\tan\delta_P + \cos\beta\sin\theta\tan\delta_A)m_{SW} - (W_A\tan\delta_P + W_P\tan\delta_A)\sin\beta\sin\theta + (W_A\tan\delta_A + W_P\tan\delta_A)\cos\beta + (C_A\sin\theta + C_P\sin\beta)m_{SW}\}$$

$$c = W_T\cos\beta\cos\theta\tan\delta_A\tan\delta_P m_{SW} - (W_A\cos\beta\sin\theta + W_P\sin\beta\cos\theta)\tan\delta_A\tan\delta_P - \tan\delta_A\tan\delta_P\sin(\beta-\theta)n_{SW} - C_A\sin\theta\tan\delta_P - C_P\sin\beta\tan\delta_A + (C_A\cos\theta\tan\delta_P + C_P\cos\beta\tan\delta_A)m_{SW}$$

$$m_{SW} = \frac{\tan\varphi_{SW}}{FS_V}$$

$$n_{SW} = \frac{C_{SW}}{FS_V}$$

5.3 Design Parameters

Table 5-1 summarises parameters used in the FS assessment for the proposed MSW landfill considering the waste filling sequence and waste mass configuration were similar to that shown in Figure 5-3.

Table 5-1: Summary of geometric and inherent solid waste parameters

Parameter	Meaning	Value	Units
B	Width of the new waste mass at the level of the existing waste mass	35.0	m
C_{SW}	Apparent cohesion of solid waste	3.0	kN/m^2
H	Depth of existing waste mass/height of side-slope	30.0	m
α	The angle of the front slope, measured from horizontal, 3.5(H):1(V)	15.9	°
ϕ_{SW}	Internal friction angle of solid waste	30.0	°
γ_{SW}	Unit weight of solid waste	10.2	kN/m^3
β	The angle of the back slope, measured from horizontal, 4(H):1(V)	18.4	°
θ	The angle of landfill cell subgrade, measured from horizontal, 2%	1.1	°

In terms of interface shear strength parameters, it was necessary to use peak strengths at the base and large displacement (LD) strengths on the side-slopes. Several scholars, for example, Qian & Koerner (2015), support this approach because the critical interface may be different at the base and the side-slopes (or back-slopes) of the lining system since it is mainly influenced by the variability of waste depth and placement routines. Therefore, it could lead to unconservative results if a landfill is lined with multi-layered geosynthetics and only one type of strength for the critical interface is used for the stability analyses. It was also imperative that the site and project-specific materials were used to determine the interface shear strength properties to achieve a good and relevant design. This study's interface shear strength parameters are seen in Table 5-2 & Table 5-3 for single and double interface testing configurations.

Table 5-2: Strength parameters for lining components tested under single interface configuration

No.	Liner Interface		Peak shear strength, used at the base		LD shear strength, used at the back slope	
	Upper Component	Lower Component	δ_P [°]	$C_{P.}$ [kPa]	δ_A [°]	C_A [kPa]
1	LCS	GTX-1	26.40	0.00	15.46	0.00
2	GTX-1	GS	36.43	0.00	28.18	0.00
3	GS	GTX-2	38.08	13.32	35.50	0.00
4	GTX-2	GMB-1	11.27	4.30	9.37	0.00
5	GMB-1	CD	18.45	0.00	18.45	0.00
6	CD	GMB-2	24.04	9.27	24.04	9.27
7	GMB-2	SAND	29.07	0.00	22.74	0.00
8	SAND	GTX-3S1	37.71	24.66	36.99	24.66
9	GTX-3S2	SAND	32.21	44.99	30.42	0.00

Table 5-3: Strength parameters for lining components tested under double interface configuration

No.	Liner Interface			Peak shear strength, used at the base		LD shear strength, used at the back slope	
	Upper Component	Middle Component	Lower Component	δ_P [°]	$C_{P.}$ [kPa]	δ_A [°]	$C_{A.}$ [kPa]
1	LCS	GTX-1	GS	44.74	0.00	44.02	0.00
2	GS	GTX-2	GMB-1	13.55	4.46	10.24	6.77
3	GTX-2	GMB-1	CD	13.40	14.80	10.59	0.00
4	GMB-1	CD	GMB-2	20.30	10.00	20.30	10.00
5	CD	GMB-2	SAND	24.51	0.00	23.99	0.00
6	SAND	GTX-3	SAND	31.11	85.71	31.11	85.71

5.4 Design Results

Since the potential translational failure surface in the lining system on the side-slope could be different to that on the base, the listed interface shear strength parameters in Table 5-2 & Table 5-3 resulted in 81 and 64 possible FS for single and double interface configurations, respectively. For this analysis, the following main assumptions were considered:

- The waste mass was sufficiently strong that failure could only occur along or within the lining system, as illustrated in Figure 5-1.

- All landfill cell variables such as waste filling mechanisms that could change the waste height/depth (H) and top width (B) remained constant. This was necessary to ensure that the objectives of this study were achieved, which were to compare the design consequences of using interface shear results obtained from single and double interface testing configurations.

5.4.1 Maximum Factor of Safety

The maximum factor of safety (FS) was evaluated using formulas presented under Equation 5-1. The value of FS_v exceeding 1 was implemented as recommended by Qian & Koerner (2004). The FS results are presented in Table 5-4 for single interface configuration and Table 5-5 for double interface configuration.

Table 5-4: Maximum factor of safety for single interface testing configuration

Interface at the back slope			1a	2a	3a	4a	5a	6a	7a	8a	9a
		δ_A [°]	15.46	28.18	35.50	9.37	18.45	24.04	22.74	36.99	30.42
		C_A [kPa]	0.00	0.00	0.00	0.00	0.00	9.27	0.00	24.66	0.00
Interface at base	δ_P [°]	C_P [kPa]	**Maximum Factor of Safety (FS_{max})**								
1p	26.40	0.00	4.02	4.68	5.14	3.74	4.16	4.45	4.38	5.25	4.81
2p	36.43	0.00	5.64	6.29	6.74	5.36	5.78	6.06	5.99	6.84	6.42
3p	38.08	13.32	5.94	6.59	7.05	5.67	6.09	6.37	6.30	7.15	6.72
4p	11.27	4.30	2.04	2.73	3.22	1.75	2.19	2.49	2.42	3.33	2.87
5p	18.45	0.00	2.93	3.61	4.08	2.65	3.08	3.37	3.30	4.19	3.74
6p	24.04	9.27	3.68	4.35	4.81	3.40	3.83	4.11	4.04	4.92	4.48
7p	29.07	0.00	4.42	5.07	5.53	4.14	4.56	4.84	4.78	5.64	5.21
8p	37.71	24.66	5.88	6.53	6.98	5.60	6.02	6.30	6.23	7.08	6.66
9p	32.21	44.99	4.92	5.57	6.03	4.64	5.06	5.34	5.28	6.13	5.70

Table 5-5: Maximum factor of safety for double interface testing configuration

Interface at the back slope			1a	2a	3a	4a	5a	6a
		δ_A [°]	44.02	10.24	10.59	20.30	23.99	31.11
		C_A [kPa]	0.00	6.77	0.00	10.00	0.00	85.71
Interface at base	δ_P [°]	C_P [kPa]	**Maximum Factor of Safety (FS_{max})**					
1p	44.74	0.00	9.07	7.10	7.12	7.57	7.75	8.15
2p	13.55	4.46	4.18	2.07	2.08	2.56	2.76	3.18
3p	13.40	14.80	4.16	2.05	2.07	2.54	2.74	3.17
4p	20.30	10.00	5.00	2.93	2.95	3.41	3.61	4.02
5p	24.51	0.00	5.55	3.51	3.52	3.98	4.18	4.59
6p	31.11	85.71	6.52	4.51	4.52	4.98	5.17	5.57

5.4.2 Minimum Factor of Safety

Equation 5-1 presented a general formula for obtaining the factor of safety (FS) under translational failure; however, to determine the minimum FS, $FS_V = \infty \,\&\, m_{SW} = n_{SW} = 0$ conditions were adopted (Qian & Koerner, 2004). Additionally, under this condition, the inclination angle of the inter-wedge (ω) was zero, while the inter-wedge force was perpendicular to the interface along with the active and passive wedges. The results of minimum FS are presented in Table 5-6 for single interface testing configuration and Table 5-7 for double interface testing configuration.

Table 5-6: Minimum factor of safety for single interface testing configuration

Interface at the back slope			1a	2a	3a	4a	5a	6a	7a	8a	9a
		δ_A [°]	15.46	28.18	35.50	9.37	18.45	24.04	22.74	36.99	30.42
		C_A [kPa]	0.00	0.00	0.00	0.00	0.00	9.27	0.00	24.66	0.00
Interface at base	δ_P [°]	C_P [kPa]	**Minimum Factor of Safety (FS_{min})**								
1p	26.40	0.00	2.12	2.86	3.36	1.79	2.29	2.62	2.53	3.49	3.01
2p	36.43	0.00	2.75	3.51	4.02	2.41	2.92	3.26	3.18	4.15	3.66
3p	38.08	13.32	2.88	3.65	4.15	2.54	3.05	3.39	3.31	4.29	3.79
4p	11.27	4.30	1.32	2.03	2.51	1.01	1.48	1.80	1.72	2.64	2.17
5p	18.45	0.00	1.69	2.41	2.90	1.36	1.85	2.17	2.09	3.03	2.55
6p	24.04	9.27	1.99	2.73	3.22	1.66	2.16	2.49	2.40	3.35	2.87
7p	29.07	0.00	2.28	3.02	3.52	1.94	2.44	2.78	2.69	3.65	3.17
8p	37.71	24.66	2.86	3.63	4.13	2.52	3.03	3.37	3.29	4.27	3.77
9p	32.21	44.99	2.51	3.26	3.76	2.17	2.67	3.01	2.92	3.89	3.40

Table 5-7: Minimum factor of safety for double interface testing configuration

Interface at the back slope			1a	2a	3a	4a	5a	6a
		δ_A [°]	44.02	10.24	10.59	20.30	23.99	31.11
		C_A [kPa]	0.00	6.77	0.00	10.00	0.00	85.71
Interface at base	δ_P [°]	C_P [kPa]	**Minimum Factor of Safety (FS_{min})**					
1p	44.74	0.00	5.42	3.12	3.13	3.70	3.92	4.45
2p	13.55	4.46	3.32	1.17	1.19	1.71	1.91	2.40
3p	13.40	14.80	3.32	1.17	1.19	1.71	1.91	2.40
4p	20.30	10.00	3.70	1.52	1.53	2.07	2.27	2.77
5p	24.51	0.00	3.94	1.74	1.75	2.29	2.50	3.01
6p	31.11	85.71	4.42	2.18	2.20	2.75	2.96	3.47

5.5 Discussion of Design Output

The following deductions were made for the internal stability of the MSW landfill's basal lining system assessed using a translational failure mechanism with LEM:

- For maximum FS assessment on single interface configuration, GTX-2 | GMB-1 interface achieved the lowest value with 1.75 for the MSW landfill cell's base and side-slope. This indicated that failure within the bottom and side-slope lining system would first occur on this interface. The highest FS value of 7.15 was achieved by GS | GTX-2 interface on the base and the SAND | GTX-3S1 interface on the side-slope.
- For a maximum FS assessment on the double interface testing configuration, an FS of between 2.05 and 2.08 was obtained for interfaces involving GTX-2 & GMB-1. These included GS | GTX-2 | GMB-1 and GTX-2 | GMB-1 | CD interfaces. If failure were to occur, both interfaces would have contributed, and it would have taken place in both landfill sub-structures, i.e., on the base and on the side-slope. The highest value of FS in the double interface configuration was 9.07, achieved by the LCS | GTX-1 | GS interface. Additionally, GMB-1 | CD | GMB-2, CD | GMB-2 | SAND and SAND | GTX-3 | SAND interfaces all achieved the highest FS as shown in Table 5-5 compared to the highest value achieved by the single interface GS | GTX-2 of 7.15.
- With the minimum FS, the lowest value of 1.01 was obtained by a single interface GTX-2 | GMB-1. This observation was similar to that of the maximum FS. Therefore, it can be deduced that the GTX-2 | GMB-1 interface was the weakest, and if failure were to occur, this interface would be the first to fail at both locations of the landfill, i.e., at the base and at the side-slope. Additionally, the highest value of FS observed under minimum FS evaluation was 4.29, with the base interface being GS | GTX-2 and the side-slope interface being SAND | GTX-3S1. For this, too, interfaces observed were like those seen in the maximum FS assessment.
- For a double interface minimum FS evaluation, it was observed that an interface with GTX-2 and GMB-1 combination had the lowest minimum FS of between 1.17 to 1.19, as can be seen in Table 5-7. This observation revealed a similar scenario as that observed with the maximum FS evaluation, in that a double interface configuration achieved a marginally higher minimum FS which had an approximately 14% increase. The highest value (5.42) of minimum FS was observed at the LCS | GTX-1 | GS interface, indicating that this interface was the most robust in both landfill locations, i.e., at the base and the side-slope. Another double interface that recorded a higher value of minimum FS than the single interface testing configuration was the SAND | GTX-3 | SAND interface, with 4.45 at the side-slope and 4.42 at the base.

Generally, it should be noted that during a landfill's operation, the only parameters that change are geometric ones, precisely the depth of the waste (H) and top width of the waste (B). As a

result, the waste filling sequence should be suitably designed to suit the minimum FS of 1.3 (DWAF, 1998). According to Qian, Koerner & Gray (2003), the lower bound results or minimum FS may be directly applied in practice due to their conservativeness. In this study, a worst-case scenario was considered where the H & B dimensions were overshot since the proposed MSW landfill cell was expected to operate for at least 15years. This led to achieving a minimum FS of 1.01 on the GTX-2 | GMB-1 interface, which was the critical interface for the basal lining system of the proposed MSW landfill.

6 Conclusions & Recommendations

6.1 Introduction

This study focused on understanding the similarities and dissimilarities of interface shear results for soil-geosynthetic and geosynthetic-geosynthetic interactions conducted in the laboratory using a *ShearTrac-III* LSA of 305mm×305mm. The study involved a series of interface shear tests implemented using two testing configurations, i.e., single and double interfaces. The test results were analysed by assessing several relationships, including shear stress - horizontal displacement, vertical displacement - time, and shear stress - normal stress relationships. Failure envelopes were studied at the peak, and large displacements (LD) and the interface shear strength parameters for both interface shear testing configurations were consequently determined. Interpretation of these results included assessing the tested specimens to pinpoint failure modes and establishing an interface at which failure could have occurred, especially for a double interface testing configuration.

Furthermore, the results obtained in both testing configurations were used in the practical design application of an MSW landfill cell through a two-part wedge limit equilibrium method (LEM) to understand the difference in the resulting minimum and maximum factors of safety (FS).

This chapter presents a summary of conclusions and recommendations established from this study.

6.2 Conclusions

The following conclusions were established from this study based on the observations of the interface shear tests and the practical design application:

i Higher shear strengths at peak and LD were generally observed under single interface configurations. This observation was attributed to specimen clamping in the LSA under a single interface configuration compared to double interface configurations where one specimen was unclamped and sandwiched between the two clamped geosynthetics or compacted geomaterials to allow failure to occur on an interface with weakest shear resistances.

ii For interfaces that involved geomaterials, i.e., soil and stone in their setups, for instance, LCS | GTX-1 | GS, GS | GTX-2 | GMB-1, CD | GMB-2 | SAND & SAND | GTX-3 | SAND; higher interface friction angles and apparent adhesion parameters were observed at peak, and there was a decline at LD. However, interfaces that involved only geosynthetics in their setups, such as GTX-2 | GMB-1 | CD & GMB | CD | GMB-2 interfaces; similar interface friction angles and apparent adhesion parameters at peak and LD were generally observed.

iii The extent of soil ploughing or blistering in the lower shear box increased with increasing applied normal pressures for interfaces that involved geomaterials in both shear boxes. This action had a negative impact on the interface shear results and posed a drawback towards double or multi-interface shear testing for this kind of specimen arrangement.

iv For tests that involved soil-geosynthetic-soil such as LCS | GTX-1 | GS & SAND | GTX-3 | SAND, a non-linearity of Mohr-Coulomb failure envelopes was observed. A non-linear/curvilinear analysis decreased the interface friction angle while an apparent adhesion value increased. However, the interface shear strength parameters obtained through a non-linear or curvilinear approach must be carefully interpreted before being applied, as more shear strength is held in the apparent adhesion parameter. Therefore, both parameters should be utilized to ensure that the shear strength is correctly captured to avoid under or overdesigning.

v The double interface configuration for the LCS | GTX-1 | GS interface set achieved higher shear strength, producing higher shear strength parameters than its constitutive single interfaces. This resulted from sufficient specimen intimate interaction in the double interface configuration where LCS (in the upper shear box) interacted with GS (in the lower shear box) through a protection geotextile. As opposed to the single interface configuration where the lower shear box constituted a heavy-duty rigid steel substrate. Additionally, when gravel materials are involved in interface shear tests, they tend to produce a minimum shear contact area due to their large particle sizes, thereby affecting shear strength estimation.

vi The double interface configuration revealed that failure occurs along the same interface as in the single interface configuration, provided that the shear plane is the weakest. For instance, tests conducted on a double interface GS | GTX-2 | GMB-1 produced interface shear strength parameters similar to those of the single interface GTX-2 | GMB-1.

vii This study also found that some of the lining components may improve shear resistances of others but only when tested consecutively as in the double interface testing configuration. For instance, due to a GS layer in the double interface configuration GS | GTX-2 | GMB-1, the shear resistances observed were 18% higher than the constitutive single interfaces.

viii Comparing both testing configurations, the lowest value of FS_{max} obtained by the double interface configuration (2.05) was higher by 15% than that obtained by the single interface configuration (1.75). Similarly, a 14% difference was observed in the FS_{min} assessment, where the lowest value of FS obtained by the double interface (1.17) was higher than that of a single interface (1.01). For both FS assessments, interfaces involving GTX-1 and GMB-1 were observed to produce the lowest values of FS. This meant that, in terms of the maximum and minimum factors of safety for the lining system on both the

base and side-slope of the proposed lining system, the double interface configuration was unconservative as it overestimated FS.

6.3 Recommendations

The following are recommendations resulting from this study:

i More research is recommended on other or similar soil-geosynthetic and geosynthetic-geosynthetic interactions with different lining arrangements to develop a large database that will, in the long run, result in a conclusive certainty with regards to double or multiple interface testing.

ii As this study utilized a 305mm×305mm LSA, other equipment with larger dimensions and possibly those that can produce horizontal displacements exceeding 75mm should be used for further studies. This is important as this study found that double interface configurations with geomaterials in lower and upper shear boxes produced a peak condition at a very large horizontal displacement, thus making them equivalent to the LD strengths.

References

Adeleke, D. 2020. An Investigation into the Effects of Asperities on Geomembrane/Geotextile Interface Shear Characteristics. MSc Thesis submitted to the University of Cape Town.

Adeleke, D., Kalumba, D. & Hardie, P. 2019. Effects of asperities on the geotextile-geomembrane interface shear characteristics. In *Proceedings of the 13th Australia New Zealand Conference on Geomechanics. H.E. Acosta-Martínez & B.M. Lehane, Eds. Perth, Western Australia: Australian Geomechanics Society, 1–3 April 2019, ISBN: 978-0-9946261-0-3, pp. 699–704*.

Adeleke, D., Kalumba, D. & Oriokot, J. 2019. Asperities effect on polypropylene & polyester geotextile-geomembrane interface shear behaviour. *E3S Web of Conferences*. 92:1–5. DOI: 10.1051/e3sconf/20199213017.

Adeleke, D., Kalumba, D., Nolutshungu, L. & Oriokot, J. 2021. Assessment of asperities geometry influence on MSW landfill critical interface side-slope stability using probabilistic analysis. In *Proceedings of The Evolution of Geotech - 25 Years of Innovation, 20-21 April 2021, pp.196-201*. 196–201.

Adeleke, D., Kalumba, D., Nolutshungu, L., Oriokot, J. & Martinez, A. 2021. The Influence of Asperities and Surface Roughness on Geomembrane/Geotextile Interface Friction Angle. *International Journal of Geosynthetics and Ground Engineering*. 7(2):1–12. DOI: 10.1007/s40891-021-00265-y.

Akpinar, M. V. & Benson, C.H. 2005. Effect of temperature on shear strength of two geomembrane-geotextile interfaces. *Geotextiles and Geomembranes*. 23(5):443–453. DOI: 10.1016/j.geotexmem.2005.02.004.

AKS Lining Systems (Pty) Ltd. 2015. *Flat Die Extruded Smooth Geomembrane Technical Data*.

Allen, A. 2001. Containment landfills: The myth of sustainability. *Engineering Geology*. 60(1–4):3–19. DOI: 10.1016/S0013-7952(00)00084-3.

Ansari, A. & Daigavane, P.B. 2021. Analysis and modelling of slope failures in municipal solid waste dumps and landfills: A review. *Nature Environment and Pollution Technology*. 20(2):825–831. DOI: 10.46488/NEPT.2021.v20i02.045.

Aquatan (Pty) Ltd. 2017. *Hi-Drain Technical Data Sheet*.

ASTM. 2020a. *ASTM D6243/D6243M - 20, Standard Test Method for Determining the Internal and Interface Shear Strength of Geosynthetic Clay Liner by the Direct Shear Method*. West Conshohocken, PA, USA.

ASTM. 2020b. *ASTM D5321/D5321M - 20, Standard Test Method for Determining the Shear Strength of Soil-Geosynthetic and Geosynthetic-Geosynthetic Interfaces by Direct Shear*. West Conshohocken, PA, USA.

Bacas, B.M., Cañizal, J. & Konietzky, H. 2015. Frictional behaviour of three critical geosynthetic interfaces. *Geosynthetics International*. 22(5):355–365. DOI: 10.1680/jgein.15.00017.

Belczyk, E.B. & Smith, C.C. 2012. Geosynthetic landfill cap stability: Comparison of limit equilibrium, computational limit analysis and finite element analyses. *Geosynthetics International*. 19(2):133–146. DOI: 10.1680/gein.2012.19.2.133.

Biswas, A. 2019. Comparative performance of different geosynthetics on sandy soil overlying clay subgrades of varying strengths. *Innovative Infrastructure Solutions*. 4(1):1–16. DOI: 10.1007/s41062-019-0204-5.

Biswas, A., Asfaque Ansari, M., Dash, S.K. & Murali Krishna, A. 2015. Behaviour of Geogrid Reinforced Foundation Systems Supported on Clay Subgrades of Different Strengths. *International Journal of*

Geosynthetics and Ground Engineering. 1(3):1–10. DOI: 10.1007/s40891-015-0023-5.

Bonaparte, R., Bachus, R.C. & Gross, B.A. 2020. Geotechnical Stability of Waste Fills: Lessons Learned and Continuing Challenges. *Journal of Geotechnical and Geoenvironmental Engineering*. 146(11):05020010. DOI: 10.1061/(ASCE)gt.1943-5606.0002291.

De Brito Galvão, T.C., Kaya, A., Ören, A.H. & Yükselen, Y. 2008. Geomechanics of landfills - Innovative technology for liners. *Soil and Sediment Contamination*. 17(4):411–424. DOI: 10.1080/15320380802146693.

Burland, J.B. 1990. On the compressibility and shear strength of natural clays. *Geotechnique*. 40(3):329–378. DOI: 10.1680/geot.1990.40.3.329.

Buthelezi, S. 2017. Comparison of Shear Strength Properties of Textured Polyethylene Geomembrane Interfaces in Landfill Liner Systems. MSc Thesis submitted to the University of Cape Town.

Buthelezi, S., Kalumba, D. & James, G. 2016. Comparison of interface shear strength characteristics of HDPE and LLDPE geomembrane interfaces. In *Proceedings of the 6th EuroGeo Conference (EuroGeo6), Ljubljana Exhibition and Convention Centre, Ljubljana, Slovenia, 25-28 September, 2016, pp. 1067-1076.*

Cen, W.J., Wang, H. & Sun, Y.J. 2018. Laboratory investigation of shear behaviour of high-density polyethylene geomembrane interfaces. *Polymers*. 10(7). DOI: 10.3390/polym10070734.

Chai, J.C. & Saito, A. 2016. Interface Shear Strengths Between Geosynthetics and Clayey Soils. *International Journal of Geosynthetics and Ground Engineering*. 2(3):1–9. DOI: 10.1007/s40891-016-0060-8.

Chang, M.H., Mitchell, J.K. & Seed, R.B. 1999. Model Studies of the 1988 Kettleman Hills Landfill Slope Failure. *Geotechnical Testing Journal*. 22(1):61–66. DOI: 10.1520/gtj11316j.

Chinkulkijniwat, A., Horpibulsuk, S., Bui Van, D., Udomchai, A., Goodary, R. & Arulrajah, A. 2017. Influential factors affecting drainage design considerations for mechanical stabilised earth walls using geocomposites. *Geosynthetics International*. 24(3):224–241. DOI: 10.1680/jgein.16.00027.

Chiu, P. & Fox, P.J. 2004. Internal and interface shear strengths of unreinforced and needle-punched geosynthetic clay liners. *Geosynthetics International*. 11(3):176–199. DOI: 10.1680/gein.11.3.152.44482.

Choudhary, A.K. & Krishna, A.M. 2016. Experimental Investigation of Interface Behaviour of Different Types of Granular Soil/Geosynthetics. *International Journal of Geosynthetics and Ground Engineering*. 2(1):1–11. DOI: 10.1007/s40891-016-0044-8.

Dai, Z., Huang, Y., Jiang, F. & Huang, M. 2016. Modelling the flow behaviour of a simulated municipal solid waste. *Bulletin of Engineering Geology and the Environment*. 75(1):275–291. DOI: 10.1007/s10064-015-0735-8.

Dananaj, I., Frankovská, J. & Janotka, I. 2005. The influence of smectite content on microstructure and geotechnical properties of calcium and sodium bentonites. *Applied Clay Science*. 28(1-4 SPEC. ISS.):223–232. DOI: 10.1016/j.clay.2004.02.006.

Department of Environmental Affairs. 2013. *Regulation 634, 635 and 636: Waste Classification and Management Regulations, National Norms and Standards for the Assessment of Waste for Landfill Disposal*. Available: http://www.greengazette.co.za/pages/national-gazette-37230-of-17-january-2014-vol-583_20140117-GGN-37230-003%0Awww.gpwonline.co.za.

Department of Environmental Affairs (DEA). 2011. *National Waste Management Strategy*. Available: https://www.environment.gov.za/sites/default/files/docs/nationalwaste_management_strategy.pdf.

Department of Water Affairs and Forestry. 1998b. *Minimum requirements for waste disposal by landfill*. 2nd Editio ed. Pretoria, Republic of South Africa: Department of Water Affairs & Forestry.

Eid, H.T. 2011. Shear strength of geosynthetic composite systems for the design of landfill liner and cover slopes. *Geotextiles and Geomembranes*. 29(3):335–344. DOI: 10.1016/j.geotexmem.2010.11.005.

El-Fadel, M., Shazbak, S., Saliby, E. & Leckie, J. 1999. Comparative assessment of settlement models for municipal solid waste landfill applications. *Waste Management and Research*. 17(5):347–368. DOI: 10.1034/j.1399-3070.1999.00059.x.

Esterhuizen, J.J.B., Filz, G.M. & Michael Duncan, J. 2001. Constitutive Behaviour of Geosynthetic Interfaces. *Geotechnical and Geoenvironmental Engineering*. 127(July):810–817.

Feng, S.J. & Lu, S.F. 2016. Repeated shear behaviours of geotextile/geomembrane and geomembrane/clay interfaces. *Environmental Earth Sciences*. 75(3):1–13. DOI: 10.1007/s12665-015-4994-2.

Feng, S.J., Chen, Y.M., Gao, L.Y. & Gao, G.Y. 2010. Translational failure analysis of landfill with retaining wall along the underlying liner system. *Environmental Earth Sciences*. 60(1):21–34. DOI: 10.1007/s12665-009-0166-6.

Fowmes, G. 2007. Analysis of Steep Sided Landfill Lining Systems. EngD Thesis submitted to Loughborough University. Available: https://www.academia.edu/26842812/Analysis_of_steep_sided_landfill_lining_systems?auto=download&email_work_card=download-paper.

Fowmes, G., Dixon, N. & Jones, D.R. V. 2007. Landfill stability and integrity: the UK design approach. *Proceedings of the Institution of Civil Engineers - Waste and Resource Management*. 160(2):51–61. DOI: 10.1680/warm.2007.160.2.51.

Fox, P.J. & Stark, T.D. 2015. State-of-the-art report: GCL shear strength and its measurement – ten-year update. *Geosynthetics International*. 22(1):3–47. DOI: 10.1680/gein.14.00030.

Gapak, Y., Yamsani, S.K., Sreedeep, S. & Rakesh, R.R. 2017. Long-term permeability characteristics of soil-geosynthetic combination used in landfill covers. *Advances in Civil Engineering Materials*. 6(1):296–309. DOI: 10.1520/ACEM20160068.

Geocomp. 2018. *Control and Report Software for Fully Automated Direct Shear Tests on ShearTrac-III Systems*. Acton, MA 01720 U.S.A.

Ghazizadeh, S. & Bareither, C.A. 2021. Failure mechanisms of geosynthetic clay liner and textured geomembrane composite systems. *Geotextiles and Geomembranes*. 49(3):789–803. DOI: 10.1016/j.geotexmem.2020.12.009.

Guarena, N., Dominijanni, A. & Manassero, M. 2020. From the design of bottom landfill liner systems to the impact assessment of contaminants on underlying aquifers. *Innovative Infrastructure Solutions*. 5(1):1–13. DOI: 10.1007/s41062-019-0251-y.

Hegde, A. & Roy, R. 2018. A Comparative Numerical Study on Soil–Geosynthetic Interactions Using Large Scale Direct Shear Test and Pullout Test. *International Journal of Geosynthetics and Ground Engineering*. 4(1):1–11. DOI: 10.1007/s40891-017-0119-1.

Hodson, E.L., Martin, D. & Prinn, R.G. 2010. The municipal solid waste landfill as a source of ozone-depleting substances in the United States and the United Kingdom. *Atmospheric Chemistry and Physics*. 10(4):1899–1910. DOI: 10.5194/ACP-10-1899-2010.

Idowu, I.A., Atherton, W., Hashim, K., Kot, P., Alkhaddar, R., Alo, B.I. & Shaw, A. 2019. Analyses of the status of landfill classification systems in developing countries: Sub Saharan Africa landfill experiences. *Waste Management*. 87:761–771. DOI: 10.1016/j.wasman.2019.03.011.

Jafari, Navid; Stark, Timothy; Thalhamer, T. 2016. Mapping Elevated Temperatures in Municipal Solid Waste Landfills 1. *GLOBAL WASTE MANAGEMENT SYMPOSIUM 2016 Mapping*. (1):2–5.

Jafari, N.H. & Stark, T.D. 2017. Service life and design implications of HDPE geomembranes at elevated temperature landfills. *Geotechnical Special Publication*. (GSP 280):198–208. DOI: 10.1061/9780784480472.021.

Jingjing, F. 2014. Leakage performance of the GM/CCL liner system for the MSW landfill. *The Scientific World Journal*. DOI: 10.1155/2014/251465.

Kalumba, D. 1998. Effect of Grading and Grain Size on the Friction Characteristics of a Sand/Geotextile Interface. MSc Thesis submitted to the University of Cape Town.

Kalumba, D. & Scheele, F. 1999. Friction Characteristics of Sand/Geotextile Interfaces for Three Selected Sand Materials. In *12th African Regional Conference: Conference Proceedings, Durban, South Africa*.

Kaytech Engineered Fabrics Ltd. 2013. *RockGrid PC Wrap Around Walls Installation Guideline*.

Kaytech Engineered Fabrics Ltd. 2014. *Bidim Storage & Installation Guide*.

Kaytech Engineered Fabrics Ltd. 2017a. *Bidim Information Sheet*.

Kaytech Engineered Fabrics Ltd. 2017b. *RockGrid PC Brochure*.

Kaytech Engineered Fabrics Ltd. 2019. *Bidim Technical Data Sheet with MARV values*.

Khilnani, K., Stark, T.D. & Bahadori, T.M. 2017. Comparison of Single and Multi-Layer Interface Strengths for Geosynthetic/Geosynthetic and Soil/Geosynthetic Interfaces. 42–51. DOI: 10.1061/9780784480434.005.

Kim, D. & Frost, J.D. 2011. Effect of geotextile constraint on geotextile/geomembrane interface shear behaviour. *Geosynthetics International*. 18(3):104–123. DOI: 10.1680/gein.2011.18.3.104.

Kiptoo, D., Aschrafi, J., Kalumba, D., Lehn, J., Moormann, C. & Zannoni, J. 2017. Laboratory Investigation of a Geosynthetic Reinforced Pavement under Static and Dynamic Loading. *American Society for Testing and Materials (ASTM) Journal of Testing and Evaluation*. Volume 45(ISSN 0090-3973: Issue 1). DOI: https://doi.org/10.1520/JTE20160170.

Kloprogge, J.T., Komarneni, S. & Amonette, J.E. 1999. Synthesis of smectite clay minerals: A critical review. *Clays and Clay Minerals*. 47(5):529–554. DOI: 10.1346/CCMN.1999.0470501.

Koda, E., Grzyb, M., Osiński, P. & Vaverková, M.D. 2019. Analysis of failure in landfill construction elements. *MATEC Web of Conferences*. 284:03002. DOI: 10.1051/matecconf/201928403002.

Koerner, R.M. 2005. *Design with Geosynthetics*. 5th ed. Upper Saddle River, New Jersey: Pearson Prentice Hall.

Lancione, M. & McFarlane, C. 2016. Life at the urban margins: Sanitation infra-making and the potential of experimental comparison. *Environment and Planning A*. 48(12):2402–2421. DOI: 10.1177/0308518X16659772.

Lin, H., Shi, J., Qian, X. & Zhang, L. 2014. An improved simple shear apparatus for GCL internal and interface stress-displacement measurements. *Environmental Earth Sciences*. 71(8):3761–3771. DOI: 10.1007/s12665-013-2810-4.

Lin, H., Zhang, L. & Xiong, Y. 2018. Research on shear strength of needle-punched GCL by simple-shear of composite liner. *Engineering Geology*. 244(August):86–95. DOI: 10.1016/j.enggeo.2018.07.022.

Lopes, M.L. & Silvano, R. 2010. Soil/Geotextile Interface Behaviour in Direct Shear and Pullout Movements. *Geotechnical and Geological Engineering*. 28(6):791–804. DOI: 10.1007/s10706-010-9339-z.

Mawer, B. & Kalumba, D. 2014. The potential for reinforcement of soft clay soils with geotextiles to resist construction loads. In *Proceedings of the 8th Young Geotechnical Engineers Conference (YGE 2014) on Cultivating the Future of Geotechnics, Spier Conference Centre, Stellenbosch, Western Cape, South Africa, 17-19 September, pp. 13-23*.

McCartney, J.S., Zornberg, J.G. & Swan, R.H. 2009. Analysis of a Large Database of GCL-Geomembrane Interface Shear Strength Results. *Journal of Geotechnical and Geoenvironmental Engineering*. 135(2):209–223. DOI: 10.1061/(ASCE)1090-0241(2009)135:2(209).

Müller, W.W. & Saathoff, F. 2015. Geosynthetics in geoenvironmental engineering. *Science and Technology of Advanced Materials*. 16(3):1–20. DOI: 10.1088/1468-6996/16/3/034605.

Müller, W., Jakob, I., Seeger, S. & Tatzky-Gerth, R. 2008. Long-term shear strength of geosynthetic clay liners. *Geotextiles and Geomembranes*. 26(2):130–144. DOI: 10.1016/j.geotexmem.2007.08.001.

Muluti, S. 2021. A Comparative Study on Shear Strength Testing of Single and Multi-layer Interfaces using Large Direct Shear Apparatus. MSc Thesis submitted to the University of Cape Town.

Nanda, S. & Berruti, F. 2021. Municipal solid waste management and landfilling technologies: a review. *Environmental Chemistry Letters*. 19(2):1433–1456. DOI: 10.1007/s10311-020-01100-y.

Naveen, B.P., Sumalatha, J. & Malik, R.K. 2018. A study on contamination of ground and surface water bodies by leachate leakage from a landfill in Bangalore, India. *International Journal of Geo-Engineering*. 9(1). DOI: 10.1186/s40703-018-0095-x.

Özer, A.T. & Akay, O. 2021. Investigation of drainage function of geosynthetics for basal-reinforced embankments. *International Journal of Physical Modelling in Geotechnics*. DOI: 10.1680/jphmg.21.00032.

Palmeira, E.M. 2009. Soil-geosynthetic interaction: Modelling and analysis. *Geotextiles and Geomembranes*. 27(5):368–390. DOI: 10.1016/j.geotexmem.2009.03.003.

Pandey, L.M.S. & Shukla, S.K. 2020. Detection of Leakage of MSW-Landfill Leachates through a Liner Defect: Experimental and Analytical Methods. *Journal of Geotechnical and Geoenvironmental Engineering*. 146(8):04020060. DOI: 10.1061/(ASCE)gt.1943-5606.0002288.

Park, H.I. & Lee, S.R. 2002. Long-term settlement behaviour of MSW landfills with various fill ages. *Waste Management and Research*. 20(3):259–268. DOI: 10.1177/0734242X0202000307.

Park, H. Il, Park, B. & Lee, S.R. 2007. Analysis of Long-Term Settlement of Municipal Solid Waste. *Journal of the Air & Waste Management Association*. 57(February):243–251.

Peng, R., Hou, Y., Zhan, L. & Yao, Y. 2016. Back-analyses of landfill instability induced by high water level: Case study of Shenzhen landfill. *International Journal of Environmental Research and Public Health*. 13(1). DOI: 10.3390/ijerph13010126.

Punetha, P. & Samanta, M. 2020. Modelling of Shear Behaviour of Interfaces Involving Smooth Geomembrane and Nonwoven Geotextile Under Static and Dynamic Loading Conditions. *Geotechnical and Geological Engineering*. 38(6):6313–6327. DOI: 10.1007/s10706-020-01437-9.

Qian, X. 2006. Translational Failures of Geosynthetic Lined Landfills under Different Leachate Buildup Conditions. 1(1):278–289. DOI: 10.1061/40860(192)32.

Qian, X. & Koerner, R.M. 2004. Effect of Apparent Cohesion on Translational Failure Analyses of Landfills. *Journal of Geotechnical and Geoenvironmental Engineering*. 130(1):71–80. DOI: 10.1061/(ASCE)1090-0241(2004)130:1(71).

Qian, X. & Koerner, R.M. 2015. Critical interfaces of multilayer geosynthetic liner systems. *Environmental Geotechnics*. 2(2):118–126. DOI: 10.1680/envgeo.13.00103.

Qian, X., Koerner, R.M. & Gray, D.H. 2003. Translational Failure Analysis of Landfills. *Journal of Geotechnical and Geoenvironmental Engineering*. 129(6):506–519. DOI: 10.1061/(ASCE)1090-0241(2003)129:6(506).

Rouncivell, W. 2007. Experimental Investigation of the Shear Characteristics of a Geosynthetic Clay Liner and Its Application in a Local Landfill. MSc Thesis submitted to the University of Cape Town.

Rowe, R.K. 2011a. Systems engineering: The design and operation of municipal solid waste landfills to minimize contamination of groundwater. *Geosynthetics International*. 18(6):391–404. DOI: 10.1680/gein.2011.18.6.391.

Rowe, R.K. 2011b. Systems engineering: The design and operation of municipal solid waste landfills to minimize contamination of groundwater. *Geosynthetics International*. 18(6):391–404. DOI: 10.1680/gein.2011.18.6.391.

Rowe, R.K. 2012. Short- and long-term leakage through composite liners. The 7th Arthur Casagrande lecture. *Canadian Geotechnical Journal*. 49(2):141–169. DOI: 10.1139/T11-092.

Rowe, R.K. 2020. Geosynthetic clay liners: Perceptions and misconceptions. *Geotextiles and Geomembranes*. 48(2):137–156. DOI: 10.1016/j.geotexmem.2019.11.012.

Rowe, R.K. & Orsini, C. 2003. Effect of GCL and subgrade type on internal erosion in GCLs under high gradients. *Geotextiles and Geomembranes*. 21(1):1–24. DOI: 10.1016/S0266-1144(02)00036-5.

Rowe, R.K. & Shoaib, M. 2017. Long-term performance of high-density polyethylene (HDPE) geomembrane seams in municipal solid waste (MSW) leachate. *Canadian Geotechnical Journal*. 54(12):1623–1636. DOI: 10.1139/cgj-2017-0049.

Schenck, C.J., Blaauw, P.F., Swart, E.C., Viljoen, J.M.M. & Mudavanhu, N. 2019. The management of South Africa's landfills and waste pickers on them: Impacting lives and livelihoods. *Development Southern Africa*. 36(1):80–98. DOI: 10.1080/0376835X.2018.1483822.

Sharma, J.S., Fleming, I.R. & Jogi, M.B. 2007. Measurement of unsaturated soil-geomembrane interface shear-strength parameters. *Canadian Geotechnical Journal*. 44(1):78–88. DOI: 10.1139/T06-097.

Shi, J., Shu, S., Qian, X. & Wang, Y. 2020. Shear strength of landfill liner interface in the case of varying normal stress. *Geotextiles and Geomembranes*. 48(5):713–723. DOI: 10.1016/j.geotexmem.2020.05.004.

Shukla, S.K. 2002. *Geosynthetics and their Applications*. 1st ed. London, UK: Thomas Telford Ltd. DOI: 10.1680/gata.31173.

Shukla, S.K. 2016. *An Introduction to Geosynthetic Engineering*. 1st ed. London, UK: CRC Press. DOI: 10.1201/b21582.

Shukla, S. & Yin, J.-H. 2006. *Fundamentals of Geosynthetic Engineering*. 1st ed. London, UK: Taylor & Francis. DOI: 10.1201/9781482288445.

Sikwanda, C. 2018. An Investigation of the Effects of Specimen Gripping Systems on Shear Stress at the Geosynthetic/Geosynthetic Interface in Landfill Applications. MSc Thesis submitted to the University of Cape Town.

Sikwanda, C., Kalumba, D. & Nolutshungu, L. 2018. An Investigation of the Effects of Specimen Gripping Systems on Shear Stress at the Geosynthetic-Geosynthetic Interface: Lecture Notes in Civil Engineering Geotechnical Characterization and Modelling Proceedings of IGC 2018. Springer International Publishing. Available: http://www.springer.com/series/15087.

Sikwanda, C., Buthelezi, S. & Kalumba, D. 2018. Review of effects of poor gripping systems in geosynthetic shear strength testing. In *Proceedings of GeoShanghai 2018 International Conference: Ground Improvement and Geosynthetics, Shanghai, China, 27–30 May 2018, pp. 420–429*.

Sikwanda, C., Kalumba, D. & Nolutshungu, L. 2019. Comparison of Single and Multi-Interface Strengths for Geosynthetic/Geosynthetic. In *Proceedings of the 17th African Regional Conference: Soil Mechanics and Geotechnical Engineering (XVII ARCSMGE), Cape Town, South Africa, 6-9 October 2019, pp. 77-81*.

Sivakumar Babu, G.L. & Lakshmikanthan, P. 2015. Estimation of the components of municipal solid waste settlement. *Waste Management and Research*. 33(1):30–38. DOI: 10.1177/0734242X14558667.

Stark, T.D. & Choi, H. 2004. Peak versus residual interface strengths for landfill liner and cover design. *Geosynthetics International*. 11(6):491–498. DOI: 10.1680/gein.2004.11.6.491.

Stark, T.D. & Newman, E.J. 2010. Design of a landfill final cover system. *Geosynthetics International*. 17(3):124–131. DOI: 10.1680/gein.2010.17.3.124.

Stark, T.D., Williamson, T.A. & Eid, H.T. 1996. HDPE Geomembrane/Geotextile Interface Shear Strength. *Journal of Geotechnical Engineering*. 122(3):197–203. DOI: 10.1061/(ASCE)0733-9410(1996)122:3(197).

Stark, T.D., Huvaj-Sarihan, N. & Li, G. 2009. Shear strength of municipal solid waste for stability analyses. *Environmental Geology*. 57(8):1911–1923. DOI: 10.1007/s00254-008-1480-0.

Stark, T.D., Choi, H., Lee, C. & Queen, B. 2012. Compacted Soil Liner Interface Strength Importance. *Journal of Geotechnical and Geoenvironmental Engineering*. 138(4):544–550. DOI: 10.1061/(ASCE)gt.1943-5606.0000556.

Stark, T.D., Niazi, F.S. & Keuscher, T.C. 2015. Strength Envelopes from Single and Multi Geosynthetic Interface Tests. *Geotechnical and Geological Engineering*. 33(5):1351–1367. DOI: 10.1007/s10706-015-9906-4.

Tammemagi, H.Y. 1999. *The Waste Crisis : Landfills, Incinerators and the search for a Sustainable Future*. Oxford, England, United Kingdom: Oxford University Press. Available: https://ebookcentral.proquest.com/lib/uoct/detail.action?docID=273258.

Touze-Foltz, N., Xie, H. & Stoltz, G. 2021. Performance issues of barrier systems for landfills: A review. *Geotextiles and Geomembranes*. 49(2):475–488. DOI: 10.1016/j.geotexmem.2020.10.016.

Vangla, P. & Latha, G.M. 2015. Influence of Particle Size on the Friction and Interfacial Shear Strength of Sands of Similar Morphology. *International Journal of Geosynthetics and Ground Engineering*. 1(1). DOI: 10.1007/s40891-014-0008-9.

Wang, J.Q., Zhang, L.L., Xue, J.F. & Tang, Y. 2018. Load-settlement response of shallow square footings on geogrid-reinforced sand under cyclic loading. *Geotextiles and Geomembranes*. 46(5):586–596. DOI: 10.1016/j.geotexmem.2018.04.009.

Wang, Q., Cui, Y.J., Tang, A.M., Delage, P., Gatmiri, B. & Ye, W.M. 2014. Long-term effect of water chemistry on the swelling pressure of a bentonite-based material. *Applied Clay Science*. 87:157–162. DOI: 10.1016/j.clay.2013.10.025.

Wilson, K.S., Kootbodien, T., Made, F., Mdleleni, S., Tlotleng, N., Ntlebi, V. & Naicker, N. 2022. Men and women waste pickers on landfills in Johannesburg, South Africa: health and socioeconomic status divergence. *International Archives of Occupational and Environmental Health*. 95(2):351–363. DOI: 10.1007/s00420-021-01787-8.

Yamsani, S.K., Sreedeep, S. & Rakesh, R.R. 2016. Frictional and Interface Frictional Characteristics of Multi-layer Cover System Materials and Its Impact on Overall Stability. *International Journal of Geosynthetics and Ground Engineering*. 2(3):1–9. DOI: 10.1007/s40891-016-0063-5.

Zaini, M.I., Kasa, A. & Nayan, K.A.M. 2012. Interface Shear Strength of Geosynthetic Clay Liner (GCL) and Residual Soil. *International Journal on Advanced Science, Engineering and Information Technology*. 2(2):156. DOI: 10.18517/ijaseit.2.2.175.

Zamara, K.A., Dixon, N., Jones, D.R. V. & Fowmes, G. 2012. Monitoring of a landfill side slope lining system: Instrument selection, installation and performance. *Geotextiles and Geomembranes*. 35:1–13. DOI: 10.1016/j.geotexmem.2012.06.003.

Zanzinger, H. 2016. Contribution to the Long-Term Shear Strength of a Needle Punched GCL. *International Journal of Geosynthetics and Ground Engineering*. 2(1):1–7. DOI: 10.1007/s40891-016-0049-3.

Zhang, Q.Q., Tian, B.H., Zhang, X., Ghulam, A., Fang, C.R. & He, R. 2013. Investigation of leachate and concentrated leachate characteristics in three landfill leachate treatment plants. *Waste Management*. 33(11):2277–2286. DOI: 10.1016/j.wasman.2013.07.021.

Appendices

A Characterization Tests

A.1 Direct Simple Shear (DSS) Tests

A.1.1 Determination of Shear Strength Parameters for Gravelly Sand (GS)

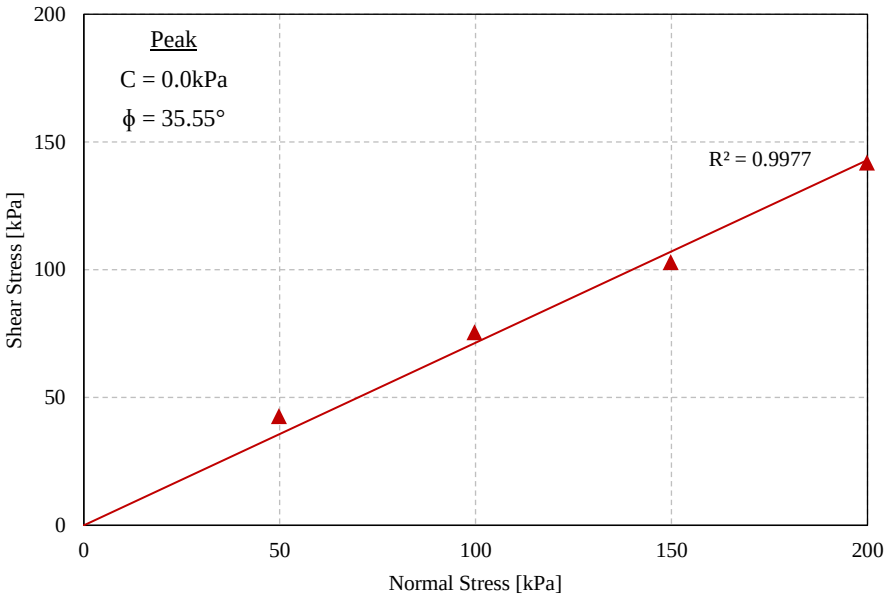

A.1.2 Determination of Shear Strength Parameters for Sand

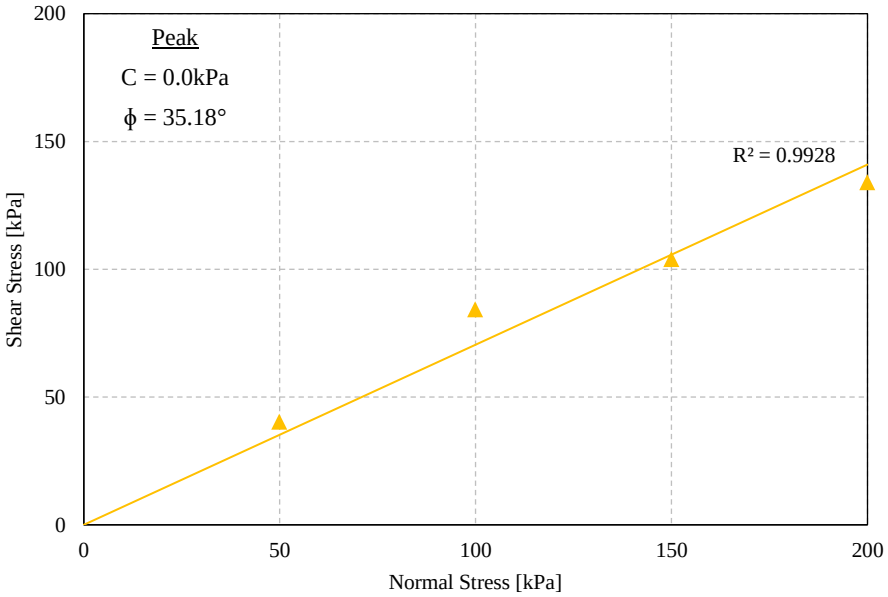

A.2 Dry Density of Geomaterials for Selected Interface Tests

A.2.1 GS | GTX-2 | GMB-1 Interface

Target Dry Density (95% MDD) = 2014kg/m^3

Target Moisture Content (W) = 4.0%

Description	Units	Applied Normal Stresses					
		150kPa		300kPa		450kPa	
		Before	After	Before	After	Before	After
Height	mm	59.74	57.01	60.55	56.70	59.28	56.03
Bulk Mass (M_{bulk})	kg	11.31	11.31	11.31	11.31	11.31	11.31
Bulk Density (γ_{bulk})	kg/m^3	2103.56	2204.29	2075.42	2216.34	2119.88	2242.85
Moisture Content (W)	%	4.20	14.67	4.46	12.90	4.47	10.87
Dry Density (DD)	kg/m^3	2018.86	1922.24	1986.90	1963.02	2029.22	2023.02

A.2.2 SAND | GTX-3 | SAND Interface

Target Dry Density (95% MDD) = 1681.5kg/m^3

Target Moisture Content (W) = 3.8%

Description	Units	Applied Normal Stresses					
		150kPa		300kPa		450kPa	
		Before	After	Before	After	Before	After
Height	mm	58.52	47.50	58.95	46.31	58.43	45.33
Bulk Mass (M_{bulk})	kg	9.43	9.43	9.43	9.43	9.43	9.43
Bulk Density (γ_{bulk})	kg/m^3	1789.51	2204.68	1776.46	2261.33	1792.27	2310.22
Moisture Content (W)	%	3.89	19.20	3.72	17.20	3.90	16.52
Dry Density (DD)	kg/m^3	1722.48	1849.56	1712.70	1929.48	1725.07	1982.66